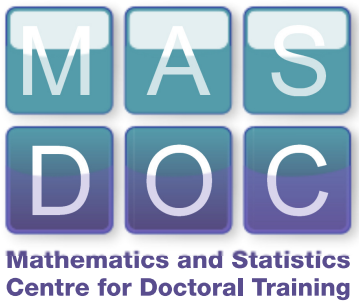

Software for Finite Element Methods and its Application to Nonvariational Problems

by

Lloyd Connellan

Thesis

Submitted to The University of Warwick

for the degree of

Doctor of Philosophy

Mathematics

The University of Warwick

September 2018

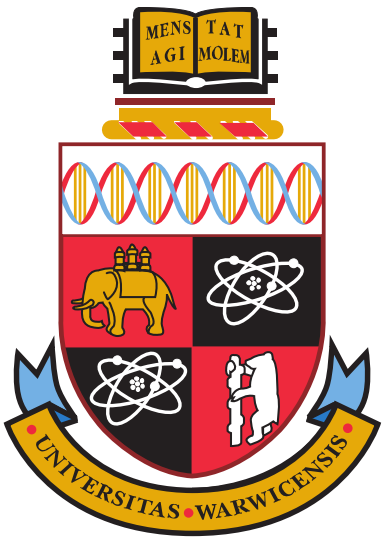

Contents

List of Tables **4**

List of Figures **6**

Acknowledgments **8**

Declarations **9**

Abstract **10**

Chapter 1 Introduction **1**

1.1 A Basic Introduction to Finite Element Methods 1
1.2 History of FEMs and Software Packages 3
1.3 Nonvariational Problems 6
1.4 Overview of Thesis 10

Chapter 2 Dune-Fempy **13**

2.1 Finite Element Methods in Dune-Fempy 13
2.1.1 Grids 16
2.1.2 Spaces 18
2.1.3 Grid Functions 19
2.1.4 Schemes 21
2.1.5 Solving 23
2.2 Alternate Solve Methods 26
2.3 Model Generation 35
2.3.1 Elliptic Models 36
2.3.2 Integrands Models 38
2.3.3 C++ Models 38
2.4 Adaptive Mesh Refinement 40
2.4.1 Re-entrant Corner Problem 41

2.4.2 Crystal Growth . . . 47
2.5 Moving Meshes . . . 52
2.5.1 Mean Curvature Flow . . . 53
2.6 Partitioned Grids . . . 59
2.6.1 Li-ion Battery Problem . . . 59
2.7 Translating Python Code to C++ . . . 71
2.8 Virtualization . . . 73

Chapter 3 Nonvariational PDEs **77**
3.1 Definition and Notation . . . 77
3.2 Existing Methods . . . 80
3.3 Minimization Method . . . 84
3.3.1 Saddle Point Formulation . . . 91
3.4 Error Analysis . . . 92
3.4.1 Error Bound for H^{-1} Method . . . 92
3.4.2 Numerical Demonstration of H^{-1} Interpolation Error . . . 99
3.5 Finite Element Hessian . . . 102
3.5.1 Derivation of FEH . . . 102
3.5.2 Numerical Implementation of FEH . . . 106
3.6 Numerical Implementation in Dune-Fempy . . . 108
3.6.1 Numerical Setup . . . 109
3.6.2 Effectiveness and Convergence Rates . . . 116
3.6.3 Efficiency . . . 125
3.7 Nonlinear Problems . . . 129
3.7.1 Numerical Setup . . . 130
3.7.2 Effectiveness and Convergence Rates . . . 131

Chapter 4 Conclusion **137**
4.1 Achieved Goals . . . 137
4.2 Future Work . . . 138

Chapter 5 Bibliography **140**

Appendix A Running this code **147**

Appendix B Derivation of Forchheimer Model **148**

Appendix C C++ Version of Forchheimer Example **150**

Appendix D List of Dune-Python modules **154**
D.1 Grids 154
D.2 Spaces 155
D.3 Grid Function 157
D.4 Schemes and Operators 159

List of Tables

2.1 Runtimes for Forchheimer solve time 40

3.1 Interpolation error in the Laplace case for different norms 100
3.2 Interpolation error with non-constant A for different norms 101
3.3 Interpolation error for a non-smooth solution with different norms . 101
3.4 Table indicating which methods are symmetric 115
3.5 Levels of drop tolerance necessary for ILU 116
3.6 Variational method applied to Poisson's equation 117
3.7 Nonvariational (DG) method applied to Poisson's equation 118
3.8 L^2 minimization method applied to Poisson's equation 118
3.9 H^{-1} minimization method applied to Poisson's equation 118
3.10 L^2 minimization method with $H[u]$ 119
3.11 H^{-1} minimization method with $H[u]$ 119
3.12 Table of EOCs for the Laplace example 119
3.13 Variational method applied to the AD equation 121
3.14 Table of EOCs for the AD problem 121
3.15 Table of EOCs for the nonD example 123
3.16 Table of EOCs for $k = 1$, for the nonD example 125
3.17 Table of EOCs for $k = 3$, for the nonD example 125
3.18 Condition numbers for the L^2 minimization method 126
3.19 Condition numbers for the H^{-1} minimization method 126
3.20 Table of EOCs for the nonvariational p-Laplace 134
3.21 Table of EOCs for the variational p-Laplace 134
3.22 Table of EOCs for the simple nonlinear problem 135
3.23 Table of EOCs for the Monge-Ampère equation 136

D.1 Grids 155
D.2 Gridviews 155
D.3 Discrete Functions 156

D.4 Spaces 156
D.5 Grid Functions 158
D.6 Solvers 160

List of Figures

2.1 Plot of a 2D grid for two different levels of refinement 17
2.2 Node maps of two Lagrange reference elements 18
2.3 The matplotlib plot of the initial function 20
2.4 Plot of solutions at each level of refinement 26
2.5 Plot of solution for Python-side Newton scheme 29
2.6 Plot of solution with Df operator 31
2.7 Plot of solution using PETSc 32
2.8 Plot of solution using PETSc and a Krylov method 33
2.9 Plot of solution using SNES 34
2.10 The first three plots of the solution 45
2.11 The second three plots of the solution 45
2.12 The final three plots of the solution 45
2.13 Zooming in on the re-entrant corner 46
2.14 Plot of the level function of the grid 46
2.15 The initial adapted grid and phase field 51
2.16 The grid, phase field and temperature after the final timestep 52
2.17 The plot of the surface at three different timesteps 56
2.18 Comparison of the error over time for varying levels of refinement . . 58
2.19 The domain, a cell split into three parts 61
2.20 The initial plot of c and ϕ 70
2.21 The plot after the final timestep 70
2.22 Comparison of time taken between the two calcRadius methods . . . 73

3.1 Plot of $\|\Delta(u - I_h u)\|$ 101
3.2 Plot of $\|\nabla \mathcal{N}_h \Delta(u - I_h u)\|$ 101
3.3 Plots of L^2 errors for Poisson's equation 120
3.4 Plots of L^2 EOCs for Poisson's equation 120
3.5 Plots of H^1 errors for Poisson's equation 120

3.6 Plots of H^1 EOCs for Poisson's equation 120
3.7 Plots of L^2 errors for the AD problem 122
3.8 Plots of L^2 EOCs for the AD problem 122
3.9 Plots of H^1 errors for the AD problem 122
3.10 Plots of H^1 EOCs for the AD problem 122
3.11 Plots of L^2 errors for the nonD problem 123
3.12 Plots of L^2 EOCs for the nonD problem 123
3.13 Plots of H^1 errors for the nonD problem 124
3.14 Plots of H^1 EOCs for the nonD problem 124
3.15 Comparison of the condition numbers for different methods 127
3.16 Plot of the iteration count for the nonD problem 128
3.17 Plot of the total time taken for the nonD problem 129

Acknowledgments

This work has been supported by the Engineering and Physical Sciences Research Council (EPSRC) within the MASDOC DTC at the University of Warwick.

First of all I would like to thank my supervisor Andreas Dedner for his continual guidance in all things mathematical and computational throughout my PhD. Without his help, often going above and beyond what I expect, I am sure this thesis would not be possible.

Secondly I would like to thank Björn Stinner for always looking out for me and giving me advice through my time at MASDOC. To Matteo Icardi who provided assistance with the battery problem, I am also very grateful.

To my colleagues at MASDOC, in particular my friends Neil and Adam, I would like to say thanks for all the support and friendly conversations over the years. To all my friends that I have met online during this time, I would also like to offer my thanks for their company.

Finally I wish to thank my family for always being there for me, and giving me their love and support. I could not have done this without you.

Declarations

The work described in this thesis is the author's own, conducted under the supervision of Andreas Dedner (University of Warwick), however we note that the software package Dune-Fempy showcased in chapter 2 is a collaborative project with Andreas Dedner, Martin Nolte (University of Freiburg), Robert Klöfkorn (International Research Institute of Stavanger), Matthew Collins (University of Warwick) and other developers. We also note that the derivation of the finite element Hessian in section 3.5 was previously carried out by Andreas Dedner and Tristan Pryer (University of Reading) in an unpublished paper (Dedner and Pryer [2013]). None of the material contained in the thesis has been used by the author in any previous publication or degree.

Abstract

We begin by introducing an extension to the software package DUNE (a C++ based toolbox for solving PDEs with the finite element method) which has the main objective of providing a Python user interface to it. First of all we explain how we have structured the interface and go into some detail about the components typical to a FEM. We then go on to demonstrate different features available in the context of worked examples. For instance, we consider the integration of different software packages such as PETSc and SciPy, as well as FEM features such as grid adaptivity, moving domains, and partitioned grids. Throughout this we highlight design decisions that are different to other similar packages and the reasoning behind them. We conclude by demonstrating how C++ code development can be integrated into the process and how that affects efficiency.

We go on to consider an application of this software to nonvariational PDEs. The key contribution of this section is the development of a new method for solving this class of problems based on minimization. We derive this method and provide results for existence and uniqueness and error convergence. We also compare this method to existing methods and highlight the advantages it has. We then derive a second aspect of this method which involves a finite element version of the Hessian. We combine these features and look at numerical results for linear nonvariational problems. We compare the new methods along with other existing methods using our software in terms of convergence rates and efficiency. Finally we take an experimental look at solving nonlinear nonvariational problems using the finite element Hessian, and an application to the Monge-Ampère equation.

Chapter 1

Introduction

1.1 A Basic Introduction to Finite Element Methods

Before talking about finite element methods (FEMs), it is only right that one first talks of the partial differential equations (PDEs) they look to solve. PDEs have existed as a mathematical model for all manner of physical phenomena for centuries, with equations describing how fluids flow, how heat transfers, and how sound waves propagate. Indeed capturing the essence of how the world works around us inherently requires complexity, meaning that in many cases the simpler ordinary differential equation is not enough. Yet with this complexity requires an added effort to solve them, and often finding an analytical solution to all but the simplest PDEs is a difficult task, and at times an impossible one. Thus in modern times we typically look to numerical solutions and computers to solve PDEs, the most common methods being the finite difference method, the finite volume method, and of course the finite element method.

To describe FEMs in an introductory sense, the general concept is to split up a problem's domain into separate smaller components (finite elements), upon which it is much easier to approximate the solution on. By moving to a finite-dimensional version of the function space, one concretely solves a discretized solution on each individual element. These elements are then combined to give the whole picture of the problem.

Let us mathematically describe this method with a relatively simple example. Let $\Omega \subset \mathbb{R}^d$ be our domain. Then **Poisson's equation** is

$$\begin{aligned} -\Delta u &= f, \quad \text{in } \Omega, \\ u &= 0, \quad \text{on } \partial\Omega. \end{aligned}$$

Whilst elementary, this equation sees use in many areas, including electrostatics and fluid mechanics. Now in FEMs, the usual procedure is to obtain the **weak form** of the PDE by multiplying by a test function v in a function space V, and integrating by parts. This results in the following equation. We want $u \in V$ such that

$$\int_\Omega \nabla u \cdot \nabla v \, \mathrm{d}x = \int_\Omega f v \, \mathrm{d}x, \quad \forall v \in V. \tag{1.1}$$

As this weak form is a common feature of FEMs, there exists a generalized form,

$$a(u, v) = (f, v), \quad \forall v \in V, \tag{1.2}$$

where $a(\cdot, \cdot)$ is a coercive bilinear form on V and $(\cdot, \cdot)$ is the L^2 inner product. In this case, the weak form of Poisson's equation can be obtained by choosing $V = H_0^1(\Omega)$ and $a(\cdot, \cdot)$ in (1.2) to be the $H_0^1(\Omega)$ inner product.

Following this, it is necessary to convert this equation into an algebraic system that can be solved elementwise, i.e. to discretize it. One aspect of this is dividing the domain Ω into a mesh of polygonal shapes $\{K_i\}$ called a *triangulation*. Specifically, we derive an approximation Ω_h such that

$$\Omega \approx \Omega_h = \bigcup_{i=1}^{N} K_i.$$

Here Ω_h is dependent on h (the mesh size) which is defined by

$$h_K := \max_{x,y \in K} |x - y| \text{ and } h := \max_{K \in \Omega_h} h_K.$$

Additionally, it is necessary to choose a discrete space V_h (typically a polynomial

space) that approximates V. With this, we are able to write the discrete solution as a linear combination of basis functions, i.e. $u_h(x) = \sum_{i=1}^{N} u_i \varphi_i(x)$ (where $\{\varphi_1, \ldots, \varphi_N\}$ is a basis of V_h). We can also write the discrete counterpart to (1.2) as follows

$$a(u_h, v_h) = (f, v_h), \quad \forall v_h \in V_h, \tag{1.3}$$

Finding $u_h \in V_h$ is known as the **Galerkin method**. Consequently, we can rewrite (1.3) in terms of basis functions, due to the linearity of $a(\cdot, \cdot)$.

$$\sum_{j=1}^{N} u_j a(\varphi_j, \varphi_i) = (f, \varphi_i), \quad i = 1, \ldots, N.$$

From here, one can form an algebraic system of equations by defining a matrix A with entries $A_{ij} = a(\varphi_i, \varphi_j)$ and a vector $\mathbf{b}$ with entries $b_i = (f, \varphi_i)$. We can then solve the linear system

$$A\mathbf{u} = \mathbf{b},$$

where $\mathbf{u} = (u_i)_{i=1}^{N}$ are the *degrees of freedom* of u_h. This system of linear equations can then be solved via an appropriate algorithm, e.g. a conjugate gradient (CG) method or generalized minimal residual (GMRES) method.

All in all this procedure allows one to consistently solve PDEs in a numerical sense, provided they can be put into a weak form.

1.2 History of FEMs and Software Packages

Now that we have introduced what FEMs are in an elementary sense, let us expand upon their history and development.

Among the different numerical methods for solving partial differential equations, finite element methods are one of the most popular. They have been used for a broad range of engineering and scientific problems, with the first computational applications originating as early as Turner et al. [1956]. Over the years there has been an extensive amount of literature analysing FEMs in general and their uses (see e.g. Khoei [2015] and Babuška and Strouboulis [2001]).

Just as the development of the theory of FEMs has progressed over the years, the landscape of FEM software itself has undergone much change. As a multidisciplinary method involving many different techniques, the scope for which direction to develop features is very high. Even within the realm of standard FEMs there exist a multitude of different options available. For instance with regards to types of finite elements, if one considers *conforming* finite elements (i.e. where $V_h \subset V$) then one has possibilities such as the well-known Lagrange element, the $H(div)$ conforming Brezzi-Douglas-Marini element used for instance for the elastic stress tensor, the $H(curl)$ conforming Nédélec element used in electromagnetism, and so on. Then, provided one uses an appropriate penalty method, one can further expand this to have nonconforming elements such as the H^2 Hermite (cubic) elements, the Morley (quadratic) elements used for fourth order problems, and the H^1 Crouzeix-Raviart element used in Stokes flow[1]. In addition one can consider the mesh itself; one can have structured grids that are more computationally efficient or unstructured ones that allow for more flexibility. Furthermore one could have different shapes such as squares, triangles, cubes, pyramids, hexahedrons and so on. This is all without going into more complex forms of FEM such as hp-FEM (see [Melenk, 2002, §1.4.3]), spectral element methods (see [Karniadakis and Sherwin, 2013, §1.2.2]) and extended finite element methods (XFEM) (see [Fries, 2008, §2]).

All in all this diversity of choice has lead to the situation of numerous competing packages that offer slightly different flavours of FEM. One preventative measure to this has been the development of large modular software libraries that offer many optional extensions in one place, thus forgoing the need to install different packages for different problems. Such examples include DUNE (Bastian et al. [2008]), deal.II (Alzetta et al. [2018, accepted]), FreeFem++ (Hecht [2012]) and Elmer (Lyly et al. [1999]). These large packages are typically written in languages such as C++ and Fortran that are efficient for large-scale computations.

In recent years however there has been a trend towards packages that favour usability. Such packages look to lower the learning curve for new developers and

[1]For a more complete list of types of elements, see Kirby et al. [2012]

non-computer focused researchers, allowing for more time to be spent productively solving problems. Additionally, higher level programming languages facilitate the use of rapid prototyping, i.e. allowing one to quickly construct new models and test their viability without having to write an intricate program. Python and MATLAB are both examples of commonly used languages that prioritize usability; in particular Python has risen to become one of the most popular programming languages of recent times (see e.g. Tio [2019]). Yet there are downsides to these languages from the standpoint of a researcher in mathematics or engineering; namely that they are not as efficient as their traditional counterparts in C, C++ and Java. Thus the goal of many new packages has been to unify an interface that combines aspects of being easier to pick up and use, without compromising the functionality and efficiency of traditional packages.

There exist many ways to go about tackling this problem. One strategy is to make use of more modern features of C++ (and other similar languages), such as `auto` types, range-based for loops and lambda functions, to increase usability. Yet arguably even the most user-friendly versions of these languages remain intimidating to programming novices, due to their core design elements that cannot be changed. A different approach is to use a language that attempts to unify usability and efficiency in one place. Julia (Bezanson et al. [2014]) is one example of such a language. The principal downside is the lack of popularity or wide-spread use of any such language in comparison to Python or C.

A third alternative, one growing in popularity, is to use two languages such as Python and C++ in the same package. The core idea behind this approach is to use a simplified interface attached to a back end with lower level code, which is typically achieved via the use of an automatic code generation tool like SWIG or Cython. This tying together of front end to back end does require additional code and maintenance of the interfacing between them, but its merit is in that it effectively combines the best of both worlds. In particular FEniCS (Alnæs et al. [2015]) and Firedrake (Rathgeber et al. [2017]) are examples of this kind of software.

One large component of both these packages is the use of Unified Form

Language (UFL) (Alnäes et al. [2013]), a domain-specific language (DSL) which allows one to write variational equations directly. For instance for equation (1.1) we have the following simple code.

Code Listing 1.1: Poisson's equation in UFL

```
a = inner(grad(u), grad(v))*dx
b = inner(f, v)*dx
```

We do however note that the code generation-style approach used in FEniCS and Firedrake does come with inherent weaknesses. In particular this generated code is not suited to direct editing, so should a binding not exist for a feature on the Python side, editing these generated files to add the feature on the C++ side is not an option. Furthermore, user interactibility with the C++ interface is not prioritized, which means porting code over to C++ for efficiency reasons or the writing of additional features are not viable.

In the first chapter of this thesis we introduce Dune-Fempy, a Dune module that is an extension to Dune-Python (Dedner and Nolte [2018]) specifically aimed at adding high-level FEM features based on the Dune-Fem module (Dedner et al. [2010]) to Dune. The aim of both of these packages is to bring the usability and speedier writing of code to Dune and its large array of existing modules whilst preserving the features available to a C++ developer. In particular the structure and functionality is designed to be analogous in many ways to Dune code, making it less difficult to port code to C++ if necessary. Additionally, attempts to increase usability have been made, such as library caching to reduce the runtime of repeated computations, and integration with modern C++11/C++14 via pybind11 (see Jakob et al. [2017]) to interface between C++ and Python.

1.3 Nonvariational Problems

Continuing onwards, there exists another reason, besides the potential for optimization, for maintaining a similar structure to Dune and other traditional C++ programming. Namely that is to facilitate the extensibility of code. In Dune-Fempy,

additional C++ code can be simply added to the interface via the use of DUNE modules and pybind11 functionality (a process that is explained in-depth in Dedner and Nolte [2018]). Considering that many interesting research topics by nature are nontrivial, it is crucial to be able to cater for problems that do not necessarily fit into the neat interface provided by many Python-style software packages.

Having said this, we note that there is a large range of problems that fit into the variational framework, and by extension the myriad of numerical software available for solving them. Indeed, since such a large variety of partial differential equations can be put into variational (or weak) form, regardless of complexities such as nonlinearity, it is usually not required to go beyond this scope.

There are however PDEs for which it is ill-advised, or sometimes impossible to put into a variational form. In particular, chapter 3 of this thesis looks at the class of PDEs that take the form

$$-A : D^2 u = f.$$

Here $D^2 u$ is the Hessian of u, f is a prescribed function and A is a matrix.

In the case that the matrix A is differentiable, we note that this has an obvious equivalence with standard variational methods. For instance in the case where A is the identity matrix, the above equation simply equates to Poisson's equation. In such cases the above is equivalent to its variational sibling.

$$-\nabla \cdot (A \nabla u) + (\nabla \cdot A) \nabla u = f.$$

However we note that because of the existence of the DA term, this cannot be done in the case where A is not differentiable. In fact even in cases where the derivatives are close to zero, the PDE becomes advection dominated, making it probably unsuited for conforming FEMs. Because of this possibility, in general PDEs of the above form are classed as *nonvariational*.

We also note that this linear case can be extended to a nonlinear version that

takes the general form

$$F(D^2u) = f(x, u, Du).$$

In this case F can be any kind of function acting on the second derivatives of u, which increases the scope further. In particular such nonvariational problems occur in a variety of different contexts, for instance the Monge-Ampère equation (see e.g. Gutiérrez [2001]) and the Hamilton-Jacobi-Bellman equations (which have many applications such as in economics (Cao and Wan [2009]) and engineering (Ioslovich et al. [2009]); a review can be found in Katzourakis and Pryer [2018]).

The Monge-Ampère equation especially has many applications. The Dirichlet version (in a domain Ω) takes the general form

$$\begin{aligned} \det(D^2u) = f(x, u, Du), \quad &\text{in } \Omega, \\ u = 0, \quad &\text{on } \partial\Omega. \end{aligned}$$

The most well-known application of this is the problem of prescribed Gauss curvature on a convex domain (Trudinger and Urbas [1983], Urbas [2004]). This is a specific example of the Monge-Ampère equation which takes the form

$$\det(D^2u) = K(x)(1 + |Du|^2)^{(n+2)/2}.$$

Another application is the mass-transfer problem (Benamou and Brenier [2000], Evans [1997]). This originates from the Monge-Kantorovich equation, which describes the transfer of mass from one area to another. This is realized via density functions ρ_0 and ρ_T, and a map M between them. For a smooth one-to-one map this reduces to

$$\det(\nabla M(x))\rho_T(M(x)) = \rho_0(x)$$

It is then possible to prove that for some convex function $\Phi(x)$ that $M(x) = \nabla\Phi(x)$, which once again returns the Monge-Ampère equation.

Furthermore more recently there has been an application to r-adaptivity on the sphere in McRae et al. [2016], i.e. moving the mesh points of a numerical

grid by solving the Monge-Ampère equation. Another recent work (Ożaǹski [2015]) demonstrates that it can also be applied to the Navier-Stokes equations.

On the whole however, whilst due consideration has been given to specific examples of nonvariational problems, as a class of equations themselves they have not been studied extensively. In particular numerical methods that target this problem are relatively few. Historically speaking, the first numerical methods developed for tackling nonvariational problems were finite difference methods (FDMs). For instance Oberman [2008] and Loeper and Rapetti [2005] studied the Monge-Ampère equation with such an approach. The most likely reason for the popularity of FDMs compared to FEMs for nonvariational problems is due to their compatibility with viscosity solutions, which are a natural type of solution for nonvariational problems. However that is not to say there is no disadvantage to FDMs, for in particular one is only able to consider structured meshes. By considering the problem from a FEM perspective, we open up the possibility of unstructured grids, and other useful tools such as grid adaptivity.

One of the first papers to consider a finite element approach to nonvariational models was Lakkis and Pryer [2010], where the concept of a *finite element Hessian* $H[u]$ was first introduced. This form comes from applying the distributional equation for the Hessian, i.e.

$$\int_\Omega D^2 u\varphi \,\mathrm{d}x = -\int_\Omega \nabla u \otimes \nabla\varphi \,\mathrm{d}x + \int_{\partial\Omega} \nabla u \otimes \mathbf{n}\varphi \,\mathrm{d}s.$$

This method has later been applied to nonlinear problems in Lakkis and Pryer [2012], and then developed into a discontinuous Galerkin (DG) method in Dedner and Pryer [2013]. Furthermore, we note that another DG finite element method was proposed around the same time in I. Smears [2013], which uses an hp-FEM, and later on an approach using a discrete version of the Hessian similar to the above was derived in Wang and Wang.

The problem has continued to see development from a FEM context. In particular a more recent paper Mu and Ye [2017] uses a symmetrised discretization

of $-A : D^2 u = f$.

$$\int_\Omega (A : D^2 u_h)(A : D^2 \varphi_h) \,\mathrm{d}x + s(u_h, \varphi_h) = \int_\Omega f A : D^2 \varphi_h \,\mathrm{d}x, \quad \forall \varphi_h \in V_h,$$

where $s(\cdot, \cdot)$ is a stabilization term. One singular property of this method is that the analysis is made easier by its inherent symmetry, which allows for less assumptions to be made of the regularity of the problem. Nonetheless the fourth-order nature of the method causes it to be less efficient numerically.

One of the main aims of chapter 3 is the development of a method that combines the symmetric properties of the above method with the numerical efficiency of other methods, and the use of the finite element Hessian. We also note that in section 3.2 we will present a more in-depth look at the methods from the literature and how they tie in with the method developed in this thesis.

1.4 Overview of Thesis

Let us provide an overview of the chapters of this thesis. On the whole it is divided into two main parts, each of which is planned to become a paper in the future.

In chapter 2 we provide an overview of the software package Dune-Fempy, the features it provides, and a discussion of the design decisions. We begin in section 2.1 by introducing the interface for a simple FEM step-by-step, where we go through the process for solving a nonlinear parabolic PDE, the Forchheimer equation. Through this section we detail each component of the FEM and why they are considered necessary. Following this, in section 2.2 we consider different ways we can solve the PDE and in doing so demonstrate how the Python interface can be fully taken advantage of. In 2.3 we instead focus on an aspect which involves the C++ back end, by considering different ways of generating the model, and how flexibility has been provided for C++ programmers. For a change of pace, the remaining sections of the chapter look at additional features in the context of more complex examples. Beginning with section 2.4, we look at two examples that use adaptive mesh refinement. The first considers a non-standard domain that requires

more precision around a certain point, and the second features a time-dependent problem that requires the grid adaption to change over time. In section 2.5 we then consider a mean curvature example, i.e. an example where the surface evolves over time due to a smoothing condition. For the last example, in section 2.6 we look at a model of a Li-ion battery where the domain is divided into three separate regions. Finally we discuss the comparison to C++ code in section 2.7, and how virtualization has been taken into consideration in section 2.8.

For chapter 3, the second part of this thesis, we consider nonvariational problems and their discretization in Dune-Fempy. We first concretely define the problem and corresponding notation in section 3.1. Then in section 3.2 we review existing methods in the literature, and compare them along with a new method proposed in this paper. We begin the analysis of this method in section 3.3, where we formally introduce this new method based on minimization, show existence and uniqueness, and derive a saddle point formulation. We then proceed in section 3.4.1 to provide error analysis for this method in terms of a bound between the solution and its discrete approximation. We also demonstrate that this error estimate may be suboptimal compared to the empirical results in part 3.4.2. We continue to consider alterations to the numerical implementation in section 3.5, where we derive a numerical version of the Hessian, which we will use to improve the previous method further. Following from this analysis, in section 3.6 we proceed to present the numerical implementation of the previous methods, implemented in Dune-Fempy. We compare them in the context of the linear case, considering convergence rates and efficiency of the approaches. Finally we will look at a purely numerical implementation of the nonlinear case in section 3.7, in which we look to solve the Monge-Ampère method and other nonlinear problems.

To summarize things, section 4 reiterates what has been achieved, and the future directions available to continue on from this project.

We note that there are two key findings to this thesis, the first of which is the contributions to developing Dune-Fempy[2], a tool for writing and developing

[2]Publically available at `https://gitlab.dune-project.org/dune-fem/dune-fempy`.

finite element methods with a Python interface, based on the well-known open source software package DUNE. DUNE-FEMPY is the first attempt to bring Python scripting to DUNE, is aimed at maintaining the flexibility of the DUNE module, and is already used in other projects. The second key finding is the minimization method for solving nonvariational problems, and the application of the finite element Hessian to said method and later on to nonlinear problems.

In particular, due to the collaborative nature of the project, I also will also emphasize the following contributions which are uniquely my own. To begin with, in DUNE-FEMPY I created the initial framework for the UFL to C++ conversion for models. Over the course of the project I have added to the underlying infrastructure, most notably to code involving grid functions and models. The code for the Forchheimer example (shown in section 2.1), the battery example (shown in section 2.6) and a Navier-Stokes example (not shown here) were written by me (other examples shown were written by others and adapted to this thesis). Otherwise, all written parts of chapter 2 (except for section 2.8) were written by me. For the nonvariational section, the code contained within the DUNE-FEMNV module[3] is almost all my own, with the Monge-Ampère code and original Finite Element Hessian computation written by my supervisor. In terms of the analysis, the minimization method posed in sections 3.3 and 3.4 and the experiments in sections 3.6 and 3.7 were done by me with help from my supervisor.

[3]Publically available at https://gitlab.dune-project.org/lloyd.connellan/dune-femnv.

Chapter 2

Dune-Fempy

2.1 Finite Element Methods in Dune-Fempy

When designing any software package, a natural challenge that arises is trying to make the user interface as simple and easy to use as possible. At the same time however, we also want to create an interface that retains all the functionality we need.

In the context of finite element methods, this leads to the question of what the minimal functional structure for a FEM looks like. In order to try to address this question, we will first outline from a mathematical standpoint the general structure we have in mind for a FEM.

To begin with, the original problem we typically want to apply a finite element method to is a continuous PDE in some infinite-dimensional space V. First let $\Omega \subset \mathbb{R}^d$ be a polygonal domain for our problem. We then choose a conforming finite element space $V_h = \{\varphi_h : \Omega \to \mathbb{R}^r\} \subset V$, where $\dim V_h = N$. This involves choosing a basis for V_h, which can vary depending on the problem, but typically involves piecewise polynomial functions.

Next the variational (or weak) form of the equation is defined. For the purpose of illustration, let us assume to start with we have a parabolic PDE of the

following general form.

$$\begin{aligned} &\partial_t u + L[u] = f(x), && \text{in } \Omega \times [0,T], \\ &u(x,0) = u^0(x), && \text{in } \Omega, \\ &D\nabla u \cdot \mathbf{n} = g(x), && \text{on } \partial\Omega \times [0,T], \end{aligned} \tag{2.1}$$

where the elliptic operator L is defined as

$$L[u] := -\nabla \cdot D(x,u,\nabla u)\nabla u + m(x,u,\nabla u), \tag{2.2}$$

and where u^0 and g are the initial and boundary conditions and $\mathbf{n}$ is the outward pointing normal. We note that we are only considering Neumann boundary conditions here for simplicity, although Dirichlet boundary conditions are also a possibility.

To obtain the discrete form, we begin by discretizing the PDE in time. This results in the following method: given u^0, for $n \in \mathbb{N}_0$, find $u^{n+1} \in V_h$ such that

$$\frac{u^{n+1} - u^n}{\Delta t} + L_I[u^{n+1}] + L_E[u^n] = f(x, t^n), \tag{2.3}$$

where Δt is the time step, and L_I and L_E are the implicit and explicit parts of L, defined using (2.2) as

$$\begin{aligned} L_I[u] &= -\nabla \cdot D_I(x,u,\nabla u)\nabla u + m_I(x,u,\nabla u), \\ L_E[u] &= -\nabla \cdot D_E(x,u,\nabla u)\nabla u + m_E(x,u,\nabla u), \end{aligned}$$

and $D_I + D_E = D$, $m_I + m_E = m$.

The variational form is then obtained from equation (2.3) by multiplying by a test function $\varphi \in V_h$ and integrating by parts.

$$\begin{aligned} \int_\Omega \frac{u^{n+1} - u^n}{\Delta t}\varphi + (D_I\nabla u^{n+1} + D_E\nabla u^n) \cdot \nabla\varphi + (m_I + m_E)\varphi \,\mathrm{d}x \\ = \int_\Omega f\varphi \,\mathrm{d}x + \int_{\partial\Omega} g\varphi \,\mathrm{d}s, \quad \varphi \in V_h. \end{aligned} \tag{2.4}$$

We note that in terms of the actual solving of this form, there exists potential variation in terms of the solver used and possible nonlinearity of the problem. We also note that this is a simple scheme for demonstration, and more complex examples involving higher order schemes or nonconforming spaces can be easily implemented along the same lines.

With this general form in mind, in Dune-Fempy we have designed the structure to take as similar a style as possible, which results in the following breakdown of parts.

- 2.1.1 Grid. The computational domain Ω the problem is set in.
- 2.1.2 Space. The finite element space V_h and type of basis functions.
- 2.1.3 Grid functions. Functions defined on the grid that store the solution u_h and other variables.
- 2.1.4 Scheme. The weak form of the equation, its boundary conditions, and method for solving.
- 2.1.5 Solving. The actual solving process and data output.

We note that there exist even further simplifications that can be made in terms of this design choice; for instance a FEM could be distilled to simply choosing a weak form (an operator) and a grid, and having all other things set to sensible defaults. Additionally the code itself used to represent these methods could be simplified to a large degree depending on the aim of the software.

Ultimately as a FEM package aimed more at extensibility and for researchers who are willing to commit to some degree of programming, we have opted for more complexity in some cases at the expense of this simplicity. In general this is quite a nuanced design decision that must be made without a clear *right* answer.

With that in mind, for the remainder of this section we shall demonstrate in more detail how each of these concepts are implemented in the context of a worked example, the FEM applied to the Forchheimer equation: a scalar, nonlinear

parabolic equation derived in Kieu [2015]. A full derivation of this equation is described in appendix B, but for the following the final form suffices.

$$\begin{aligned}&\int_\Omega \frac{1}{\Delta t}(u^{n+1}-u^n)\varphi \ + \frac{1}{2}K(\nabla u^{n+1})\nabla u^{n+1}\cdot\nabla\varphi \\ &+ \frac{1}{2}K(\nabla u^n)\nabla u^n\cdot\nabla\varphi\,\mathrm{d}x = \int_\Omega f\varphi\,\mathrm{d}x + \int_{\partial\Omega} g\varphi\,\mathrm{d}s, \quad \varphi\in V_h,\end{aligned} \tag{2.5}$$

where $K(\nabla u)$ is a scalar function. We note that this corresponds to taking $D_E = D_I = \frac{1}{2}K(\nabla u)I$ (where I is the identity matrix) and $m_E = m_I = 0$ in equation (2.4).

2.1.1 Grids

The first aspect of FEMs that we consider is probably the most fundamental aspect, that of the grid (or mesh). Naturally, before looking at the equations we want to solve themselves, we must look at the computational domain and how we want to discretize it. Ideally numerical software looking to emulate FEMs should be able to construct both simple triangulated 2D domains and more complex surfaces and meshes.

For now we will look at a simple example. Let us suppose we have a domain of the following form.

$$\Omega = \{(x,y)\in\mathbb{R}^2 : 0\le x\le 1, 0\le y\le 1\}.$$

In creating a computational grid for this domain, it will be necessary to specify the following things.

1. The shape of the domain (a square) and its vertices.
2. The number of elements.
3. The type of elements (e.g. square elements or triangles).

With these points in mind, we implement the grid in the following way in DUNE-FEMPY and plot the result in figure 2.1.

Code Listing 2.1: Creating and plotting two simple rectangular grids

```
from dune.grid import structuredGrid
grid = structuredGrid([0, 0], [1, 1], [4, 4])
grid.plot()
grid.hierarchicalGrid.globalRefine(1)
grid.plot()
grid.hierarchicalGrid.globalRefine(-1)  # revert grid refinement
```

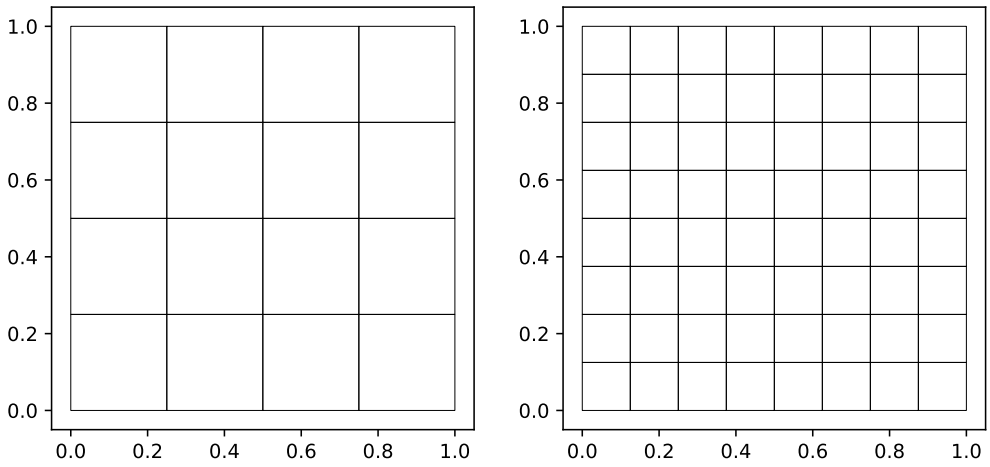

Figure 2.1: Plot of a 2D grid for two different levels of refinement

Here we create a simple square domain by specifying two opposite corners $(0, 0)$ and $(1, 1)$, and the number of elements in each direction $(4, 4)$. We then refine the grid and plot the results, before coarsening it again. We note that this is a simplified example and in general grids in DUNE-FEMPY can additionally be constructed via a dictionary containing vertex and element information, gmsh files or *dune grid format* (dgf) files when more complexity is required, which is demonstrated in the DUNE-PYTHON paper Dedner and Nolte [2018]. A list of more complicated grids and other modules is given in appendix D.

Conceptually it is worth stating that from a design standpoint, assumptions could potentially be made to cut down on the complexity needed. For instance in situations where the exact details are not necessary, a basic square grid could simply be made with `grid = square()`. However such a design comes at the cost of it being

(a) Second order element (b) Third order element

Figure 2.2: Node maps of two Lagrange reference elements

unclear how to make small modifications.

2.1.2 Spaces

The next key part of a FEM after constructing the grid is defining the kind of elements we want to use, and by extension their space. In particular this is important because the order of elements used as well as the type of element space can dictate the solvability and the efficiency of the method.

Let us consider a simple case of Lagrange elements. Since we have a 2D domain with a quadrilateral mesh, we consider shape functions that are 1 on each separate node, and 0 on the others. For orders 2 and 3, the shape functions would be quadratic and cubic polynomials respectively (as shown in figure 2.2). The creation of such a Lagrange space in DUNE-FEMPY is done by the following code.

Code Listing 2.2: Creating a Lagrange space with polynomial basis functions

```
1 import dune.create as create
2 space = create.space('lagrange', grid, dimrange=1, order=2)
```

We note that the above space is called with two default arguments and two keyword arguments.

- `'lagrange'` indicates that we will use a space with Lagrange basis functions.
- `grid` passes in the grid we constructed previously.
- `dimrange=1` (optional) sets the dimension of the range space to 1 (deduced from the UFL expression by default).

- `order=2` (optional) sets the order of the finite elements to 2 (2 is the default).

Of particular note is that the first argument corresponds to a DUNE discrete space realization that can come from anywhere within a DUNE installation, provided Python bindings are created for it. For instance we could use a discontinuous Galerkin space with orthonormal basis functions instead by using `'dgonb'`.

2.1.3 Grid Functions

Having defined the computational domain and function space, we look towards functions that we may need to define, e.g. for containing the solution. In particular we want to be able to store what initial values it can take, its value at the previous time step and so on.

Let us begin by just considering a function for the initial condition. In DUNE-FEMPY, we use Unified Form Language (UFL) (Alnäes et al. [2013]) to define equations, which is essentially a human-readable way of writing a variational form. We can also use UFL to define a simple function. To this end, we must begin by defining a variable.

Code Listing 2.3: Creating an `x` variable in UFL

```
1 from ufl import SpatialCoordinate
2 x = SpatialCoordinate(space)
```

Here we create `x` as a spatial coordinate from UFL by using the `space` object from the previous section. The `space` gives UFL the dimensions of the grid and the range space, so it knows `x` is two dimensional. So now for initial condition $u = \frac{1}{2}(x_0^2 + x_1^2) - \frac{1}{3}(x_0^3 - x_1^3) + 1$, we would have the following code.

Code Listing 2.4: Creating a grid function using UFL

```
1 initial = 1/2*(x[0]**2 + x[1]**2) - 1/3*(x[0]**3 - x[1]**3) + 1
```

Now this function can be used in a variety of ways. Let us first show how we would compute the L^2 norm of the initial function. We do this using the `integrate` function, which we note takes as arguments the `grid` defined previously, the function

`initial` and the quadrature order `5`. Also note that in DUNE-FEMPY functions are vectors by default, so we add `[0]` so that it is treated as a scalar.

Code Listing 2.5: Integrating the initial data

```
1 from dune.fem.function import integrate
2 mass = integrate(grid, initial**2, order=5)[0]
3 print(mass)
```

Output

```
1 1.840079345703125
```

We can also plot functions fairly easily. The two main ways to do this in DUNE-FEMPY are either a quick plot in `matplotlib` (see Hunter [2007]), or writing to a VTK file for use in Paraview (see Ahrens et al. [2005]), which we do below, resulting in figure 2.3.

Code Listing 2.6: Plotting a function using two different methods

```
1 from dune.fem.plotting import plotPointData as plot
2 plot(initial, grid=grid)
3 grid.writeVTK('initial', pointdata={'initial': initial})
```

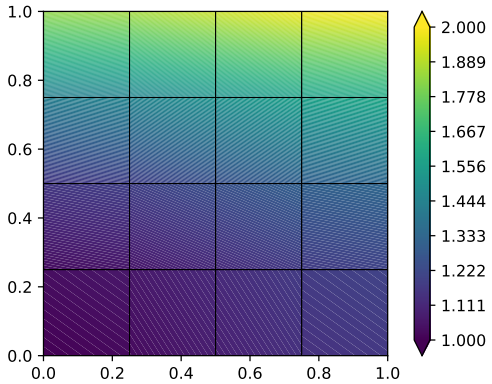

Figure 2.3: The matplotlib plot of the initial function

For the vtk output the function needs to be assigned a name, which is given by the key argument of the dictionary passed as the `pointdata` argument.

Note that so far we have simply evaluated the UFL expression `initial` directly, i.e., without using any approximation. It is equally possible to do the

above with a discrete function, which can be created through interpolation into the discrete function space as shown below.

Code Listing 2.7:

```
u_h = space.interpolate(initial, name='u_h')
```

So we have created a discrete function `u_h` over the discrete finite element space to contain the solution and used an interpolation over the space to assign its initial value to the UFL expression `initial`. The name is used later for plotting purposes, for example in the VTK output.

To define the weak formulation given by (2.5) we need two discrete functions, one to store the next time step (u^{n+1}) and a second one (u^n) containing the approximation of the previous time step. We use `u_h` to store the former and construct a copy, `u_h_n`, to store the latter.

Code Listing 2.8: Copying a discrete function

```
u_h_n = u_h.copy(name="previous")
```

2.1.4 Schemes

In Dune-Fempy, we define schemes as the object containing the weak form of the PDE, its boundary conditions and the method used to approximate the inverse e.g. the iterative linear solver to use. Specifically, for an operator $L : V_h \to V_h^*$, schemes have two main methods.

1. Apply the operator. That is to calculate $w_h = L[v_h]$ given some $v_h \in V_h$.
2. Solve the PDE. That is to compute the solution u_h to $L[u_h] = v_h$ given some $v_h \in V_h^*$, by using a solve method.

Remark. In the case where only the operator application is required/possible (e.g. when $L : V \to W \neq V$, an `operator` object can be constructed instead of a scheme which comes without a solve method.

Recall the parabolic equation (2.5), which we will focus on in the following example. To begin with, it is necessary to define the variables that are used in the

equation.

Code Listing 2.9: Setting up UFL variables to be used

```
from ufl import TestFunction, TrialFunction
from dune.ufl import NamedConstant
u = TrialFunction(space)
v = TestFunction(space)
dt = NamedConstant(space, "dt")     # time step
t  = NamedConstant(space, "t")      # current time
```

The trial function u and the test function v are defined on the same `space` as before. Additionally Δt and t are defined as `NamedConstant`, which is simply a UFL `Constant` variable that can be given a name so it can be more easily modified later on.

Now for the equation (2.5) itself, let us prescribe the following value for K.

$$K(\nabla u) = \frac{2}{1+\sqrt{1+4|\nabla u|}}. \tag{2.6}$$

This results in an implementation of the following form.

Code Listing 2.10: Implementing the weak form

```
from ufl import dx, grad, div, inner, sqrt
abs_du = lambda u: sqrt(inner(grad(u), grad(u)))
K = lambda u: 2/(1 + sqrt(1 + 4*abs_du(u)))
a = ( inner((u - u_h_n)/dt, v) \
    + 0.5*inner(K(u)*grad(u), grad(v)) \
    + 0.5*inner(K(u_h_n)*grad(u_h_n), grad(v)) ) * dx
```

For the exact solution we will use the following (which is consistent with the initial data)

$$u(x,t) = e^{-2t}\left(\frac{1}{2}(x_0^2+x_1^2) - \frac{1}{3}(x_0^3-x_1^3)\right) + 1 \tag{2.7}$$

We can use `initial` to define this using some algebra, and we write a lambda function that takes `t` as argument.

Code Listing 2.11: The exact solution

```
from ufl import as_vector, exp
```

```
exact = lambda t: as_vector([exp(-2*t)*(initial - 1) + 1])
```

To set the right hand side of the equation, i.e. f, we put the exact solution into the strong form of the equation (i.e. $u_t - \nabla \cdot (K(\nabla u) \cdot \nabla u)$. We also add in Neumann boundary conditions by substituting the exact solution into the boundary term (obtained after differentiation by parts).

Code Listing 2.12: Setting up the right hand side

```
from ufl import dot, FacetNormal, ds
n = FacetNormal(space)
b = inner(-2*exp(-2*t)*(initial - 1) \
    - div(K(exact(t))*grad(exact(t)[0])), v[0]) * dx \
    + K(exact(t))*dot(grad(exact(t)[0]), n) * v[0] * ds
```

Finally, having defined the weak form and right hand side, we can now set up a scheme object which we can use to solve the PDE.

Code Listing 2.13: Creating an H^1 scheme

```
scheme = create.scheme("galerkin", a == b, solver='cg')
```

The above function creates a simple Galerkin method for H^1 conforming elements, with the space and equation passed in. We note that DUNE automatically solves nonlinear PDEs using Newton's method so it is sufficient to simply pass in the weak form as shown. As before we also note there exist other such premade DUNE schemes for different problems (see D.4)

Additionally the linear solver for the method can be specified, so for this instance we use `'cg'` for a conjugate gradient method, since the PDE is symmetric and positive definite.

Lastly we note that it is possible to explicitly define a model object to hold the method, and we investigate the different ways of doing this in section 2.3.

2.1.5 Solving

The last natural part of a FEM is the solving, which includes time loops, mesh refinements, data output, plotting, and so on. Let us begin by setting up the time

step, $\Delta t = 0.001$, by assigning it in the model (using the name given to the coefficient previously).

Code Listing 2.14: Setting up time variables before the loop

```
scheme.model.dt = 0.001
```

Next we write the following method for solving the problem over the time range. Since the problem is time-dependent, we solve over a for loop with $t_0 = 0$ and $t_N = 1$, using `u_h_n` for the old solution and `u_h` for the new one.

Code Listing 2.15: Evolve method for solving in time

```
def evolve(scheme, u_h, u_h_n):
    time = 0
    endTime = 1.0
    while time < (endTime - 1e-6):
        scheme.model.t = time + 0.5*scheme.model.dt
        u_h_n.assign(u_h)
        scheme.solve(target=u_h)
        time += scheme.model.dt
```

Lastly we want to have a way of computing the error. Say for instance we want to look at the L^2 and H^1 errors for our computed solution. For the error we will consider the difference between an exact solution u at the final time of the simulation and our computed solution, as follows.

$$L^2 \text{ error} = \left(\int_\Omega |u - u_h|^2 \, \mathrm{d}x \right)^{1/2}, \qquad H^1 \text{ error} = \left(\int_\Omega |\nabla(u - u_h)|^2 \, \mathrm{d}x \right)^{1/2}. \quad (2.8)$$

We can calculate the squared norm with the following code.

Code Listing 2.16: Writing expressions for the error computed at the final time

```
exact_end = exact(1)
l2error_fn = inner(u_h - exact_end, u_h - exact_end)
h1error_fn = inner(grad(u_h - exact_end), grad(u_h - exact_end))
```

First of all we define the exact solution (`exact_end`) at the end time $T = 1$. Then we simply write expressions in UFL to calculate the L^2 and H^1 errors. We

note that this works even though `u_h` is a discrete function and not a UFL term itself, since the expression is extracted from it automatically.

We also want to compute the estimated order of convergence (EOC), to test our method.

$$EOC = \frac{\log(e_{new}/e_{old})}{\log(h_{new}/h_{old})}.$$

This is calculated by refining the grid and comparing the errors (e_{old} and e_{new}) to the grid sizes (h_{old} and h_{new}), where the errors are computed using the error function `l2error_fn` from 2.16. In particular for a grid size that is being halved at each step, we do the following after each solve step.

Code Listing 2.17: Calculating the EOCs

```
error_old = error                                  # store old error
error = sqrt(integrate(grid, l2error_fn, 5)[0]) # integrate
eoc = log(error/error_old)/log(0.5)                # do the EOC calc
grid.hierarchicalGrid.globalRefine(1)              # refine the grid
```

Combining these concepts into one solve method in DUNE-FEMPY, we have the following program (with resulting figure 2.4).

Code Listing 2.18: Solving the Forchheimer equation in time and refining the grid

```
from math import log
error = 0
for eocLoop in range(3):
    print('# step:', eocLoop, ', size:', grid.size(0))
    u_h.interpolate(initial)
    evolve(scheme, u_h, u_h_n)
    error_old = error
    error = sqrt( integrate(grid, l2error_fn, 5)[0] )
    if eocLoop == 0:
        eoc = '-'
    else:
        eoc = log(error/error_old)/log(0.5)
    print('|u_h - u| =', error, ', eoc =', eoc)
    plot(u_h)
    grid.writeVTK('forchheimer', pointdata={'u': u_h, 'l2error':
```

```
                    l2error_fn, 'h1error': h1error_fn},
                        number=eocLoop)
    grid.hierarchicalGrid.globalRefine(1)
    scheme.model.dt /= 2
```

Output

```
# step: 0 , size: 16
|u_h - u| = 2.9194982026064784e-05 , eoc = -
# step: 1 , size: 64
|u_h - u| = 3.6106320903708674e-06 , eoc = 3.0153970951632156
# step: 2 , size: 256
|u_h - u| = 4.5004939236970754e-07 , eoc = 3.0040961733992497
```

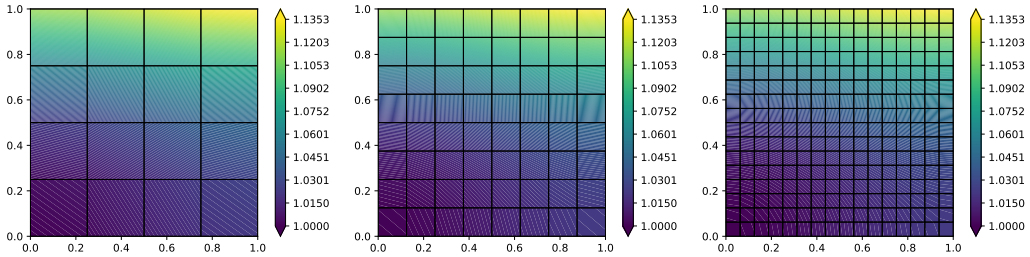

Figure 2.4: Plot of solutions at each level of refinement

We compile a table of the errors and EOCs for additional refinement steps and also including the H^1 error below.

Elements	$\|u - u_h\|_{L^2}$	EOC	$\|u - u_h\|_{H^1}$	EOC
16	2.919e-05	-	8.917e-04	-
64	3.611e-06	3.015	2.223e-04	2.000
256	4.500e-07	3.004	5.573e-05	2.000
1024	5.621e-08	3.001	1.393e-05	2.000
4096	7.031e-09	2.999	3.483e-06	2.000

2.2 Alternate Solve Methods

We carry on our explanation of different DUNE-FEMPY features by looking at the different methods of solving the PDE, which is facilitated by the different storage

back ends for spaces. DUNE-FEM allows one to store DoF vectors and matrices directly based on the data structures from different linear algebra packages.

We can specify alternate storage types as follows.

Code Listing 2.19: Accessing different storage types

```
space = create.space('lagrange', grid, dimrange=1, order=2,
    storage='istl')
```

As before we construct the space, but now with the additional argument that specifies the usage of DUNE-ISTL (see Blatt and Bastian [2006]) as a linear algebra backend. By default we use a very simple storage structure directly provided in DUNE-FEM, consequently not requiring any additional packages. A number of simple Krylov type solvers are available. Changing the `storage` argument in the construction of the space makes it possible to use more sophisticated solvers (e.g., better preconditioners or direct solvers). Available possibilities are shown in appendix D.3.

In particular one thing that we can do with certain storage methods is integrate methods from SciPy (Jones et al. [2001–]) into our code. This allows for more complex ways of writing numerical methods without the need to explicitly write it on the C++ side. Additionally we will show that it is possible to store the degrees of freedom in such a way that they can be treated as vectors from the NumPy package (Oliphant [2006]) and an assembled system matrix can be stored in a SciPy sparse matrix.

We present these methods once again via the Forchheimer example from section 2.1.

In the following we implement a simple Newton solver: given an initial guess u^0 (here taken to be zero) solve for $n \geq 0$,

$$u^{n+1} = u^n - DS(u^n)(S(u^n) - g),$$

where g is a discrete function containing the Dirichlet boundary conditions if they exist.

Usually this would be automatically taken care of in DUNE-FEMPY by

`scheme.solve`, however this time we will use the call operator on the `scheme` to compute $S(u^n)$ as well as `scheme.assemble` to get a copy of the system matrix in form of a SciPy sparse row matrix. Note that this method is not available for all storage types. We present this alternative below, and plot the result in figure 2.5.

Code Listing 2.20: Creating a class to hold a different solve method

```
import numpy as np
from scipy.sparse.linalg import spsolve
class Scheme:
  def __init__(self, scheme):
      self.model = scheme.model

  def solve(self, target=None):
      # create a copy of target for the residual
      res = target.copy(name="residual")

      # create numpy vectors to store target and res
      sol_coeff = target.as_numpy
      res_coeff = res.as_numpy

      n = 0
      while True:
          scheme(target, res)
          absF = math.sqrt( np.dot(res_coeff,res_coeff) )
          if absF < 1e-10:
              break
          matrix = scheme.assemble(target).as_numpy
          sol_coeff -= spsolve(matrix, res_coeff)
          n += 1

scheme_cls = Scheme(scheme)

grid.hierarchicalGrid.globalRefine(-2)  # revert grid refinement
u_h.interpolate(initial)                # reset u_h to initial
scheme.model.dt = 0.05                  # reset time step
evolve(scheme_cls, u_h, u_h_n)
plot(u_h)
```

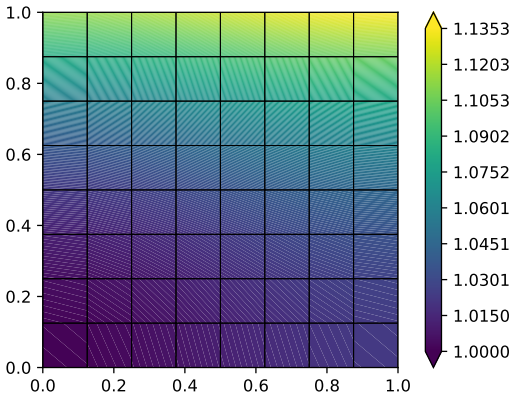

Figure 2.5: Plot of solution for Python-side Newton scheme

We can redo the above computation using a Newton-Krylov solver from SciPy. We do this by constructing a class `Df` containing the derivative of the operator. This would normally be done within DUNE, but here we do it purely through Python, giving figure 2.6 which is identical to before.

Code Listing 2.21: Implementing a Newton-Krylov solver with SciPy

```
from scipy.optimize import newton_krylov
from scipy.sparse.linalg import LinearOperator

def f(x_coeff):
    res = u_h.copy(name="residual")
    res_coeff = res.as_numpy
    x = space.numpyFunction(x_coeff, "tmp")
    scheme(x, res)
    return res_coeff

# class for the derivative DS of S
class Df(LinearOperator):
    def __init__(self, x_coeff):
        self.shape = (x_coeff.shape[0], x_coeff.shape[0])
        self.dtype = x_coeff.dtype
        # the following converts a given numpy array
        # into a discrete function over the given space
```

```
        x = space.numpyFunction(x_coeff, "tmp")
        # store the assembled matrix
        self.jac = scheme.assemble(x).as_numpy
    # reassemble the matrix DF(u) given a DoF vector for u
    def update(self, x_coeff, f):
        x = space.numpyFunction(x_coeff, "tmp")
        # Note: the following does produce a copy of the matrix
        # and each call here will reproduce the full matrix
        # structure - no reuse possible in this version
        self.jac = scheme.assemble(x).as_numpy
    # compute DS(u)^{-1}x for a given DoF vector x
    def _matvec(self, x_coeff):
        return spsolve(self.jac, x_coeff)

class Scheme2:
    def __init__(self, scheme):
        self.scheme = scheme
        self.model = scheme.model
    def solve(self, target=None):
        sol_coeff = target.as_numpy
        # call the newton krylov solver from scipy
        sol_coeff[:] = newton_krylov(f, sol_coeff,
                    verbose=0, f_tol=1e-8,
                    inner_M=Df(sol_coeff))

scheme2_cls = Scheme2(scheme)
u_h.interpolate(initial)
evolve(scheme2_cls, u_h, u_h_n)
plot(u_h)
```

We can also solvers from the PETSc package (see Balay et al. [2018]) to solve the problem. This can be done either through bindings available in DUNE-FEM or through the `petsc4py` package (Dalcin et al. [2011]).[1]

The first step is to change the storage in the space. This also requires setting

[1]For this to work, one must make sure that DUNE has been configured using the same version of PETSc used for `petsc4py`.

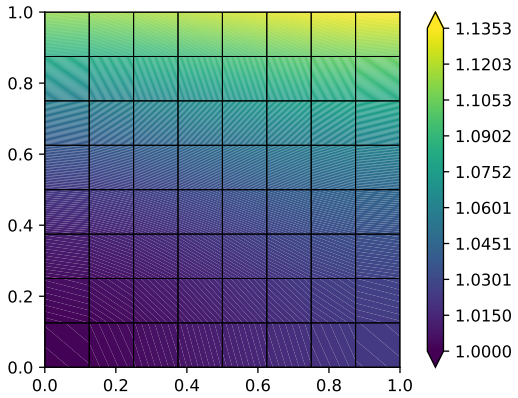

Figure 2.6: Plot of solution with Df operator

up the scheme and discrete functions again to use the new storage structure.

We can directly use the PETSc solvers by invoking `solve` on the scheme as before. Note that to do this we must change the storage type by creating a new `space`. Then we have the following code, with the same results found once again in figure 2.7.

Code Listing 2.22: Using petsc4py to solve using PETSc

```
space = create.space("lagrange", grid, dimrange=1, order=2,
    storage='petsc')
scheme = create.scheme("galerkin", a == b, space=space,
                       parameters={"petsc.preconditioning.method":"sor"})
# first we will use the petsc solver available in the dune-fem
    package (using the sor preconditioner)
u_h = space.interpolate(initial, name='u_h')
u_h_n = u_h.copy(name="previous")
scheme.model.dt = 0.05
evolve(scheme, u_h, u_h_n)
plot(u_h)
```

Next we will implement the Newton loop in Python using `petsc4py` to solve the linear systems. We can access the PETSc vectors by calling `as_petsc` on the discrete function. Note that this property will only be available if the discrete function is an element of a space with storage `'petsc'`. The method `assemble` on the scheme now returns the sparse PETSc matrix and so we can directly use the

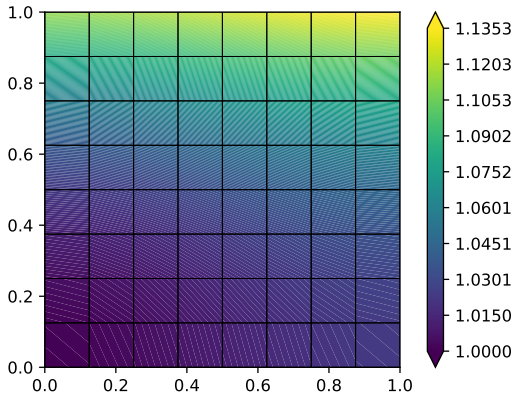

Figure 2.7: Plot of solution using PETSc

KSP class from `petsc4py`.

Code Listing 2.23: Using petsc4py and its Krylov solvers to define a Newton scheme and solve

```
import petsc4py, sys
petsc4py.init(sys.argv)
from petsc4py import PETSc
ksp = PETSc.KSP()
ksp.create(PETSc.COMM_WORLD)
# use conjugate gradients method
ksp.setType("cg")
# and incomplete Cholesky
ksp.getPC().setType("icc")

class Scheme3:
  def __init__(self, scheme):
      self.model = scheme.model
  def solve(self, target=None):
      res = target.copy(name="residual")
      sol_coeff = target.as_petsc
      res_coeff = res.as_petsc
      n = 0
      while True:
          scheme(target, res)
          absF = math.sqrt( res_coeff.dot(res_coeff) )
```

```
            if absF < 1e-10:
                break
            matrix = scheme.assemble(target).as_petsc
            ksp.setOperators(matrix)
            ksp.setFromOptions()
            ksp.solve(res_coeff, res_coeff)
            sol_coeff -= res_coeff
            n += 1

u_h.interpolate(initial)
scheme3_cls = Scheme3(scheme)
evolve(scheme3_cls, u_h, u_h_n)
plot(u_h)
```

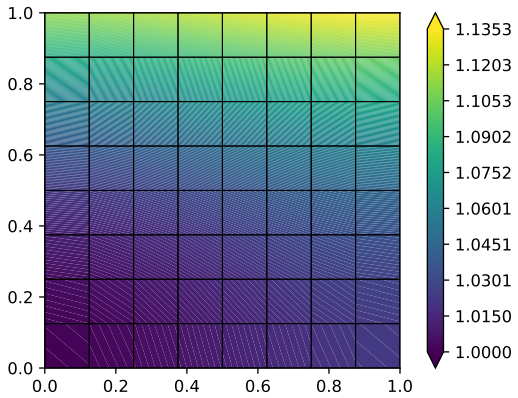

Figure 2.8: Plot of solution using PETSc and a Krylov method

Finally we we will use PETSc's nonlinear solvers (the `snes` classes) directly.

Code Listing 2.24: Using petsc4py and their nonlinear solvers (SNES) directly

```
def f(snes, X, F):
    inDF = space.petscFunction(X)
    outDF = space.petscFunction(F)
    scheme(inDF,outDF)
def Df(snes, x, m, b):
    inDF = space.petscFunction(x)
    matrix = scheme.assemble(inDF).as_petsc
    m.createAIJ(matrix.size, csr=matrix.getValuesCSR())
    b.createAIJ(matrix.size, csr=matrix.getValuesCSR())
```

```
    return PETSc.Mat.Structure.SAME_NONZERO_PATTERN

class Scheme4:
    def __init__(self, scheme):
        self.scheme = scheme
        self.model = scheme.model

    def solve(self, target=None):
        res = target.copy(name="residual")
        sol_coeff = target.as_petsc
        res_coeff = res.as_petsc

        snes = PETSc.SNES().create()
        snes.setMonitor(lambda snes, i, r:print())
        snes.setFunction(f, res_coeff)
        matrix = self.scheme.assemble(target).as_petsc
        snes.setJacobian(Df, matrix, matrix)
        snes.getKSP().setType("cg")
        snes.setFromOptions()
        snes.solve(None, sol_coeff)

u_h.interpolate(initial)
scheme4_cls = Scheme4(scheme)
evolve(scheme4_cls, u_h, u_h_n)
plot(u_h)
```

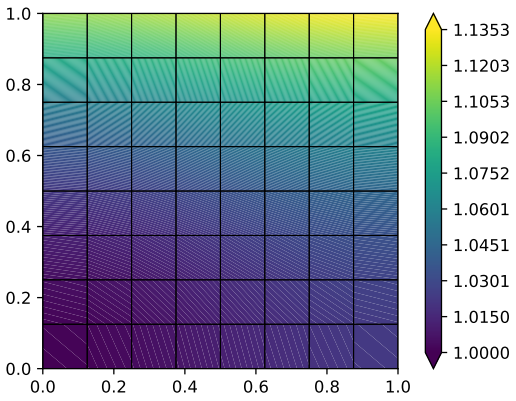

Figure 2.9: Plot of solution using SNES

Remark. The methods `as_numpy` and `as_petsc` (returning the DoF vector either as a `numpy` or a `petsc` vector) do not lead to a copy of the data and the same is true for the `function` objects returned by the `function` method on the discrete space. In the `numpy` case we can use Python's buffer protocol to use the same underlying storage. In the case of `petsc` the underlying `Vec` can be shared. In the case of matrices the situation is not yet as clear; `scheme.assemble` returns a copy of the data in the SciPy case while the `Mat` structure is shared between C++ and Python in the `petsc` case. But at the time of writing it is not possible to pass in the `Mat` structure to the `scheme.assemble` method from the outside. That is why it is necessary to copy the data when using the `snes` nonlinear solver as seen above.

2.3 Model Generation

After having looked at the basics of the Python interface, let us now consider features more aimed at C++ integration and code extensibility.

We briefly alluded to a way of creating a model independent of a scheme in section 2.1.4, so let us expand upon this idea here. We can separate the process into two steps as follows.

Code Listing 2.25: A simple elliptic model

```
1 model = create.model('elliptic', grid, a == b)
2 scheme = create.scheme("galerkin", model)
```

where `a == b` refers to the UFL expression used to represent the weak form, and `'elliptic'` refers to the elliptic operator class in DUNE. The purpose of this class is to have a set list of virtualized methods that represent the standard structure of what we consider is necessary for an elliptic PDE model. This is then implemented in DUNE-FEMPY by translating the UFL input into a DUNE class compatible format.

We note that this is a different approach to similar packages, like Fenics Alnæs et al. [2015] and Firedrake Rathgeber et al. [2017], which in general do not create a virtual class and instead use the UFL form directly. In fact such an approach is also available in DUNE-FEMPY, using the `'integrands'` identifier. The choice

between `'elliptic'` and `'integrands'` models each lead to separate advantages and disadvantages, which is what we would like to discuss in this section.

2.3.1 Elliptic Models

First let us consider the elliptic model. Summarized briefly, the elliptic model is the version of model generation in DUNE-FEMPY that follows as closely as possible the structure used in DUNE-FEM. In mathematical terms, consider the same general operator we defined previously.

$$L[u] = -\nabla \cdot D(x, u, \nabla u)\nabla u + m(x, u, \nabla u). \tag{2.2}$$

In variational form, after multiplying with a test function and integration by parts (ignoring boundary terms for now), we arrive at

$$\langle L[u], v\rangle = \int_\Omega D(x, u, \nabla u)\nabla u \cdot \nabla v + m(x, u, \nabla u)v \,\mathrm{d}x.$$

Now the elliptic model class in DUNE-FEMPY has methods that represent the above form in general terms. Suppose for instance we were to take the case of $m(x, u, \nabla u) = u$ above. In the model class, this would be defined under the method `source`.

Code Listing 2.26: A function in the elliptic model C++ class

```
1 template< class Point >
2 void source ( const Point &x, const RangeType &u, const
      JacobianRangeType &du, RangeType &result ) const
3 ]
4   result[ 0 ] = u[ 0 ];
5 }
```

A similar method exists for $D(x, u)$, as well as linearised versions for the purposes of nonlinear methods. Additionally there are methods for the associated Dirichlet or Neumann boundary conditions. Together these form the elliptic model class which is one way of expressing weak forms in DUNE-FEMPY. Generally this class is then

used to create a shared object file that is exported to Python using pybind11 for use in Python scripts and notebooks.

Another possibility provided for by the modular design of DUNE-PYTHON and the elliptic class structure is the ability to extend the model to more complex cases. This approach involves the writing of additional C++ classes (one example would be an elliptic discontinuous Galerkin model) based on the elliptic model class except with extra modifications that one might want to make to the underlying structure. Whilst this approach is more in-depth than simply editing a few lines in the model file, it allows one to change the functions themselves beyond what the default elliptic model accepts.

An example of this approach is the *nonvariational* model for the DUNE-FEMNV module (see chapter 3). This comes from the desire to write weak forms that can accept a Hessian as as argument as follows.

$$L[u] = -\nabla \cdot D(x, u, \nabla u)\nabla u(x) + m(x, u, \nabla u, D^2 u).$$

Such a change would require different arguments to be made available to the methods from the elliptic model. Suppose we wanted to implement the nonvariational Poisson equation, i.e. taking $m = -\Delta u$ above. Then we would need the following method.

Code Listing 2.27: A nonvariational method

```
1 template< class Point >
2 void source ( const Point &x, const RangeType &u, const
3 JacobianRangeType &du, const HessianRangeType &d2u, RangeType
     &result ) const
4 {
5   result[ 0 ] = d2u[ 0 ][ 0 ] + d2u[ 1 ][ 1 ];
6 }
```

Whilst this may not be immediately possible with the standard elliptic model, it is possible to create a model `'nvdg'` that can use such functions, which results in the ability to write functional DUNE-FEMPY code as follows.

Code Listing 2.28: The DUNE-FEMPY code for a nonvariational model

```
a = -(grad(grad(u[0])[0])[0] + grad(grad(u[0])[1])[1])*v[0]*dx
b = rhs(A, exact)
model = create.model("nvdg", grid, a == b)
```

Thus it becomes possible to write schemes that expect different arguments from the operator.

2.3.2 Integrands Models

We note however that as mentioned before, there exists another way of constructing operators, by using `'integrands'`. This method bypasses the virtual methods used in the elliptic operator class and creates methods purely using the UFL expressions given to it. This again allows for expressions that are not by default allowed in the default elliptic class, as shown below.

Code Listing 2.29: Usage of integrands operators for skeleton terms

```
a = -(grad(grad(u[0])[0])[0] + grad(grad(u[0])[1])[1])*v[0]*dx
    + jump(A*grad(u[0]), n)*avg(v[0])*dS
b = rhs(A, exact)
scheme = create.model("integrands", space, a == b)
```

Here we take the nonvariational equation from before and add a term defined only on the skeleton (the edges) of the mesh. Due to the ability to add such interior terms, the `'integrands'` class is particularly useful for discontinuous Galerkin methods.

In summary, we state that the `'integrands'` model is the most versatile version of model generation for most ordinary cases (it is also more efficiently implemented due to its recency); however the elliptic model lends itself better to code extension possibilities.

2.3.3 C++ Models

In addition to the automatic creation of a shared library object that is done when `create` is called, it is possible to generate a model class separately as a header file. That is, it is possible to generate a C++ file (e.g. `'model.hh'`) that can be used

flexibly in both DUNE-FEMPY and regular C++ compatible DUNE code. We can do this by writing a pure UFL file and calling cmake on it.

Let us examine what this file looks like for the Forchheimer model.

Code Listing 2.30: UFL file used for C++ header file generation

```
space = Space(2, 1)
u = TrialFunction(space)
v = TestFunction(space)
x = SpatialCoordinate(space.cell())
dt = NamedConstant(triangle, "dt")     # time step
t  = NamedConstant(triangle, "t")      # current time
n = FacetNormal(space)
u_h_n = NamedCoefficient(space,"previous")

from ufl import as_vector, exp
exact = lambda t: as_vector([exp(-2*t)*(initial - 1) + 1])

initial = 1/2*(x[0]**2 + x[1]**2) - 1/3*(x[0]**3 - x[1]**3) + 1
abs_du = lambda u: sqrt(inner(grad(u), grad(u)))
K = lambda u: 2/(1 + sqrt(1 + 4*abs_du(u)))
a = ( inner((u - u_h_n)/dt, v) \
    + 0.5*inner(K(u)*grad(u), grad(v)) \
    + 0.5*inner(K(u_h_n)*grad(u_h_n), grad(v)) ) * dx
b = inner(-2*exp(-2*t)*(initial - 1) \
    - div(K(exact(t))*grad(exact(t)[0])), v[0]) * dx \
    + K(exact(t))*dot(grad(exact(t)[0]), n) * v[0] * ds

F = a - b
```

Once the corresponding `forchheimer.hh` file has been generated, it can then be edited manually in C++, and then used in place of a UFL expression in DUNE-FEMPY. This choice of default shared library generation or usable header files falls in line with attempts we have made to improve extensibility of the code, since in particular it allows for the user to write in more complex features in C++ that do not necessarily have Python bindings written for them.

One natural question that arises is that of the efficiency between using the

full Dune-Fempy interface to run problems and simply using it to just generate a model file to be used in C++. To look at this problem we constructed an identical Forchheimer example in C++ which can be found in appendix C. We compare the runtime of the two solve-steps below.

Table 2.1: Runtimes for Forchheimer solve time

Elements	Time step (Δt)	Python runtime (s)	C++ runtime (s)
256	6.25e-4	13.7	33.0
1024	3.125e-4	109.3	101.9
4096	1.5625e-4	890.0	864.3

Thus we see there is not a sizable difference between the Dune-Fem and Dune-Fempy versions (and to begin with the Python version even appears to be faster).

Remark. We remark that both versions use preprocessing, since in use-cases such as long-running simulations, this extra time is negligible. We also note that the most *costly* aspect of pure Python code are generally callbacks, and in this example this amounts to just the solve call. An additional example that taxes the two versions differently can be found in section 2.7.

2.4 Adaptive Mesh Refinement

We shall now consider the implementation of adaptive mesh refinement in Dune-Fempy. Adaptive mesh refinement is a technique that allows for the targeted refinement of the computational domain in specific areas where there is greater turbulence or activity, for greater precision. In problems where uniform refinement of a mesh is not required, this allows for more precision of the results at less computational cost.

The method considered here uses so-called h-adaptivity that adds additional mesh points to the grid at areas of small scale activity. It does so based on a marking procedure that evaluates the gradient of the solution at each element and determines whether to refine the grid based on a level of tolerance.

In this section we present two examples which use adaptive grid refinement

in slightly different ways.

2.4.1 Re-entrant Corner Problem

Here we will consider the classic *re-entrant corner* problem,

$$\begin{aligned} -\Delta u &= f, && \text{in } \Omega, \\ u &= g, && \text{on } \partial\Omega, \end{aligned}$$

where the domain is given using polar coordinates,

$$\Omega = \{(r, \varphi) \colon r \in (0, 1), \varphi \in (0, \Phi)\} \ .$$

For the boundary condition g, we set it to the trace of the function u, given by

$$u(r, \varphi) = r^{\frac{\pi}{\Phi}} \sin\left(\frac{\pi}{\Phi}\varphi\right)$$

Now we start by importing some necessary modules.

```
1 import math
2 import numpy
3 import dune.create as create
4 import matplotlib.pyplot as pyplot
5 from dune.fem.view import adaptiveLeafGridView
6 from dune.fem.plotting import plotPointData as plot
7 import dune.grid as grid
8 import dune.fem as fem
```

We set the angle for the corner Φ, (where $0 < \Phi <= 2\pi$), and the order for the space.

```
1 Phi = 16/9*math.pi
2 order = 2
```

We now define the grid for this domain, which has its vertices at the origin and 7 equally spaced points on the unit sphere, starting with $(1, 0)$ and ending at $(cos(\Phi), sin(\Phi))$. We also define the interior triangles using these numbered vertices.

```
vertices = numpy.zeros((8, 2))
vertices[0] = [0, 0]
for i in range(0, 7):
    vertices[i+1] = [math.cos(Phi/6*i),
                     math.sin(Phi/6*i)]
triangles = numpy.array([[2,1,0], [0,3,2], [4,3,0],
                         [0,5,4], [6,5,0], [0,7,6]])
domain = {"vertices": vertices, "simplices": triangles}
view = create.view("adaptive", "ALUConform", domain, dimgrid=2)
view.hierarchicalGrid.globalRefine(2)
space  = create.space("lagrange", view, dimrange=1, order=order)
```

Next we define the model. We obtain ϕ from the x and y coordinates, define the exact solution $u(r, \phi)$ and the weak form $\int_\Omega \nabla u \cdot \nabla v \, \mathrm{d}x = 0$.

```
from ufl import *
from dune.ufl import DirichletBC
u = TrialFunction(space)
v = TestFunction(space)
x = SpatialCoordinate(space.cell())

phi = atan_2(x[1], x[0]) + conditional(x[1] < 0, 2*pi, 0)
# define the exact solution u(r, phi)
exact = as_vector([inner(x, x)**(pi/2/Phi) * sin(pi/Phi * phi)])
# define the bilinear form
a = inner(grad(u), grad(v)) * dx

# set up the scheme
laplace = create.scheme("galerkin", [a==0,
                        DirichletBC(space, exact, 1)])
uh = space.interpolate(lambda x: [0], name="solution")
```

For the following we use the well-known a-posteriori error estimate (see e.g. [Verfürth, 1994, |p71])

$$\int_\Omega |\nabla(u - u_h)|^2 \leq C \sum_K \eta_K^2,$$

where on each element K of the grid the local estimator is given by

$$\eta_K^2 = h_K^2 \int_K |\Delta u_h|^2 \, \mathrm{d}x + \frac{1}{2} \sum_{S \subset \partial K} h_S \int_S [\nabla u_h]^2 \, \mathrm{d}s.$$

Here $[\cdot]$ is the jump in the normal direction over the edges of the grid, $h_K = \max_{x,y \in K} |x - y|$ and h_S is the length of side S.

We compute the elementwise indicator by defining a weak form

$$\eta(u, v) = h_K^2 \int_K |\Delta u_h|^2 v \, \mathrm{d}x + \sum_{S \subset \partial K} h_S \int_S [\nabla u_h]^2 \{v\} \, \mathrm{d}s,$$

where $\{\cdot\}$ is the average over the cell edges. This weak form can be easily written in UFL and by using it to define a discrete operator L from the second order Lagrange space into a space containing piecewise constant functions we have $L[u_h]|_K = \eta_K$.

```
# energy error
h1_error = inner(grad(uh - exact), grad(uh - exact))

# define a FV space to do the error estimation
fvspace = create.space("finitevolume", view,
                       dimrange=1, storage="istl")

# define hK, hS, n and the elementwise estimator
hK = MaxCellEdgeLength(space.cell())
hS = MaxFacetEdgeLength(space.cell())('+')
n = FacetNormal(space.cell())
estimator_ufl = hK**2 * (div(grad(u[0])))**2 * v[0] * dx + hS * \
                inner(jump(grad(u[0])), n('+'))**2 * avg(v[0]) * dS
# we define an operator that takes uh and applies the above formula
estimator = create.operator("galerkin", estimator_ufl == 0,
                            space, fvspace)
```

Lastly let us set up a marking function for the grid adaptivity. The function `mark` (that gets directly passed into the grid), estimates the error locally, compares it to the tolerance, and refines the grid if necessary.

```
tolerance = 0.1
```

```
gridSize = view.size(0)
estimate = fvspace.interpolate([0], name="estimate")
def mark(element):
    estLocal = estimate(element, element.geometry.
                        referenceElement.center)
    return grid.Marker.refine if estLocal[0] \
            > tolerance / gridSize else grid.Marker.keep
```

Let us solve over a time loop and plot the solutions side by side.

```
# adaptive loop (solve, mark, estimate)
fig = pyplot.figure(figsize=(10,10))
count = 0
while count < 20:
    laplace.solve(target=uh)
    if count%3 == 0:
        pyplot.show()
        pyplot.close('all')
        fig = pyplot.figure(figsize=(10,10))
    plot(uh, figure=(fig, 131+count%3), colorbar=False)
    # compute the actual error and the estimator
    error = math.sqrt(fem.function.integrate(view, h1_error, 5)[0])
    estimator(uh, estimate)
    eta = sum(estimate.dofVector)
    if eta < tolerance:
        break
    if tolerance == 0.:
        view.hierarchicalGrid.globalRefine(2)
        uh.interpolate([0])  # initial guess needed
    else:
        marked = view.hierarchicalGrid.mark(mark)
        fem.adapt(view.hierarchicalGrid, [uh])
        fem.loadBalance(view.hierarchicalGrid, [uh])
    gridSize = view.size(0)
    laplace.solve( target=uh )
    count += 1
pyplot.show()
pyplot.close('all')
```

```
<matplotlib.figure.Figure at 0x7f143f475630>
```

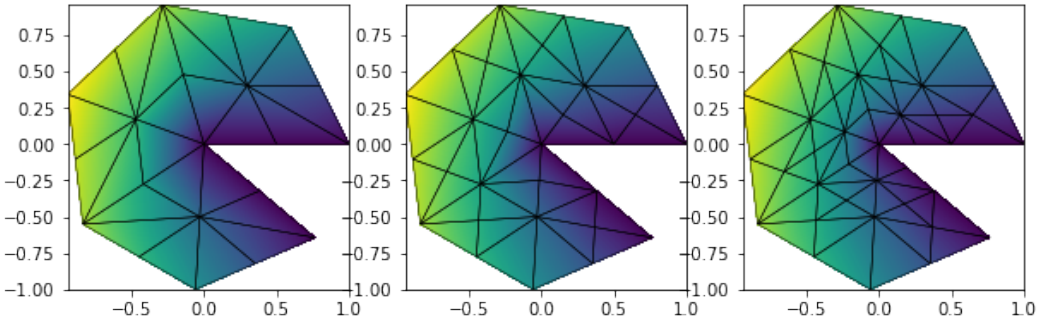

Figure 2.10: The first three plots of the solution

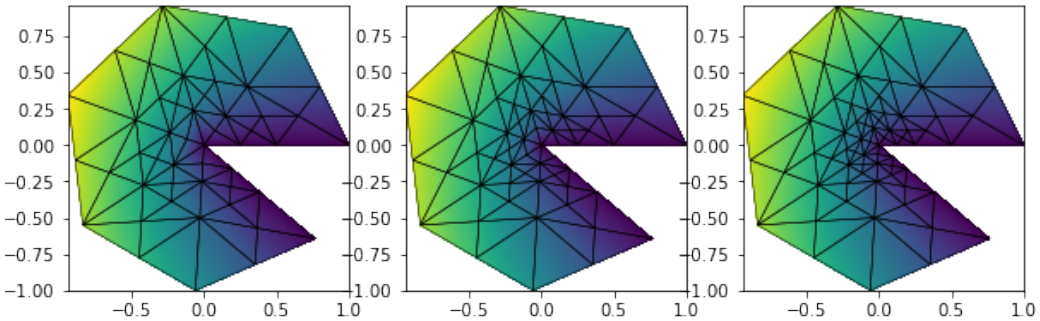

Figure 2.11: The second three plots of the solution

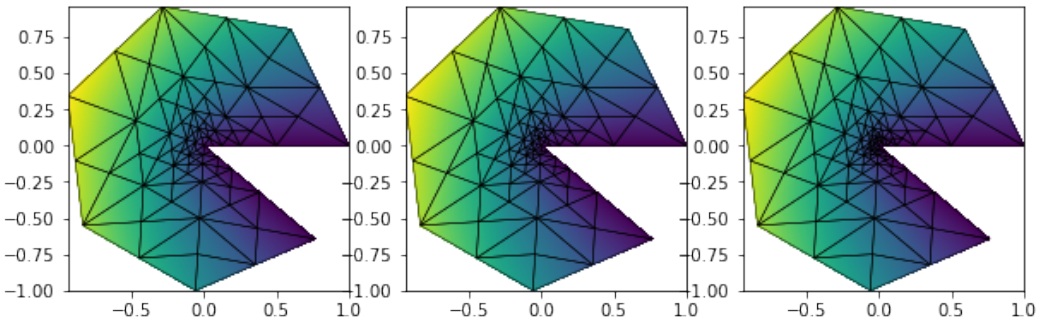

Figure 2.12: The final three plots of the solution

Let's have a look at the center of the domain:

```
fig = pyplot.figure(figsize=(15,15))
plot(uh, figure=(fig, 131), xlim=(-0.5, 0.5),
```

```
     ylim=(-0.5, 0.5), colorbar={"shrink": 0.25})
plot(uh, figure=(fig, 132), xlim=(-0.25, 0.25),
     ylim=(-0.25, 0.25),colorbar={"shrink": 0.25})
plot(uh, figure=(fig, 133), xlim=(-0.125, 0.125),
     ylim=(-0.125, 0.125),colorbar={"shrink": 0.25})
pyplot.show()
pyplot.close('all')
```

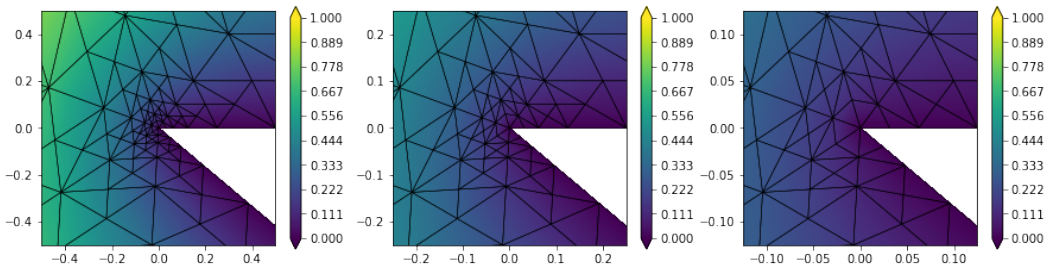

Figure 2.13: Zooming in on the re-entrant corner

Finally, let us have a look at the grid levels.

```
from dune.fem.function import levelFunction
plot(levelFunction(view), xlim=(-0.2,1), ylim=(-0.2,1))
```

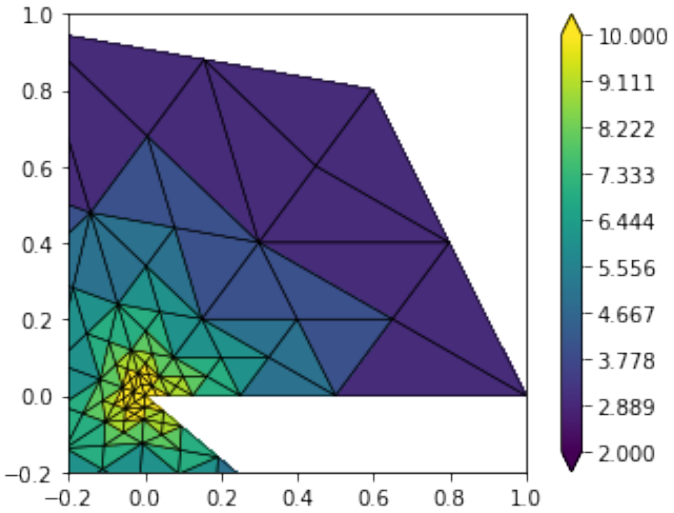

Figure 2.14: Plot of the level function of the grid

We shall now look at a model for crystallization on the surface of a liquid.

2.4.2 Crystal Growth

Here we demonstrate crystallisation on the surface of a liquid due to cooling from Guyer et al. [2009]. Before anything else let us set up the grid and the function space. We use the default DoF storage available in DUNE-FEM (this can be changed for example to `istl`, `eigen` or `petsc`).

```
import dune.fem as fem
from dune.grid import Marker, cartesianDomain
import dune.create as create
order = 1
dimDomain = 2      # we are solving this in 2D
dimRange = 2       # we have a system with two unknowns
domain = cartesianDomain([4, 4], [8, 8], [3, 3])
grid   = create.view("adaptive", grid="ALUConform",
                     constructor=domain, dimgrid=dimDomain)
space  = create.space("lagrange", grid, dimrange=dimRange,
                      order=order, storage="fem")
```

We want to solve the following system of equations of variables ϕ (phase field) and T (temperature field)

$$\sigma\frac{\partial\phi}{\partial t} = \nabla\cdot D(\phi)\nabla\phi + m(\phi,T),$$
$$\frac{\partial T}{\partial t} = 2.25\Delta T + \frac{\partial\phi}{\partial t},$$

where σ is a constant, $m(\phi,T)$ is given by

$$m(\phi,T) = \phi(1-\phi)(\phi - \frac{1}{2} - \frac{\kappa_1}{\pi}\arctan(\kappa_2 T)),$$

(here κ_1 and κ_2 are constants) and $D(\phi)$ is a matrix representing anisotropic diffusion given by

$$D(\phi) = \alpha^2(1+c\beta)\begin{pmatrix} 1+c\beta & -c\frac{\partial\beta}{\partial\psi} \\ c\frac{\partial\beta}{\partial\psi} & 1+c\beta \end{pmatrix},$$

and where $\beta = \frac{1-\Phi^2}{1+\Phi^2}$, $\Phi = \tan\left(\frac{N}{2}\psi\right)$, $\psi = \theta + \arctan\left(\frac{\partial\phi/\partial y}{\partial\phi/\partial x}\right)$ and α, c, θ and N are

constants.

Let us first set up the parameters for the problem.

```
alpha  = 0.015
sigma  = 3.e-4
kappa1 = 0.9
kappa2 = 20.
c      = 0.02
N      = 6.
```

As we will be discretising in time, we define the unknown data as $\mathbf{u}_n = (\phi_n, T_n)^T$, with given data (from the previous time step) as $\mathbf{u}_{n-1} = (\phi_{n-1}, T_{n-1})^T$ and test function as $\mathbf{v} = (v_0, v_1)^T$.

```
from ufl import TestFunction, TrialFunction, Constant
from dune.ufl import NamedConstant
u = TrialFunction(space)
v = TestFunction(space)
dt = NamedConstant(space, "dt")     # time step
```

We define the initial data and create a function from it. We use this value to set up our solution $\mathbf{u}_n$ and previous solution $\mathbf{u}_{n-1}$.

```
def initial(x):
    r  = (x - [6, 6]).two_norm
    return [ 0 if r > 0.3 else 1, -0.5 ]
initial_gf = create.function("global", grid, "initial",
                             order+1, initial)
u_h = space.interpolate(initial_gf, name="solution")
u_h_n = u_h.copy()     # previous solution
```

To obtain the numerical scheme, we begin by multiplying the first equation by v_0 and the second by v_1 and integrate by parts to obtain

$$\int \sigma \frac{\partial \phi}{\partial t} v_0 \, \mathrm{d}x = \int \left(-(D(\phi)\nabla\phi) \cdot \nabla v_0 + m(\phi, T) v_0\right) \, \mathrm{d}x,$$
$$\int \frac{\partial T}{\partial t} v_1 \, \mathrm{d}x = \int \left(-2.25 \nabla T \cdot \nabla v_1 + \frac{\partial \phi}{\partial t} v_1\right) \, \mathrm{d}x.$$

We then discretise the time derivatives via $\partial\phi/\partial t = (\phi_n - \phi_{n-1})/\Delta t$ and $\partial T/\partial t =$

$(T_n - T_{n-1})/\Delta t$. For the other terms we discretize implicitly (i.e. using ϕ_n and T_n), with the exception of $D(\phi_{n-1})$. This ultimately results in

$$\int (\phi_n - \phi_{n-1})v_0 \, \mathrm{d}x = \int \frac{\Delta t}{\sigma} \left(-(D(\phi_{n-1})\nabla\phi_n) \cdot \nabla v_0 + m(\phi_n, T_n)v_0\right) \, \mathrm{d}x,$$
$$\int (T_n - T_{n-1})v_1 \, \mathrm{d}x = \int \left(-2.25\nabla T_n \cdot \nabla v_1 + (\phi_n - \phi_{n-1})v_1\right) \, \mathrm{d}x.$$

To finally get the desired equation, we add both equations together and rewrite using vector notation.

$$\int \left(\frac{\Delta t}{\sigma}(D(\phi_{n-1})\nabla\phi_n) \cdot \nabla v_0 + \Delta t \; 2.25\nabla T_n \cdot \nabla v_1 + \mathbf{u}_n \cdot \mathbf{v} - \mathbf{s} \cdot \mathbf{v}\right) \mathrm{d}x$$
$$= \int (\mathbf{u}_{n-1} \cdot \mathbf{v} - \phi_{n-1}v_1) \, \mathrm{d}x,$$

where

$$\mathbf{s} = \left(\frac{\Delta t}{\sigma} m(\phi_n, T_n), \phi_n\right)^T.$$

Let us put this into code. First we put in the right hand side which only contains explicit data.

```
from ufl import inner, dx
a_ex = (inner(u_h_n, v) - inner(u_h_n[0], v[1])) * dx
```

For the left hand side we have the spatial derivatives and the implicit parts.

```
from ufl import pi, atan, atan_2, tan, grad, as_vector, inner, dot
psi         = pi/8.0 + atan_2(grad(u_h_n[0])[1], (grad(u_h_n[0])[0]))
Phi         = tan(N / 2.0 * psi)
beta        = (1.0 - Phi*Phi) / (1.0 + Phi*Phi)
dbeta_dPhi  = -2.0 * N * Phi / (1.0 + Phi*Phi)
fac         = 1.0 + c * beta
diag        = fac * fac
offdiag     = -fac * c * dbeta_dPhi
d0          = as_vector([diag, offdiag])
d1          = as_vector([-offdiag, diag])
m = u[0] * (1.0 - u[0]) * (u[0] - 0.5 - kappa1/pi*atan(kappa2*u[1]))
s = as_vector([dt / sigma * m, u[0]])
a_im = (alpha*alpha*dt / sigma * (inner(dot(d0, grad(u[0])),
```

```
        grad(v[0])[0]) + inner(dot(d1, grad(u[0])), grad(v[0])[1]))
        + 2.25 * dt * inner(grad(u[1]), grad(v[1]))
        + inner(u,v) - inner(s,v)) * dx
```

We set up the scheme with some parameters.

```
solverParameters = {
        "fem.solver.newton.tolerance": 1e-5,
        "fem.solver.newton.linabstol": 1e-8,
        "fem.solver.newton.linreduction": 1e-8,
        "fem.solver.newton.verbose": 0,
        "fem.solver.newton.linear.verbose": 0
    }
scheme = create.scheme("galerkin", a_im == a_ex, space,
                       solver="gmres", parameters=solverParameters)
```

We set up the adaptive method. We start with a marking strategy based on the value of the gradient of the phase field variable.

```
def mark(element):
    u_h_local = u_h.localFunction(element)
    grad = u_h_local.jacobian(element.geometry.
                              referenceElement.center)
    if grad[0].infinity_norm > 1.2:
        return Marker.refine if element.level < maxLevel \
                else Marker.keep
    else:
        return Marker.coarsen
```

We do the initial refinement of the grid.

```
maxLevel = 11
hgrid    = grid.hierarchicalGrid
hgrid.globalRefine(6)
for i in range(0, maxLevel):
    hgrid.mark(mark)
    fem.adapt(hgrid, [u_h])
    fem.loadBalance(hgrid, [u_h])
    u_h.interpolate(initial_gf)
```

Let us start by plotting the initial state of the material, which is just a small circle in the centre.

```
from dune.fem.plotting import plotComponents as plotComponents
import matplotlib.pyplot as pyplot
from dune.fem.function import levelFunction, partitionFunction
import matplotlib
vtk = grid.sequencedVTK("crystal", pointdata=[u_h],
       celldata=[levelFunction(grid), partitionFunction(grid)])

matplotlib.rcParams.update({'font.size': 10})
matplotlib.rcParams['figure.figsize'] = [10, 5]
plotComponents(u_h, cmap=pyplot.cm.rainbow, show=[0])
```

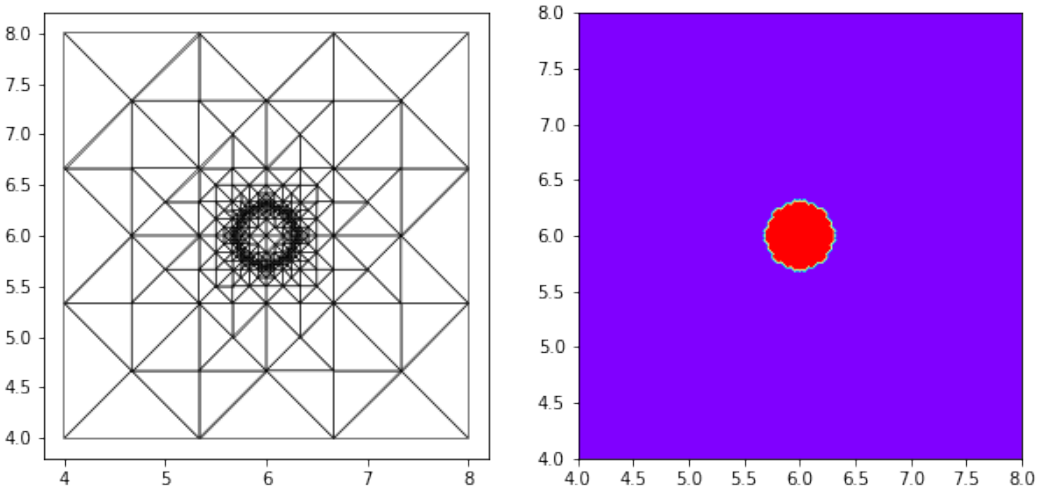

Figure 2.15: The initial adapted grid and phase field

We set `dt` and the initial time $t = 0$.

```
scheme.model.dt = 0.0005
t = 0.0
```

Finally we set up the time loop and solve the problem - each time this cell is run the simulation will progress to the given `endTime` and then the result is shown. The simulation can be progressed further by rerunning the cell while increasing the `endTime`.

```
endTime = 0.05
```

```
while t < endTime:
    u_h_n.assign(u_h)
    scheme.solve(target=u_h)
    print(t, grid.size(0), end="\r")
    t += scheme.model.dt
    hgrid.mark(mark)
    fem.adapt(hgrid, [u_h])
    fem.loadBalance(hgrid, [u_h])
print()
```

```
plotComponents(u_h, cmap=pyplot.cm.rainbow)
```

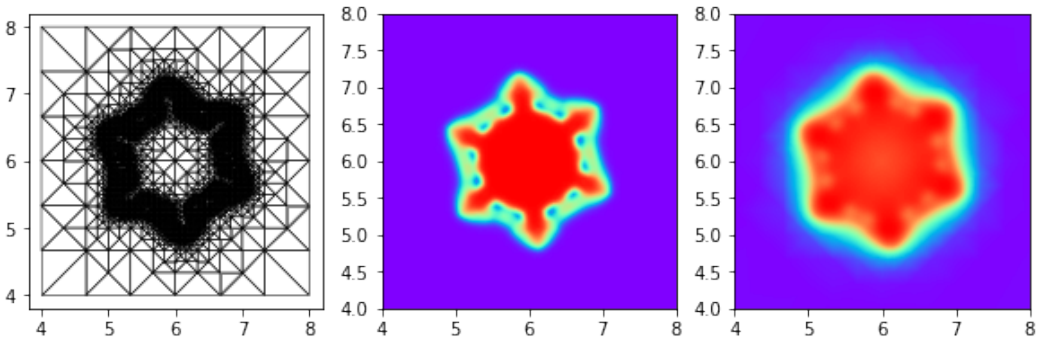

Figure 2.16: The grid, phase field and temperature after the final timestep

2.5 Moving Meshes

In this section we will consider an example where the grid itself changes over time subject to PDEs. Specifically we refer to a *geometric evolution equation*, which describes the motion of a hypersurface by prescribing its velocity geometrically. In DUNE-FEMPY, it is possible to accomplish this through the following process.

1. Create an interpolated function that describes the initial surface, i.e.

```
positions = space.interpolate(lambda x: some_function(x),
    name="position")
```

2. Create a surface from `positions` using this function

```
surface = create.view("geometry", positions)
```

3. Create the scheme that describes the surface evolution and solve it in the usual way.

4. Update the surface using the computed solution.

```
positions.dofVector.assign(solution.dofVector)
```

With this process the surface (and by extension the mesh) can be changed over time. We will now demonstrate this in a mean curvature flow example.

2.5.1 Mean Curvature Flow

Mean curvature flow is a specific example of a geometric evolution equation where the evolution is governed by the mean curvature H. One real-life example of this is in how soap films change over time, although it can also be applied to image processing (e.g. Malladi and Sethian [1996]). Assume we can define a reference surface Γ_0 such that we can write the evolving surface $\Gamma(t)$ in the form

$$\Gamma(t) = X(t, \Gamma_0).$$

Then we can say Γ moves by mean curvature if $X = X(t, x)$ satisfies for $x \in \Gamma_0$,

$$\frac{\partial}{\partial t} X = -H(X)\mathbf{n}(X), \tag{2.9}$$

where H is the mean curvature of $\Gamma(t)$ and $\mathbf{n}(X)$ is its outward pointing normal.

For the following we will use the *tangential gradient* operator (or surface gradient) defined by

$$\nabla_\Gamma u = \nabla u - (\nabla u \cdot \mathbf{n})\mathbf{n}.$$

We note that ∇_Γ is the orthogonal projection of ∇ onto the tangent space of Γ.

Now we will solve (2.9) using a finite element approach based on the following

time discrete approximation from [Deckelnick et al., 2005, Eqn 4.16].

$$\int_{\Gamma^n} \left(U^{n+1} - \mathrm{id}\right) \cdot \varphi + \Delta t \int_{\Gamma^n} \nabla_{\Gamma^n} U^{n+1} : \nabla_{\Gamma^n} \varphi = 0.$$

Here U^n parametrizes $\Gamma(t^{n+1})$ over $\Gamma^n := \Gamma(t^n)$, I is the identity matrix and Δt is the time step. Finally we apply a θ-scheme to arrive at the following form.

$$\int_{\Gamma^n} \left(U^{n+1} - \mathrm{id}\right) \cdot \varphi + \Delta t \int_{\Gamma^n} \left(\theta \nabla_{\Gamma^n} U^{n+1} + (1-\theta) I\right) : \nabla_{\Gamma^n} \varphi = 0.$$

where $\theta \in [0, 1]$ is a discretization parameter.

```
from __future__ import print_function
try:
    %matplotlib inline # can also use notebook or nbagg
except:
    pass

import math

from ufl import *
from dune.ufl import NamedConstant
import dune.ufl
import dune.create as create
import dune.geometry as geometry
import dune.fem as fem
from dune.fem.plotting import plotPointData as plot
import matplotlib.pyplot as pyplot
from IPython import display

# polynomial order of surface approximation
order = 2

# initial radius
R0 = 2.
```

We begin by setting up reference domain Γ_0 (`grid`), and the space on Γ_0 that describes $\Gamma(t)$ (`space`). From this we interpolate the non-spherical initial surface

positions, and, then reconstruct space for the discrete solution on $\Gamma(t)$.

```
grid = create.grid("ALUConform", "sphere.dgf",
                   dimgrid=2, dimworld=3)
space = create.space("lagrange", grid,
                     dimrange=grid.dimWorld, order=order)
positions = space.interpolate(lambda x: x * (1 + 0.5*math.sin(2*
                              math.pi*x[0]*x[1])*math.cos(math.pi*
                              x[2])), name="position")
surface = create.view("geometry", positions)
space = create.space("lagrange", surface,
                     dimrange=surface.dimWorld, order=order)
solution = space.interpolate(lambda x: x, name="solution")
```

We set up the theta scheme with $\theta = 0.5$.

```
theta = 0.5   # Crank-Nicholson
u = TrialFunction(space)
v = TestFunction(space)
x = SpatialCoordinate(space)
I = Identity(3)
dt = NamedConstant(space, "dt")

a = (inner(u - x, v) + dt * inner(theta*grad(u)
    + (1 - theta)*I, grad(v))) * dx
scheme = create.scheme("galerkin", a == 0, space, solver="cg")
```

Now we solve the scheme in time. We first set up the initial time variables, then we plot the initial figure's mesh, and finally we begin the loop, updating positions on each step and plotting the results side-by-side.

```
count = 0
t = 0.
end_time = 0.05
scheme.model.dt = 0.005

fig = pyplot.figure(figsize=(10, 10))
plot(solution, figure=(fig, 131+count%3), colorbar=False,
     gridLines="", triplot=True)

```

```
while t < end_time:
    scheme.solve(target=solution)
    t += scheme.model.dt
    count += 1
    positions.dofVector.assign(solution.dofVector)
    if count % 4 == 0:
        plot(solution, figure=(fig, 131+count%3), colorbar=False,
             gridLines="", triplot=True)
pyplot.show()
pyplot.close('all')
```

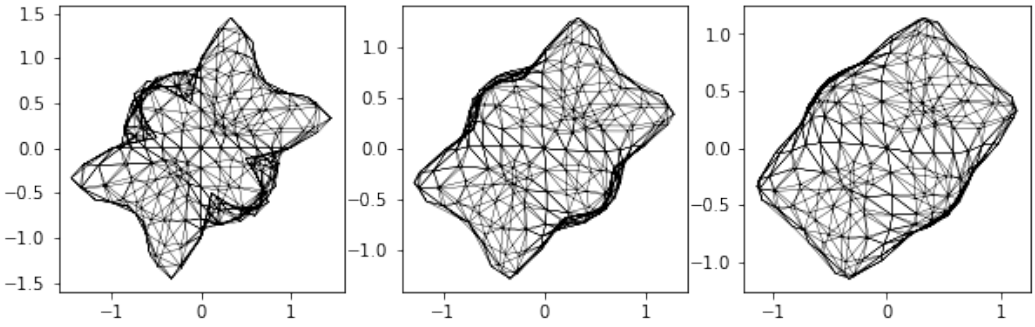

Figure 2.17: The plot of the surface at three different timesteps

In case we start with a spherical initial surface, i.e., $\Gamma(0) = R_0\ S^2$, the solution to the mean curvature flow equation is easy to compute:

$$\Gamma(t) = R(t)\ S^2$$
$$R(t) = \sqrt{R_0^2 - 4t}$$

We can use this to check that our implementation is correct. To do so we first define a function that computes the averaged radius of the surface.

```
def calcRadius(surface):
    # compute R = int_x |x| / int_x 1
    R   = 0
    vol = 0
    for e in surface.elements:
        rule = geometry.quadratureRule(e.type, 4)
```

```
        for p in rule:
            geo = e.geometry
            weight = geo.volume * p.weight
            R   += geo.toGlobal(p.position).two_norm * weight
            vol += weight
    return R/vol
```

Now we test the convergence rate by solving over a loop, and calculating the error in terms of the difference between the above analytical solution and our calculated one. We plot this in a figure.

```
end_time = 0.1
scheme.model.dt = 0.02

import numpy as np
pyplot.figure()
pyplot.gca().set_xlim([0, end_time])
pyplot.gca().set_ylabel("error")
pyplot.gca().set_xlabel("time")

number_of_loops = 3
errors = np.zeros(number_of_loops)
totalIterations = np.zeros(number_of_loops, np.dtype(np.uint32))
gridSizes = np.zeros(number_of_loops, np.dtype(np.uint32))
for i in range(number_of_loops):
    positions.interpolate(lambda x: x * (R0/x.two_norm))
    solution.interpolate(lambda x: x)
    t = 0.
    R = calcRadius(surface)
    Rexact = math.sqrt(R0**2 - 4.*t)
    x = np.array([t])
    y = np.array([R - Rexact])
    iterations = 0
    while t < end_time:
        solution,info = scheme.solve(target=solution)
        # move the surface
        positions.dofVector.assign(solution.dofVector)
        # store some information about the solution process
```

```
        iterations += int( info["linear_iterations"] )
        t += scheme.model.dt
        R = calcRadius( surface )
        Rexact = math.sqrt(R0*R0-4.*t)
        x = np.append(x, [t])
        y = np.append(y, [R - Rexact])
        pyplot.plot(x, y, label='i = '+ str(i) if t >= end_time \
                    else '')
        pyplot.legend()
        display.clear_output(wait=True)
        display.display(pyplot.gcf())
    errors[i] = abs(R - Rexact)
    totalIterations[i] = iterations
    gridSizes[i] = grid.size(2)
    if i < number_of_loops - 1:
        grid.hierarchicalGrid.globalRefine(1)
        scheme.model.dt /= 2.
```

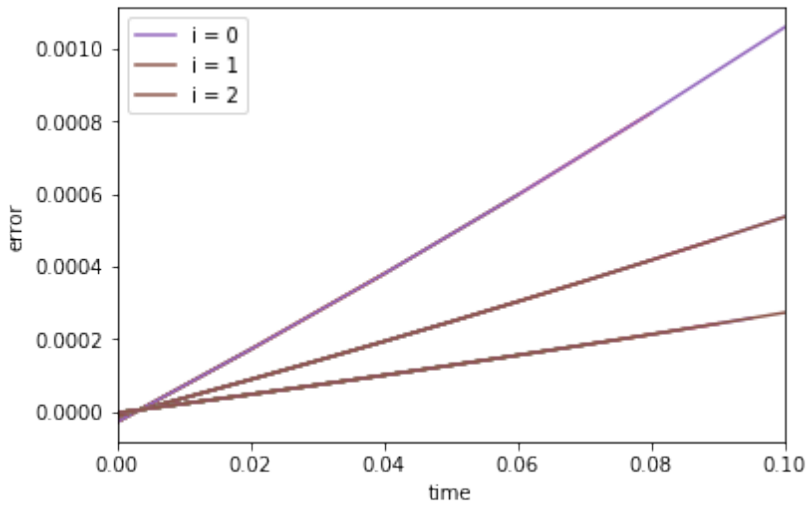

Figure 2.18: Comparison of the error over time for varying levels of refinement

The estimated orders of convergence (EOCs) are calculated as shown.

```
eocs = np.log(errors[0:][:number_of_loops-1] / errors[1:]) \
             / math.log(2.)
print(eocs)
```

```
[ 0.82367854  1.13117264]
```

Finally we organise this information into a table using `pandas`.

```
try:
    import pandas as pd
    keys = {'size': gridSizes, 'error': errors,
            "eoc": np.insert(eocs, 0, None),
            'iterations': totalIterations}
    table = pd.DataFrame(keys, index=range(number_of_loops),
                         columns=['size', 'error', 'eoc',
                                  'iterations'])
    print(table)
except ImportError:
    print("pandas could not be used to show table with results")
    pass
```

```
   size      error        eoc  iterations
0   318   0.001060        NaN          80
1   854   0.000599   0.823679         339
2  2065   0.000273   1.131173         777
```

2.6 Partitioned Grids

As another application of grid techniques, we look at a problem where we want to divide the grid into three regions. We do this using an `'adaptive'` grid that allows for grid filters to be applied. We note that another way of creating multi-domain grids in DUNE is described in Müthing and Bastian [2012] (though DUNE-FEMPY bindings are not yet available).

2.6.1 Li-ion Battery Problem

In this example we provide an implementation of a Li-ion battery model described in Popov et al. [2011]. The aim is to model how the concentration of Lithium (Li) ions and the electric potential vary over time in a battery as it discharges.

Li-ion batteries are among the most popular types of rechargeable batteries available, having widespread use in phones, laptops and other portable devices. Due to the desire to improve their capacities, charge times and overall lifetime, they have been studied extensively (see e.g. Efendiev et al. [2013], Taralov et al. [2012], Taralov [2015] and Latz et al. [2011]).

In particular this model considers smaller scale behaviour of the system, by looking at an individual cell split into three parts, as described below.

We consider the following PDE system.

$$\begin{aligned}\frac{\partial c}{\partial t} - \nabla \cdot (\mathbf{A}(\mathbf{u})\nabla \mathbf{u}) &= 0, \quad \text{in } \Omega_a, \Omega_e \text{ and } \Omega_c, \\ -\nabla \cdot (\mathbf{B}(\mathbf{u})\nabla \mathbf{u}) &= 0, \quad \text{in } \Omega_a, \Omega_e \text{ and } \Omega_c,\end{aligned}$$

where $\mathbf{u} = (c, \phi)$, i.e. the concentration and electric potential, $\nabla \mathbf{u}$ is the Jacobian, and $\mathbf{A}(\mathbf{u}), \mathbf{B}(\mathbf{u})$ are defined as

$$\begin{aligned}\mathbf{A}(\mathbf{u}) &= \left(D_e + \frac{RT}{F^2} \frac{t_+^2 \kappa}{c}, \frac{t_+ \kappa}{F} \right), \\ \mathbf{B}(\mathbf{u}) &= \left(\frac{RT}{F} \frac{t_+ \kappa}{c}, \kappa \right),\end{aligned}$$

where $F = 96485$ C mol^1 is the Faraday constant, $R = 8.314$ J mol^1 K^1 is the gas constant and $T = 300$ K. D_e, κ and t_+ are constants that depend on the domain and are given as

Domain	D_e	κ	t_+
Anode	$3.9x10^{-10}$	1.0	0
Electrolyte	$7.5x10^{-7}$	0.002	0.2
Cathode	$1.0x10^{-9}$	0.038	0

The domain is given by a rectangle Ω split into three parts. Ω_a on left (anode), Ω_e in middle (electrolyte), Ω_c on right (cathode). The inner boundaries are $\Gamma_a = \bar{\Omega}_a \cap \bar{\Omega}_e$, $\Gamma_c = \bar{\Omega}_e \cap \bar{\Omega}_c$. The outer boundary is Γ_{out}. Note that $\mathbf{u}$ is considered discontinuous across the inner boundaries, therefore we denote $\mathbf{u}$ separately as $\mathbf{u}_a, \mathbf{u}_e$ and $\mathbf{u}_c$ in

each respective domain.

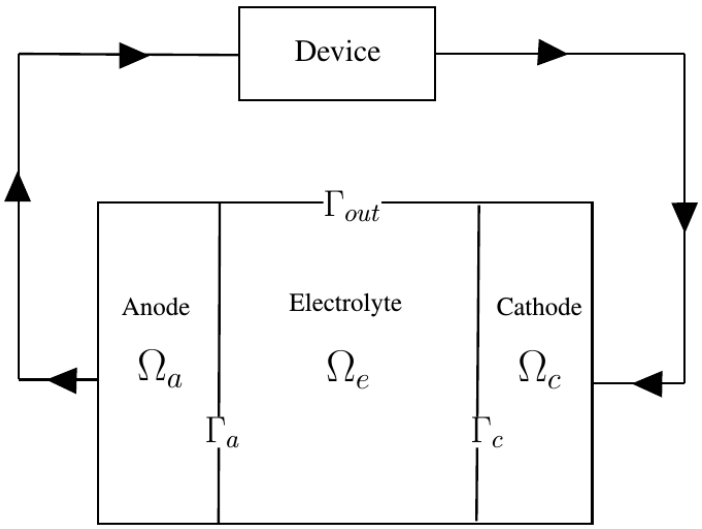

Figure 2.19: The domain, a cell split into three parts

For the outer boundary Γ_{out} we set the Neumann conditions (no flux),

$$(\mathbf{A}(\mathbf{u})\nabla\mathbf{u})\cdot\mathbf{n} = 0,$$
$$(\mathbf{B}(\mathbf{u})\nabla\mathbf{u})\cdot\mathbf{n} = 0,$$

where $\mathbf{n}$ is the unit normal pointing out the domain. Additionally on the inner boundaries Γ_a we set the Neumann conditions,

$$\begin{aligned}(\mathbf{A}(\mathbf{u}_a)\nabla\mathbf{u}_a)\cdot\mathbf{n} = -(\mathbf{A}(\mathbf{u}_e)\nabla\mathbf{u}_e)\cdot\mathbf{n} &= N(\mathbf{u}_a,\mathbf{u}_e),\\ (\mathbf{B}(\mathbf{u}_a)\nabla\mathbf{u}_a)\cdot\mathbf{n} = -(\mathbf{B}(\mathbf{u}_e)\nabla\mathbf{u}_e)\cdot\mathbf{n} &= J(\mathbf{u}_a,\mathbf{u}_e),\end{aligned}$$

(note that the negative sign on the Ω_e side accounts for the fact the normal is inverted) and similarly for Γ_c, where N and J are defined on Γ_a (and equivalently Γ_c) as follows.

$$J(\mathbf{u}_a,\mathbf{u}_e) = k\left(\frac{c_e}{c_e^0}\right)^{\alpha_a}\left(\frac{c_a}{c_a^0}\right)^{\alpha_a}\left(1-\frac{c_a}{c_{a,max}}\right)^{\alpha_c}\left(\exp\left(\frac{\alpha_a F}{RT}\eta_a\right)-\exp\left(-\frac{\alpha_c F}{RT}\eta_a\right)\right),$$
$$N(\mathbf{u}_a,\mathbf{u}_e) = \frac{J(\mathbf{u}_a,\mathbf{u}_e)}{F},$$

where $\eta_a = \phi_a - \phi_e - U_{a,0}$ (and correspondingly $\eta_c = \phi_c - \phi_e - U_{c,0}$) and $\alpha_a + \alpha_c = 1$ are anodic and cathodic weightings respectively. Additionally c^0 (the initial condition for c), c_{max} and U_0 are defined on each domain by

Domain	c^0	c_{max}	U_0
Anode	0.002639	0.02639	0
Electrolyte	0.001	–	–
Cathode	0.020574	0.02286	0.001

We will now write the weak form of the above PDE. Introducing a test function $\mathbf{v} = (v_0, v_1)$ and integrating over the domain, we get,

$$\begin{aligned}\int_\Omega \frac{\partial c}{\partial t} v_0 - \nabla \cdot (\mathbf{A}(\mathbf{u})\nabla \mathbf{u}) v_0 \, \mathrm{d}V = 0,\\ -\int_\Omega \nabla \cdot (\mathbf{B}(\mathbf{u})\nabla \mathbf{u}) v_1 \, \mathrm{d}V = 0.\end{aligned}$$

We then apply an implicit time discretisation, denoting the data from the previous time step by $\mathbf{u}^0 = (c^0, \phi^0)$, the new time step by $\mathbf{u}^1 = (c^1, \phi^1)$ and the size of the time step by Δt. This gives us the following.

$$\begin{aligned}\int_\Omega c^0 v_0 \, \mathrm{d}V = \int_\Omega c^1 v_0 - \Delta t \nabla \cdot (\mathbf{A}(\mathbf{u}^1)\nabla \mathbf{u}^1) v_0 \, \mathrm{d}V,\\ -\int_\Omega \nabla \cdot (\mathbf{B}(\mathbf{u}^1)\nabla \mathbf{u}^1) v_1 \, \mathrm{d}V = 0.\end{aligned}$$

We now apply Green's identity to get rid of the divergence terms. Note that for the following, we will separate the PDE into 3 equations for each part of the domain, since the boundaries are different in each case. For Ω_a, we get the following.

$$\begin{aligned}\int_{\Omega_a} c_a^0 v_0 \, \mathrm{d}V = \int_{\Omega_a} c_a^1 v_0 + \Delta t (\mathbf{A}(\mathbf{u}_a^1)\nabla \mathbf{u}_a^1) \cdot \nabla v_0 \, \mathrm{d}V - \int_{\Gamma_a} \Delta t (\mathbf{A}(\mathbf{u}^1)\nabla \mathbf{u}^1) \cdot \mathbf{n} v_0 \, \mathrm{d}S,\\ \int_{\Omega_a} (\mathbf{B}(\mathbf{u}_a^1)\nabla \mathbf{u}_a^1) \cdot \nabla v_1 \, \mathrm{d}V - \int_{\Gamma_a} \Delta t (\mathbf{B}(\mathbf{u}^1)\nabla \mathbf{u}^1) \cdot \mathbf{n} v_1 \, \mathrm{d}S = 0.\end{aligned}$$

For Ω_e,

$$\int_{\Omega_e} c_e^0 v_0 \; dV = \int_{\Omega_e} c_e^1 v_0 + \Delta t(\mathbf{A}(\mathbf{u}_e^1)\nabla \mathbf{u}_e^1) \cdot \nabla v_0 \; dV - \int_{\Gamma_a \cup \Gamma_c} \Delta t(\mathbf{A}(\mathbf{u}^1)\nabla \mathbf{u}^1) \cdot \mathbf{n} v_0 \; dS,$$
$$\int_{\Omega_e} (\mathbf{B}(\mathbf{u}_e^1)\nabla \mathbf{u}_e^1) \cdot \nabla v_1 \; dV - \int_{\Gamma_a \cup \Gamma_c} \Delta t(\mathbf{B}(\mathbf{u}^1)\nabla \mathbf{u}^1) \cdot \mathbf{n} v_1 \; dS = 0.$$

And for Ω_c,

$$\int_{\Omega_c} c_c^0 v_0 \; dV = \int_{\Omega_a} c_c^1 v_0 + \Delta t(\mathbf{A}(\mathbf{u}_c^1)\nabla \mathbf{u}_c^1) \cdot \nabla v_0 \; dV - \int_{\Gamma_c} \Delta t(\mathbf{A}(\mathbf{u}^1)\nabla \mathbf{u}^1) \cdot \mathbf{n} v_0 \; dS,$$
$$\int_{\Omega_c} (\mathbf{B}(\mathbf{u}_c^1)\nabla \mathbf{u}_c^1) \cdot \nabla v_1 \; dV - \int_{\Gamma_c} \Delta t(\mathbf{B}(\mathbf{u}^1)\nabla \mathbf{u}^1) \cdot \mathbf{n} v_1 \; dS = 0.$$

Finally we apply our boundary conditions for the integrands with $\mathrm{d}S$. For Ω_a,

$$\int_{\Omega_a} c_a^0 v_0 \; \mathrm{d}V = \int_{\Omega_a} c_a^1 v_0 + \Delta t(\mathbf{A}(\mathbf{u}_a^1)\nabla \mathbf{u}_a^1) \cdot \nabla v_0 \; \mathrm{d}V - \int_{\Gamma_a} \Delta t N(\mathbf{u}_a^1, \mathbf{u}_e^1) v_0 \; \mathrm{d}S,$$
$$\int_{\Omega_a} (\mathbf{B}(\mathbf{u}_a^1)\nabla \mathbf{u}_a^1) \cdot \nabla v_1 \; \mathrm{d}V - \int_{\Gamma_a} J(\mathbf{u}_a^1, \mathbf{u}_e^1) v_1 \; \mathrm{d}S = 0.$$

For Ω_e,

$$\int_{\Omega_e} c_e^0 v_0 \; \mathrm{d}V = \int_{\Omega_e} c_e^1 v_0 + \Delta t(\mathbf{A}(\mathbf{u}_e^1)\nabla \mathbf{u}_e^1) \cdot \nabla v_0 \; \mathrm{d}V$$
$$+ \int_{\Gamma_a} \Delta t N(\mathbf{u}_a^1, \mathbf{u}_e^1) v_0 \; \mathrm{d}S + \int_{\Gamma_c} \Delta t N(\mathbf{u}_e^1, \mathbf{u}_c^1) v_0 \; \mathrm{d}S,$$
$$\int_{\Omega_e} (\mathbf{B}(\mathbf{u}_e^1)\nabla \mathbf{u}_e^1) \cdot \nabla v_1 \; \mathrm{d}V + \int_{\Gamma_a} J(\mathbf{u}_a^1, \mathbf{u}_e^1) v_1 \; \mathrm{d}S + \int_{\Gamma_c} J(\mathbf{u}_e^1, \mathbf{u}_c^1) v_1 \; \mathrm{d}S = 0.$$

And for Ω_c,

$$\int_{\Omega_c} c_c^0 v_0 \; \mathrm{d}V = \int_{\Omega_a} c_c^1 v_0 + \Delta t(\mathbf{A}(\mathbf{u}_c^1)\nabla \mathbf{u}_c^1) \cdot \nabla v_0 \; \mathrm{d}V - \Delta t \int_{\Gamma_c} N(\mathbf{u}_e^1, \mathbf{u}_c^1) v_0 \; \mathrm{d}S,$$
$$\int_{\Omega_c} (\mathbf{B}(\mathbf{u}_c^1)\nabla \mathbf{u}_c^1) \cdot \nabla v_1 \; \mathrm{d}V - \int_{\Gamma_c} J(\mathbf{u}_e^1, \mathbf{u}_c^1) v_1 \; \mathrm{d}S = 0.$$

We will now look at an implementation of the above in DUNE-FEMPY. First, let us import the necessary Python modules.

```
1 import math
2 from ufl import *
```

```
3
4  import dune.ufl
5  import dune.fem
6
7  import dune.create as create
8  from dune.fem.view import filteredGridView
```

Let us define the parameters for the problem.

```
1  dune.fem.parameter.append("parameter")
2
3  # general parameters
4  dimDomain = 2
5  dimRange = 2
6  order = 1  # order of FE space
7  numRefines = 1  # number of refinements of inital grid
8  timeStep = 50  # size of timeStep
9  maxIter = 20  # max number of solver iterations
10
11 # problem parameters (from battery paper)
12 R = 8.314
13 T = 300
14 F = 96485
15 t_plus = [0, 0.2, 0]
16 kappa = [1.0, 0.002, 0.038]
17 D_e = [3.9e-10, 7.5e-7, e-9]
18 c_init = [0.002639, 0.001, 0.020574]  # initial value for c
19 phi_init = [0, 0, 0]  # initial value for potential
20 c_max = [0.02639, None, 0.02286]
21 U_0 = [0, None, 0.001]
22 alpha_a = 0.5
23 alpha_c = 1 - alpha_a
```

In the usual way we define the variables in UFL.

```
1  # define u^1 = (c^1, phi^1) and v = (v_0, v_1)
2  space = dune.ufl.Space(dimDomain, dimRange)
3  u = TrialFunction(space)
4  v = TestFunction(space)
```

```
5
6  # define un = (c^0, phi^0), u_a is for storing u
7  # in Omega_a and so on for u_e and u_c
8  un = Coefficient(space)
9  u_a = Coefficient(space)
10 u_e = Coefficient(space)
11 u_c = Coefficient(space)
12 dt = Constant(space.cell())
```

Let us define the PDE and boundary conditions, starting with variables that we might want to modify.

```
1  # define A_1 and A_2 in PDE (for the Id, a = 0, e = 1, c = 2)
2  def A1(Id):
3      return D_e[Id] + R*T/(F**2)*t_plus[Id]**2*kappa[Id]/u[0]
4  def A2(Id):
5      return kappa[Id]*t_plus[Id]/F
6
7  # define B_1 and B_2 in PDE
8  def B1(Id):
9      return R*T/F*t_plus[Id]*kappa[Id]/u[0]
10 def B2(Id):
11     return kappa[Id]
12
13 # define Neumann boundary term J for inner boundaries
14 def J(uElec, uSolid):
15     J1 = (uElec[0]/c_init[1])**alpha_a
16     J2 = (uSolid[0]/c_init[0])**alpha_a
17     J3 = (1 - uSolid[0]/c_max[0])**alpha_c
18     J4 = (exp(alpha_a*F/(R*T)*(uSolid[1] - uElec[1] - U_0[0])) \
19           - exp(-alpha_c*F/(R*T)*(uSolid[1] - uElec[1] - U_0[0])))
20     return J1*J2*J3*J4
21
22 # define dirichlet conditions on the left and right boundaries
23 tmp_a = 0.000951 # these should be removed
24 tmp_c = 0.018454 #
25 diric_a = as_vector([tmp_a, 2.5e-8])
26 diric_c = as_vector([tmp_c, 1.9e-2])
```

We continue defining the PDE and boundary conditions, this time with parts of the framework that should mostly remain the same.

```
# define J, N in Omega_a and Omega_c
J_s = J(u_e, u)
N_s = J_s/F
# define J, N in Omega_e on Gamma_a and Gamma_c respectively
J_ea = J(u, u_a)
N_ea = J_ea/F
J_ec = J(u, u_c)
N_ec = J_ec/F

# define the bilinear form's explicit part using B1, B2
def eq_ex(Id):
    ex = inner(un[0], v[0])*dx
    ex += inner(B1(Id)*grad(u[0])
          + B2(Id)*grad(u[1]), grad(v[1]))*dx
    return ex
# define the implicit part using A1, A2
def eq_im(Id):
    im = (inner(u[0], v[0]))*dx
    im += dt*inner(A1(Id)*grad(u[0])
          + A2(Id)*grad(u[1]), grad(v[0]))*dx
    return im

# let's combine the bilinear forms with the BCs in each domain
a_ex = eq_ex(0) - J_s*v[1]*ds(4)
a_im = eq_im(0) - dt*N_s*v[0]*ds(4)
# same for Omega_e
e_ex = eq_ex(1) + J_ec*v[1]*ds(5)
e_im = eq_im(1) + dt*N_ea*v[0]*ds(3) + dt*N_ec*v[0]*ds(5)
# and Omega_c
c_ex = eq_ex(2) - J_s*v[1]*ds(4)
c_im = eq_im(2) - dt*N_s*v[0]*ds(4)
```

The remaining code involves setting up the FEM and is mostly independent of the problem paramaters, thus should not need to be changed.

Let us construct the three separate grids using a grid filter. We label the three domains by 3, 4 and 5 to correspond with the inner BCs defined above.

```
def filter(e):
    if e.geometry.center[0] <= 0.2:
        return 3
    elif 0.2 <= e.geometry.center[0] <= 0.8:
        return 4
    elif 0.8 <= e.geometry.center[0]:
        return 5

unitcube = 'unitcube-' + str(dimDomain) + 'd.dgf'
grid = create.view("adaptive", create.grid("ALUCube", unitcube,
                   dimgrid=dimDomain))
grid.hierarchicalGrid.globalRefine(numRefines)
anode       = filteredGridView(grid, filter, 3)
electrolyte = filteredGridView(grid, filter, 4)
cathode     = filteredGridView(grid, filter, 5)
```

We construct the FE spaces and the solutions.

```
space_a = create.space("Lagrange", anode, dimrange=dimRange,
                       order=order)
space_e = create.space("Lagrange", electrolyte, dimrange=dimRange,
                       order=order)
space_c = create.space("Lagrange", cathode, dimrange=dimRange,
                       order=order)

solution_a  = space_a.interpolate(lambda x: [c_init[0],
                                  phi_init[0]], name="solution_a")
solution_a_n = solution_a.copy()
solution_a_n.assign( solution_a )
solution_e = space_e.interpolate(lambda x: [c_init[1],
                                 phi_init[1]], name="solution_e")
solution_e_n = solution_e.copy()
solution_e_n.assign( solution_e )
solution_c = space_c.interpolate(lambda x: [c_init[2],
                                 phi_init[2]], name="solution_c")
solution_c_n = solution_c.copy()
```

```
solution_c_n.assign( solution_c )
```

We construct the models and schemes.

```
# omega_a
model_a  = create.model("split", anode, a_ex == a_im,
             dirichlet={6: diric_a},
             coefficients={u_e: solution_e_n, un: solution_a_n})
model_a.setConstant(dt, timeStep)
scheme_a = cr eate.scheme("galerkin", model_a, space_a)

# omega_e
model_e  = create.model("split", electrolyte, e_ex == e_im,
            coefficients={u_a: solution_a_n, u_c: solution_c_n,
                          un: solution_e_n})
model_e.setConstant(dt, timeStep)
scheme_e = create.scheme("galerkin", model_e, space_e)

# omega_c
model_c  = create.model("split", cathode, c_ex == c_im,
             dirichlet={7: diric_c},
             coefficients={u_e: solution_e_n, un: solution_c_n})
model_c.setConstant(dt, timeStep)
scheme_c = create.scheme("galerkin", model_c, space_c)
```

We define the method for plotting the solution. We do this using matplotlib and by plotting each solution to its own domain. We also calculate a `global_max` and `global_min` of all solutions to create the colour plot.

```
from numpy import amin, amax, linspace
import matplotlib
from matplotlib import pyplot
from IPython import display
matplotlib.rcParams.update({'font.size': 10})
matplotlib.rcParams['figure.figsize'] = [10, 5]

def matplot(grid, solution, sol2, sol3, a=False):
    triangulation = grid.triangulation()
    for p in range(2):
```

```
        pyplot.subplot(121 + p)
        pyplot.gca().set_aspect('equal')
        pyplot.gca().locator_params(tight=True, nbins=4)
        data = solution.pointData()
        data2 = sol2.pointData()
        data3 = sol3.pointData()
        global_min = min(amin(data[:,p]), amin(data2[:,p]),
                         amin(data3[:,p])) - 1e-4
        global_max = max(amax(data[:,p]), amax(data2[:,p]),
                         amax(data3[:,p])) + 1e-4
        if global_min != global_max:
            levels = linspace(global_min, global_max, 256)
            pyplot.tricontourf(triangulation, data[:,p],
                        cmap=pyplot.cm.rainbow, levels=levels)
        else:
            pyplot.tricontourf(triangulation, data[:,p],
                               cmap=pyplot.cm.rainbow)
        if a == True:
            pyplot.colorbar(shrink=0.725)
```

Finally we start the solving process over a loop. We plot the initial solution and the result after 20 steps, and we save each step to a paraview file.

```
anode.writeVTK("battery_anode_", pointdata=[solution_a], number=0)
electrolyte.writeVTK("battery_electrolye_", pointdata=[solution_e],
                     number=0)
cathode.writeVTK("battery_cathode_", pointdata=[solution_c],
                 number=0)
matplot(anode, solution_a, solution_e, solution_c, a=True)
matplot(electrolyte, solution_e, solution_a, solution_c)
matplot(cathode, solution_c, solution_a, solution_e)
display.display(pyplot.gcf())
pyplot.close('all')
for i in range(1, 20):
    scheme_a.solve(target=solution_a)
    scheme_e.solve(target=solution_e)
    scheme_c.solve(target=solution_c)
    solution_a_n.assign(solution_a)
```

```
    solution_e_n.assign(solution_e)
    solution_c_n.assign(solution_c)
    anode.writeVTK("battery_anode_",
                   pointdata=[solution_a], number=i)
    electrolyte.writeVTK("battery_electrolye_",
                         pointdata=[solution_e], number=i)
    cathode.writeVTK("battery_cathode_",
                     pointdata=[solution_c], number=i)
matplot(anode, solution_a, solution_e, solution_c, a=True)
matplot(electrolyte, solution_e, solution_a, solution_c)
matplot(cathode, solution_c, solution_a, solution_e)
display.display(pyplot.gcf())
```

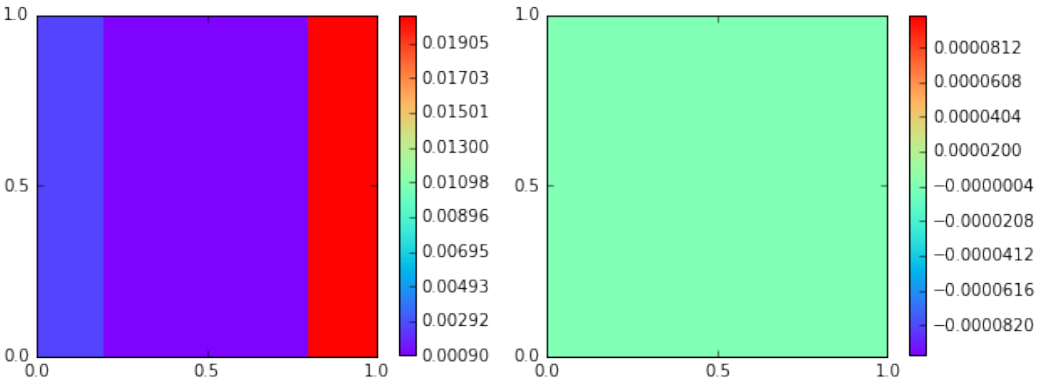

Figure 2.20: The initial plot of c and ϕ

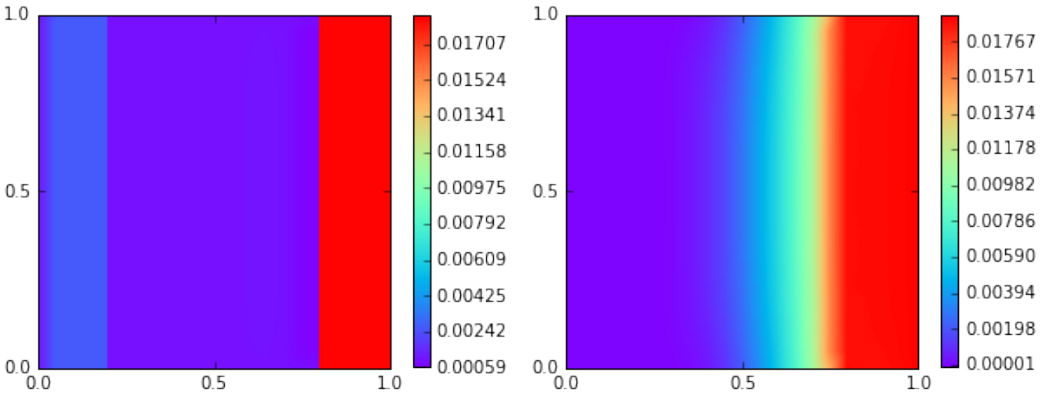

Figure 2.21: The plot after the final timestep

2.7 Translating Python Code to C++

Having looked at some of the functionality available for solving various FEM problems, we now shift our focus towards more in-depth features that concern efficiency and C++ development. Here we consider the idea of moving sections of Python code over to C++ for efficiency. A key aspect of the design of Dune-Fempy has been about keeping the structure of the C++ code in the Python code's design, to the point where translating between the two is relatively painless. In particular this allows for rapid prototyping of methods in Python with its relative ease of use, after which code can be ported to C++ for efficiency if necessary in large-scale computation.

Here we will demonstrate this translation process, and additionally provide comparisons for the difference in efficiency timewise. We will examine the function used for calculating the averaged radius of a surface used in the mean curvature flow example from section 2.5.

Code Listing 2.31: A Pythonic function for calculating the radius of a surface

```
def calcRadius(surface):
    # compute R = int_x |x| / int_x 1
    R   = 0
    vol = 0
    for e in surface.elements:
        rule = geometry.quadratureRule(e.type, 4)
        for p in rule:
            geo = e.geometry
            weight = geo.volume * p.weight
            R   += geo.toGlobal(p.position).two_norm * weight
            vol += weight
    return R/vol
```

As a relatively simple example, this code is not particularly slow in Python, however the existence of callbacks inside a looped statement are not insignificant. Now let us look at a C++ translation of the above code.

Code Listing 2.32: The C++ version of the calcRadius function

```
#include <dune/geometry/quadraturerules.hh>

template< class Surface >
double calcRadius( const Surface &surface )
{
  double R = 0.;
  double vol = 0.;
  for( const auto &entity : elements( surface ) )
  {
    const auto& rule = Dune::QuadratureRules<double,
        2>::rule(entity.type(), 4);
    for ( const auto &p : rule )
    {
      const auto geo = entity.geometry();
      const double weight = geo.volume() * p.weight();
      R   += geo.global(p.position()).two_norm() * weight;
      vol += weight;
    }
  }
  return R/vol;
}
```

We note that we take advantage of C++11 features such as `auto` and range based for loops to keep a similar structure to the Python code.

Supposing we save the above as `radius.hh`, we can then call it in a Python script and use it like a regular function as follows.

Code Listing 2.33: Calling our C++ function using algorithm

```
from dune.generator import algorithm
calcRadius = algorithm.load('calcRadius', 'radius.hh', surface)
```

Doing this, we can quite easily swap between the two versions and compare the runtime of the solve method. Specifically, we test the runtime of the mean curvature flow example with the original Python version of `calcRadius` and compare it to the runtime with the above substitution. We show these results for a relatively large number of elements, as shown in figure 2.22.

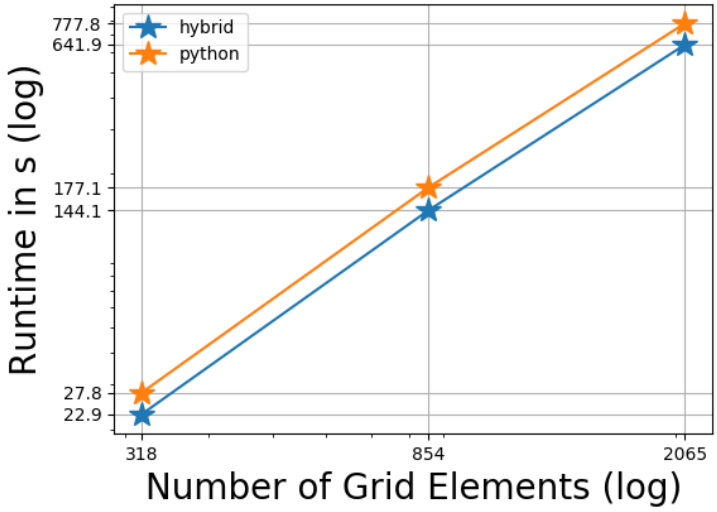

Figure 2.22: Comparison of time taken between the two calcRadius methods

What we see is that the C++ version is roughly 18% faster. On a small scale this is not a significant change, but it could be potentially worth it for a particularly long-running simulation. Naturally the more of the code that is written in C++, the faster it will be overall, though whether it is justifiable to do this depends on a case-by-base basis.

2.8 Virtualization

One final topic we want to discuss is virtualization, by which we mean the use of virtual classes and functions in C++ to abstractly represent objects such as grids and spaces.

In the development of the Python bindings for DUNE-PYTHON, the decision was made was to avoid introducing such a virtual layer when exporting classes from C++ to Python or vice versa; the reason being that it would introduce additional code maintenance and more importantly perhaps lead to loss in performance when a C++ object is passed through Python back into C++. In this case code optimization steps like inlining or loop unrolling could not be utilized to their full potential.

Take as an example a discrete function which is constructed using `df = space.interpolate([0],name="df")`. The call to `interpolate` goes back to the corresponding function in DUNE-FEM and returns an instance of the discrete function. To store the solution to a PDE problem in `df`, the `solve` method on a `scheme` is called. While executing `scheme.solve(target=df)` the discrete function instance is passed back to another DUNE-FEM function. If `df` were virtualized (i.e. type erased) in either of the two steps, i.e. when passed to or from Python, then the `solve` method could not work with the same efficiency as when used in a pure C++ environment. The number of degrees of freedom, local structure, etc. of the discrete function would only be known as dynamic properties, making code optimization by the compiler or the DUNE developer implementing the `solve` method more difficult or even impossible. Note that virtualizing the discrete function for example, would almost certainly also require virtualization of the underlying discrete function spaces (with mapper and basis function set), and the underlying grid view (with its iterators). The cumulative effect of this would be quite severe on performance.

To avoid this issue, no type erasure is carried out when an object is passed into Python. So in the above example the call to `interpolate` returns an object which still contains the full type information of the underlying DUNE-FEM function. This approach leads to compilation overhead the first time a new type of discrete function is used since a new Python module needs to be generated. But this overhead occurs only the first time the discrete function is used during the development of a project and is thus negligible. Since no type erasure has occurred, any DUNE object can now be passed back to it. The `solve` method on the scheme is exported in such a way that the target argument has to be of the same discrete function type that was defined by the `storage` argument provided during the space construction. Consequently a scheme over a given space (e.g. a Lagrange space of a fixed order using an `istl` storage) will only accept one type of discrete function as `target` argument for its solve method. As described before the advantage of this is that the full static type information is available at the cost of more compilation requirements when changes (e.g. to the storage back end) are made.

There are a few exceptions to the above rule, where Python objects passed as arguments to C++ functions undergo type erasure if their type does not match the exact type of the arguments of that function.

An example is the `__call__` method on an `operator`. When calling `op(arg,dest)`, the destination parameter (`dest`) has to be of the correct discrete function type, but for the argument parameter (`arg`) it can make sense to allow for a wide range of grid functions, e.g. an exact solution given by a UFL expression or a different type of discrete function. In many cases the implementation of the operator does not require the argument to even be discrete since only the evaluation of `arg` at quadrature points is required; in this case any grid function is a valid argument. On the C++ side the operator call is simply implemented as a template method on the operator class with the signature

```
1 template <class GF> Operator::operator()(const GF &arg, typename
      Operator::DiscreteFunction &dest);
```

We note that it is not possible to export a template method to Python without fixing all of its arguments. Since an optimized version of such a method is often implemented for the case that `arg` is of the same type as `dest`, the default method that will always be exported to Python has `GF=Operator::DiscreteFunction`. In addition, a second version is exported where `GF=VirtualizedGridFunction<...>`, which is a type erased implementation of a grid function. Any grid function exported to Python (e.g. UFL expressions, discrete function etc.) will implicitly convert to a `VirtualizedGridFunction` so that `op(arg,dest)` can be used in Python even in the case that `arg` is not of the same type as `dest`. Optimal code is still produced in the case where both parameters are of the same type.

A second use of type erasure where objects are passed back to C++ occurs when an `operator` or `scheme` is constructed from a given model. Since the development of a new model can involve repeated changes being made to it (e.g. its underlying UFL form) we aimed to avoid the situation of each change requiring a recompilation of the `operator` or `scheme`. To this end the model is virtualized when it is passed to the constructor of the `operator` or `scheme` class. Consequently, these

classes only depend on some type information like the underlying type of the grid view and the range dimension of the model but not on the actual details of the weak form. The consequence of this approach is that evaluating some part of the form introduces a virtual function call.

Chapter 3

Nonvariational PDEs

3.1 Definition and Notation

We start this chapter by concretely defining our problem for the linear case and providing some notation for the following sections.

Let the computational domain for our finite element method be $\Omega \subset \mathbb{R}^d$. Then let us once again state the problem in general terms. For $u \in W := H^2(\Omega) \cap H_0^1(\Omega)$, we would like to solve

$$\begin{aligned} -A : D^2 u &= f, \quad \text{in } \Omega, \\ u &= 0, \quad \text{on } \partial\Omega. \end{aligned} \tag{3.1}$$

Here $D^2 u$ is the Hessian of u, $f \in L^2$ is a real-valued prescribed function, $M : N = \sum_{i,j} M_{ij} N_{ij}$ is the Frobenius inner product and $A(x) \in \mathrm{Sym}(\mathbb{R}^{d\times d}) \cap C^0(\Omega^{d\times d})$ is a coefficient matrix that is elliptic in the following sense.

Definition 3.1.1 (Ellipticity of Symmetric Matrices)**.** We say A is *elliptic* on $\mathrm{Sym}(\mathbb{R}^{d\times d})$ if, for each $M \in \mathbb{R}^{d\times d}$, there exist $\Lambda \geq \lambda > 0$ such that

$$\lambda \sup_{|\xi|=1} |N\xi| \leq A(M+N) - A(M) \leq \Lambda \sup_{|\xi|=1} |N\xi|, \quad \forall N \in \mathrm{Sym}(\mathbb{R}^{d\times d}).$$

Additionally for the next theorem we will use the following definition.

Definition 3.1.2 (Hölder Domain)**.** A domain $\Omega \subset \mathbb{R}^d$ is $C^{k,\alpha}$, if each point on the boundary $\partial\Omega$ has a neighbourhood in which $\partial\Omega$ can be represented by a function in the Hölder space $C^{k,\alpha}$, after a change of coordinates.

Then we have the following theorem for the existence of a strong solution from [Gilbarg and Trudinger, 2015, Thm 9.15].

Theorem 3.1.1 (Existence of a strong solution to (3.1))**.** *Let $\Omega \subset \mathbb{R}^d$ be a $C^{1,1}$ domain. Let $A \in Sym(\mathbb{R}^{d\times d}) \cap C^0(\Omega)^{d\times d}$ be an elliptic matrix and $f \in L^2(\Omega)$. Then the equation*

$$\begin{aligned} -A : D^2u = f, \quad & \text{in } \Omega, \\ u = 0, \quad & \text{on } \partial\Omega. \end{aligned}$$

has a unique solution $u \in H^2(\Omega) \cap H_0^1(\Omega)$. There also exists a constant C independent of u such that

$$\|u\|_2 \leq C\|f\|.$$

where $\|\cdot\|_k$ denotes the $H_k(\Omega)$ norm.

Now in future sections we will be working in the discrete case of this problem, therefore to streamline the analysis, let us define the notation we will be using here.

Regarding the domain, let $\mathcal{T}$ denote a triangulation of Ω, and $\mathcal{E}$ denote the edges of the elements (with $\mathcal{E}_0 := \mathcal{E}\backslash\partial\Omega$). For measuring the refinement of the mesh, we define $h = \max_{K\in\mathcal{T}} h_K$ to be the mesh size (where h_K is the diameter of element K).

In the future we will be working in a conforming finite element space V_h, for which the discretized problem is defined. Let $P^k(\mathcal{T})$ denote the space of piecewise polynomials of degree k over $\mathcal{T}$, i.e.

$$P^k(\mathcal{T}) = \{\phi : \phi|_K \in P^k(K)\}.$$

Then we let $V_h = C^0(\Omega) \cap P^k(\mathcal{T})$. We remark that this space is the typical choice used for Lagrange finite elements.

Now as a lot of the upcoming methods use discontinuous Galerkin (DG) techniques, we shall also define some of these concepts here.

Definition 3.1.3 (Jumps and Averages)**.** Consider an edge $e \in \mathcal{E}$ (if $e \in \mathcal{E}_0$ then let it be between two elements K_1 and K_2). We define the **jump** and **average** of $v \in L^2(\Omega)$ on e respectively as

$$[\![v]\!] = \begin{cases} v|_{K_1}\mathbf{n}_{K_1} + v|_{K_2}\mathbf{n}_{K_2}, & e \in \mathcal{E}_0, \\ v\mathbf{n}, & e \subset \partial\Omega, \end{cases}$$

$$\{v\} = \begin{cases} \frac{1}{2}(v|_{K_1} + v|_{K_2}), & e \in \mathcal{E}_0, \\ v, & e \subset \partial\Omega, \end{cases}$$

where $\mathbf{n}_K$ is the outward pointing normal to K. Additionally for a vector $\mathbf{v} \in L^2(\Omega)^d$ we have the following natural extensions to the definitions.

$$[\![\mathbf{v}]\!] = \begin{cases} \mathbf{v}|_{K_1} \cdot \mathbf{n}_{K_1} + \mathbf{v}|_{K_2} \cdot \mathbf{n}_{K_2}, & e \in \mathcal{E}_0, \\ \mathbf{v} \cdot \mathbf{n}, & e \subset \partial\Omega, \end{cases}$$

$$\{\mathbf{v}\} = \begin{cases} \frac{1}{2}(\mathbf{v}|_{K_1} + \mathbf{v}|_{K_2}), & e \in \mathcal{E}_0, \\ \mathbf{v}, & e \subset \partial\Omega, \end{cases}$$

And we have a similar version of the jump for the outer product,

$$[\![\mathbf{v}]\!]_\otimes = \begin{cases} \mathbf{v}|_{K_1} \otimes \mathbf{n}_{K_1} + \mathbf{v}|_{K_2} \otimes \mathbf{n}_{K_2}, & e \in \mathcal{E}_0, \\ \mathbf{v} \otimes \mathbf{n}, & e \subset \partial\Omega. \end{cases}$$

Finally we note there exists an alternate form of the jump sometimes used in the

literature, which we define now.

$$[\![v]\!]_0 = \begin{cases} v|_{K_1} - v|_{K_2}, & e \in \mathcal{E}_0, \\ v, & e \subset \partial\Omega. \end{cases}$$

Remark. We note that the $[\![\cdot]\!]$ definition returns a vector when applied to a scalar, and a scalar when applied to a vector, whilst the $[\![\cdot]\!]_0$ definition always returns a variable of the same dimension. Thus it is important to keep this distinction in mind.

In the discontinuous Galerkin case, note that we use a discontinuous version of V_h for our space, which we denote by V_{DG}.

One more concept we would like to mention used in some nonvariational approaches (e.g. Dedner and Pryer [2013] and Wang and Wang) is to discretize the Hessian as follows.

Definition 3.1.4 (Finite Element Hessian)**.** We define the **finite element Hessian** $H[u]$ to be a unique element of $V_{DG}^{d\times d}$ such that for all $\varphi \in V_h$,

$$\int_\Omega H[u]\,\varphi \,\mathrm{d}x = -\int_\Omega \nabla_h u \otimes \nabla_h \varphi \,\mathrm{d}x + \int_{\mathcal{E}} [\![u]\!] \otimes \{\nabla_h \varphi\} + [\![\varphi]\!] \otimes \{\nabla_h u\} \,\mathrm{d}s, \quad (3.2)$$

where $\nabla_h = (D_h)^T$ is the elementwise gradient. In section 3.5 we will return to this concept and provide a full derivation.

3.2 Existing Methods

Now that we have provided a background for the mathematical concepts of (3.1) in section 3.1, we start our analysis of nonvariational problems by considering the methods from the literature that have been developed to solve this kind of problem numerically.

Before we go into the specifics of these approaches, let us briefly state the

variational method we use in the case when A is assumed to be smooth. We introduce this for the purpose of a benchmark to compare nonvariational methods to in later sections.

Example 3.2.1 (Variational)**.** We begin by rewriting $A : D^2u$ into divergence form.

$$A : D^2u = \nabla \cdot (A\nabla u) - (\nabla \cdot A)\nabla u.$$

Substituting this form into (3.1), multiplying by v and integrating by parts, we obtain the following bilinear form.

$$\int_\Omega (A\nabla u \cdot \nabla v - (\nabla \cdot A) \cdot \nabla u v)\,\mathrm{d}x - \int_{\partial\Omega} A\nabla u \cdot \mathbf{n} v\,\mathrm{d}s = \int_\Omega f v\,\mathrm{d}x.$$

Lastly we incorporate the boundary condition $u = 0$ by adding the following term which is a weak implementation of Dirichlet boundary conditions.[1]

$$\beta h^{-1} \int_{\partial\Omega} uv\,\mathrm{d}s, \quad \beta > 0, \tag{3.3}$$

where $\beta > 0$ is a constant. This results in the following bilinear form for the variational approach.

$$\int_\Omega (A\nabla u \cdot \nabla v + (\nabla \cdot A) \cdot \nabla u v)\,\mathrm{d}x + \int_{\partial\Omega} \left(\beta h^{-1} uv - A\nabla u \cdot \mathbf{n} v\right)\mathrm{d}s = \int_\Omega f v\,\mathrm{d}x, \tag{3.4}$$

With the variational method stated, we shall now consider the nonvariational approaches.

Example 3.2.2 (Pryer)**.** Let us consider the numerical method used in Lakkis and Pryer [2010], which is equivalent to finding $u_h \in V_h$ such that

$$-\int_\Omega A : \hat{H}[u_h]\varphi_h\,\mathrm{d}x = \int_\Omega f\varphi_h\,\mathrm{d}x, \quad \forall \varphi_h \in V_h, \tag{3.5}$$

[1] This is an alternative to a strong Dirichlet BC implementation which in the numerical implementation requires one to manually set columns in the system matrix to zero. As we will later formulate the problem as a saddle point problem, for comparison reasons it is easier to use the same penalty term for all methods to enforce boundary conditions.

where $\hat{H}[u_h] \in [V_h]^{d\times d}$ satisfies

$$\int_\Omega \hat{H}[u_h]\varphi_h \,\mathrm{d}x = -\int_\Omega \nabla u_h \otimes \nabla\varphi_h \,\mathrm{d}x + \int_{\partial\Omega} \nabla u_h \otimes \mathbf{n}\varphi_h \,\mathrm{d}s.$$

We note that, assuming strong treatment of the Dirichlet boundary conditions, this form of $\hat{H}[u]$ is equivalent to (3.2) in the case of Lagrange finite elements (i.e. continuity across elements is assumed so $[\![v]\!] = 0$ on $\mathcal{E}_0$).

A-priori error estimates are not formulated in this paper, and instead quantitative results are the focus[2]. In terms of convergence rates, they show (for a sufficiently smooth solution and) for P^k elements that $\|u - u_h\| = \mathcal{O}(h^{k+1})$ and $|u - u_h|_1 = \mathcal{O}(h^k)$. We note that these are the usual results observed in FEMs for variational problems, and among the upcoming examples, we will see that convergence rates of this order are also typical for nonvariational problems of the form (3.1).

Example 3.2.3 (NVDG)**.** A discontinuous Galerkin version of the above method was later derived in Dedner and Pryer [2013].

$$-\int_\Omega A : H[u_h]\varphi_h \,\mathrm{d}x + \int_{\mathcal{E}} \sigma h^{-1}[\![u_h]\!]\cdot[\![\varphi_h]\!]\,\mathrm{d}s = \int_\Omega f\varphi_h \,\mathrm{d}x, \quad \forall\varphi_h \in V_h. \tag{3.6}$$

where $H[u]$ is defined as in (3.2).

In comparison to (3.5), the DG formulation leads to a slightly more complex form of the finite element Hessian, and there is the addition of a stabilization term.

The method is implemented in DUNE, and numerically the same convergence rates are observed as in example 3.2.2. Additionally, they prove the analytical result that for sufficiently smooth A and u that

$$\|u - u_h\|_{DG,1} \leq C\left(h^k|u|_{k+1} + h^{k+1}|u|_{k+3}\right),$$

[2]The results were computed in MATLAB with a GMRES (generalized minimal residual method) used for the linear solver.

where k is the polynomial order and $\|u_h\|_{DG,1}$ is the broken norm defined by

$$\|u_h\|_{DG,1}^2 := \|\nabla_h u_h\|^2 + h^{-1}\|[\![u_h]\!]\|_{\mathcal{E}}^2.$$

We note that in theory the smoothness conditions limit the usability of this result, although they still show numerically that optimal convergence holds even for a nondifferentiable operator.

Given that this form of the method can be considered an advancement to example 3.2.2, we will focus mostly on this version for comparative purposes.

Example 3.2.4 (Feng)**.** We now consider a method that takes a similar form to the above, but without the finite element Hessian. In Feng et al. [2015] they used the following method.

$$-\int_\Omega A : D_h^2 u_h \varphi_h \,\mathrm{d}x + \sum_{e\in\mathcal{E}} \int_e [\![A\nabla u_h]\!]\varphi_h \,\mathrm{d}s = \int_\Omega f\varphi_h \,\mathrm{d}x, \quad \forall \varphi_h \in V_h. \tag{3.7}$$

where D_h^2 is a piecewise defined Hessian. We also note that the stabilization term is different to the above case.

For sufficiently smooth u, they obtain the following a-priori error bound.

$$\|u - u_h\|_{W^{2,p}(\Omega)} \leq h^{k-1}\|u\|_{W^{k+1,p}(\Omega)},$$

i.e. in the case $p = 2$,

$$\|u - u_h\|_2 \leq h^{k-1}\|u\|_{k+1}. \tag{3.8}$$

This result is roughly equivalent to the estimate for 3.2.2[3], and furthermore they verify numerically that $|u - u_h|_1 = \mathcal{O}(h^k)$ and $\|D_h^2(u - u_h)\|_{L^2(\Omega)} = \mathcal{O}(h^{k-1})$.

Example 3.2.5 (Mu)**.** Recently in Mu and Ye [2017], they introduced a method that takes a different approach.

$$\int_\Omega \left(A : D_h^2 u_h\right)\left(A : D_h^2 \varphi_h\right) \mathrm{d}x + s(u_h, \varphi_h) = \int_\Omega fA : D_h^2\varphi_h \,\mathrm{d}x, \quad \forall \varphi_h \in V_h, \tag{3.9}$$

[3]Since moving from the H^1 norm to the H^2 norm is roughly the same as adding h^{-1} to the estimate.

where $s(\cdot,\cdot)$ is a stabilization term defined by

$$s(u_h,\varphi_h) = \int_{\mathcal{E}} h^{-3}[\![u_h]\!]_0[\![\varphi_h]\!]_0 \,\mathrm{d}s + \int_{\mathcal{E}_0} h^{-1}[\![\nabla u_h]\!]_0 \cdot [\![\nabla\varphi_h]\!]_0 \,\mathrm{d}s.$$

This term has been added to enforce smoothness and continuity across elements.

We note that the principal difference to the above methods is the change from φ_h to $A : D^2\varphi_h$, which gives the problem symmetry, but results in a higher order approximation. This leads to the benefit of higher regularity, however the fourth order nature of the problem could lead to higher computational costs.

In terms of convergence results, an equivalent approximation to (3.8) is proved, and this is verified for the $k = 2$ case in the L^2, H^1 and H^2 norms.

Now for the derivation within this paper, we consider a method that is similar to example 3.2.5, but takes a more general form. In section 3.3 we will fully introduce this idea and explain the differences to the above methods.

3.3 Minimization Method

In the following we look at a derivation for a new method which comes from minimizing the problem. We will first give an outline of the continuous formulation of the problem, before moving to the discrete case which will be the basis for our numerical method. Specifically the saddle point formulation in section 3.3.1 is used in the computations.

First of all, in order to set up the problem in general terms, let V be a Hilbert space with inner product $a(\cdot,\cdot) : V \times V \to \mathbb{R}$ (i.e. a symmetric, positive definite, bilinear form). We wish to consider two different cases for this method. In the first case we will choose $V = L^2(\Omega)$ and $a(v,w) = \int_\Omega vw \,\mathrm{d}x$ and in the second we will choose $V = H^1(\Omega)$ and $a(v,w) = \int_\Omega \nabla v \cdot \nabla w \,\mathrm{d}x + \beta h^{-1} \int_{\partial\Omega} vw \,\mathrm{d}s$, where $\beta > 0$.

Now the Riesz representation theorem says that for every $w \in V^*$, there exists a unique $u \in V$ such that,

$$a(u,v) = \langle w, v\rangle, \quad \forall v \in V.$$

where $\langle \cdot, \cdot \rangle : V^* \times V \to \mathbb{R}$ is the dual pairing. From this we can define an invertible projection operator $\mathcal{N} : V^* \to V$ which has the property

$$a(\mathcal{N}w, v) = \langle w, v \rangle, \quad \forall v \in V, \tag{3.10}$$

We can additionally define a norm using $\mathcal{N}$ and a as

$$\|w\|_{\mathcal{N}}^2 := a(\mathcal{N}w, \mathcal{N}w), \quad \forall w \in V^*. \tag{3.11}$$

We note that this norm is defined in the dual of V, however in the case of $V = L^2$, they are equivalent.

Using the above definitions, we can reformulate (3.1) as a minimization problem as follows.

Definition 3.3.1 (Continuous Minimization Formulation)**.** Let $u \in H^2(\mathcal{T}) \cap H_0^1(\Omega) \subset V$ such that for $J : H^2(\mathcal{T}) \cap H_0^1(\Omega) \to \mathbb{R}^+$

$$J(u) := \frac{1}{2}\|A : D_h^2 u + f\|_{\mathcal{N}}^2 \quad \to \quad \min, \tag{3.12}$$

Then we call (3.12) the **continuous minimization formulation** of (3.1).

Here $D_h^2 u \in L^2(\Omega)$ is a piecewise approximation to the Hessian, i.e. $D_h^2 v|_K = D^2 v|_K$ for all $K \in \mathcal{T}$, which we will use for the remainder of this method.

Remark. We note that it is necessary to have $u \in H^2(\mathcal{T}) \cap H_0^1(\Omega)$ for the continuous case, however for the discrete case we will instead be working with $u \in V_h$.

Now by formulating the Euler-Lagrange equation of the above, by taking the functional derivative, we get a variational version of (3.12).

Definition 3.3.2 (Continuous Euler-Lagrange Formulation)**.** Let $u \in W$ such that

$$a(\mathcal{N}(A : D_h^2 u), \mathcal{N}(A : D_h^2 \varphi)) = l(\varphi), \quad \forall \varphi \in W, \tag{3.13}$$

where the right-hand side is defined by

$$l(\varphi) = -a(\mathcal{N}f, \mathcal{N}(A : D_h^2\varphi)).$$

Then (3.13) is the **continuous Euler-Lagrange formulation** of (3.12).

We note that this formulation is written in a general way so that it can take different forms depending on the choices of $a(\cdot,\cdot)$ (and by extension V). These different cases will be considered later on.

Now let us consider a discrete version of the problem. Note that the discrete version keeps virtually the same structure, with the only changes being the use of V_h, $\mathcal{N}_h$, and u_h, which are discrete versions of the above.

In particular $\mathcal{N}_h$ is a standard Galerkin approximation to $\mathcal{N}$, and takes a similar form to (3.10).

Definition 3.3.3 ($\mathcal{N}_h$ projection)**.** Recall $V_h = C^0(\Omega) \cap P^k(\mathcal{T})$. We define $\mathcal{N}_h : V^* \to V_h$ by

$$a(\mathcal{N}_h v_h, \varphi_h) = (v_h, \varphi_h)_{L^2}, \quad \forall \varphi_h \in V_h. \tag{3.14}$$

First, we note that we make a standard assumption related to the difference between our non-discrete and discrete projection operators $\mathcal{N}$ and $\mathcal{N}_h$.

Assumption 3.3.1. *For $\mathcal{N}v \in H^k$, $k \in \mathbb{N}$ and $0 \leq m \leq k$*

$$\|(\mathcal{N} - \mathcal{N}_h)v\|_m \leq Ch^{k-m}\|\mathcal{N}v\|_k. \tag{3.15}$$

We can also derive the following bound on the discrete projector by the non-discrete version.

Lemma 3.3.1 ($\mathcal{N}_h$ bound)**.** *Let $\|v\|_a := a(v,v)$ for $v \in V$. Then*

$$\|\mathcal{N}_h v\|_a \leq C\|\mathcal{N}v\|_a, \quad \forall v \in V^*. \tag{3.16}$$

Proof.

$$\begin{aligned}
\|\mathcal{N}_h v\|_a^2 &= a(\mathcal{N}_h v, \mathcal{N}_h v), \\
&= a(\mathcal{N} v, \mathcal{N}_h v), && \text{(due to Galerkin orthogonality of } \mathcal{N}_h) \\
&\leq C\|\mathcal{N} v\|_a \|\mathcal{N}_h v\|_a, && \text{(by boundedness of } a(\cdot,\cdot))
\end{aligned}$$

Thus we divide through by $\|\mathcal{N}_h v\|_a$ to get $\|\mathcal{N}_h v\|_a \leq C\|\mathcal{N} v\|_a$. □

Having defined these discretized concepts, let us now consider the minimization formulation which we will use as the basis for our finite element method.

Definition 3.3.4 (Euler-Lagrange Formulation)**.** Let $u_h \in V_h$ such that

$$a(\mathcal{N}_h(A : D_h^2 u_h), \mathcal{N}_h(A : D_h^2 \varphi_h)) + s(u_h, \varphi_h) = l_h(\varphi_h), \quad \forall \varphi_h \in V_h, \tag{3.17}$$

where we have added a stabilization term $s(\cdot,\cdot)$, defined by

$$s(v,w) := \int_{\mathcal{E}} \beta_1 h^p [\![\nabla v]\!] \cdot [\![\nabla w]\!] \,\mathrm{d}s + \beta_2 h^q \int_\Omega A : D_h^2 v A : D_h^2 w \,\mathrm{d}x + \beta_3 h^r \int_{\partial\Omega} vw \,\mathrm{d}s,$$

where $\beta_1, \beta_2, \beta_3 > 0$ are parameters, h is the grid size, $p, q, r \in \mathbb{Z}$ and $l_h(\cdot)$ is

$$l_h(v) := -a(\mathcal{N}_h f, \mathcal{N}_h(A : D_h^2 v)) - \beta_2 h^q \int_\Omega f A : D_h^2 v \,\mathrm{d}x.$$

Then (3.17) is the discrete **Euler-Lagrange formulation** of (3.1).

For convenience we denote the left hand side of (3.17) by

$$b_h(v,w) := a(\mathcal{N}_h(A : D_h^2 v), \mathcal{N}_h(A : D_h^2 w)) + s(v,w). \tag{3.18}$$

Remark. The values of p, q, r will vary depending on the choice of $a(\cdot,\cdot)$, as this will change the h-scaling of the first term in b_h, thus we leave them unspecified.

It is quite easy to show Galerkin orthogonality for this problem, which shows that it is consistent with the original one.

Lemma 3.3.2 (Galerkin Orthogonality)**.** *Let $u \in W = H^2(\Omega) \cap H_0^1(\Omega)$ be the*

solution to (3.1), and $b_h(\cdot,\cdot)$ be defined as in (3.18). Then we have

$$b_h(u,v) = l_h(v), \quad \forall v \in V_h. \tag{3.19}$$

Consequently,

$$b_h(u - u_h, v) = 0, \quad \forall v \in V_h.$$

Proof.

$$\begin{aligned}
&b_h(u,v) - l_h(v),\\
=&a(\mathcal{N}_h(A:D_h^2 u), \mathcal{N}_h(A:D_h^2 v)) + \int_{\mathcal{E}} \beta_1 h^p [\![\nabla u]\!]\cdot[\![\nabla v]\!]\,\mathrm{d}s + \beta_2 h^q (A:D_h^2 u, A:D_h^2 v)_{L^2},\\
&+\beta_3 h^r \int_{\partial\Omega} uv\,\mathrm{d}s + a(\mathcal{N}_h f, \mathcal{N}_h A:D_h^2 v) + \beta_2 h^q (A:D_h^2 f, A:D_h^2 v)_{L^2}\\
=&(A:D_h^2 u + f, \mathcal{N}_h(A:D_h^2 v))_{L^2} + \beta_2 h^q (A:D_h^2 u + f, A:D_h^2 v)_{L^2}\\
&+\beta_3 h^r \int_{\partial\Omega} uv\,\mathrm{d}s, \qquad \text{(using (3.14) and } [\![\nabla u]\!] = 0),\\
=&0,
\end{aligned}$$

where we have used the fact $-A:D_h^2 u = f$ in Ω and $u = 0$ on $\partial\Omega$. □

We can also prove the existence of a unique solution fairly easily due to the choice of stabilization term.

Lemma 3.3.3 (Existence and Uniqueness)**.** *Assume that the original equation (3.1) has a unique solution $u_h \in W$. Then for $\beta_1, \beta_2, \beta_3 > 0$, the approximation (3.17) has a unique solution $u_h \in V_h$.*

Proof. This follows by taking $f = 0$ and showing the solution u_h must be zero. Setting $f = 0$ in (3.17) and taking $\varphi_h = u_h$ gives

$$\begin{aligned}
0 =&a(\mathcal{N}_h(A:D_h^2 u_h), \mathcal{N}_h(A:D_h^2 u_h)) + s(u_h, u_h),\\
=&\|N_h(A:D_h^2 u_h)\|_a^2 + \beta_1 h^p \|[\![\nabla u_h]\!]\|_{\mathcal{E}}^2 + \beta_2 h^q \|A:D_h^2 u_h\|_0^2 + \beta_3 h^r \|u_h\|_{\partial\Omega}^2.
\end{aligned}$$

where $\|\cdot\|_{\mathcal{E}}$ denotes the L^2 norm over the skeleton of the grid and $\|\cdot\|_{\partial\Omega}$ denotes the L^2 norm over the boundary.

Since every term in this expression is ≥ 0, they must each be zero. Thus we have $[\![\nabla u_h]\!] = 0$ on $\mathcal{E}$, which means u_h is smooth across elements, so $u_h \in C^1(\Omega)$. We already had $u_h \in C^0(\Omega) \cap P^k(\mathcal{T})$, so $u_h \in C^1(\Omega) \cap P^k(\mathcal{T})$, which by extension means $u_h \in H^2(\Omega)$. Additionally since $u_h|_{\partial\Omega} = 0$, we have that $u_h \in W$. Next since $A : D_h^2 u_h = 0$ (and $u_h|_{\partial\Omega} = 0$), u_h is a piecewise solution to (3.1) when $f = 0$. Since at the start we assumed the solution to (3.1) was unique, and $u_h \in W$, this means $u_h = 0$. □

Let us now return to the two specific examples of the method, which come from selecting appropriate choices for V and $a(\cdot, \cdot)$.

Example 3.3.1 (L^2 Minimization)**.** Let $V = L^2(\Omega)$ and $a(v, w) = \int_\Omega vw \, \mathrm{d}x$ (thus $\|\cdot\|_{\mathcal{N}}$ is simply the L^2 norm). In this case $\mathcal{N}_h$ defined in (3.14) is the discrete L^2 projection $P_h : L^2(\Omega) \to V_h$ defined by

$$\int_\Omega P_h v \varphi_h \, \mathrm{d}x = \int_\Omega v \varphi_h \, \mathrm{d}x, \quad \forall \varphi_h \in V_h. \tag{3.20}$$

So the discrete problem becomes

$$\int_\Omega P_h(A : D_h^2 u_h) P_h(A : D_h^2 \varphi_h) \, \mathrm{d}x + s(u_h, \varphi_h) = l_h(\varphi_h), \quad \forall \varphi \in V_h, \tag{3.21}$$

where we choose $p = -1, q = 0, r = -3$ in $s(u_h, \varphi_h)$.

Remark 1. The formulation in (3.21) is similar to the one presented in Mu and Ye [2017], with the discrete projection P_h and a different penalty term being the main differences.

Remark 2. The choice of p, q and r comes from examining how each term scales in magnitude with regards to the grid size h. For the main component,

$$\int_\Omega P_h(A : D_h^2 u_h) P_h(A : D_h^2 \varphi_h) \, \mathrm{d}x$$

we can state that the $D_h^2 u_h$ and $D_h^2 \varphi_h$ each provide approximately $\mathcal{O}(h^{-2})$ scaling, whilst the integral $\mathrm{d}x$ itself provides $\mathcal{O}(h^2)$ scaling, giving $\mathcal{O}(h^{-2}h^{-2}h^2) = \mathcal{O}(h^{-2})$

overall. Applying similar logic to the $s(u_h, \varphi_h)$ terms, we find that

$$\begin{aligned}
&\beta_1 h^p \int_{\mathcal{E}} [\![\nabla v]\!]_0 \cdot [\![\nabla w]\!]_0 \,\mathrm{d}s \approx \mathcal{O}(h^p h^{-2} h) = \mathcal{O}(h^{p-1}) \\
&\beta_2 h^q \int_{\Omega} A : D_h^2 v, A : D_h^2 w \,\mathrm{d}x \approx \mathcal{O}(h^q h^{-4} h^2) = \mathcal{O}(h^{q-2}) \\
&\beta_3 h^r \int_{\partial\Omega} vw \,\mathrm{d}s \approx \mathcal{O}(h^r h^0 h) = \mathcal{O}(h^{r+1})
\end{aligned}$$

In order to match the original $\mathcal{O}(h^{-2})$, we thus choose $p = -1, q = 0, r = -3$.

Example 3.3.2 (H^{-1} Minimization)**.** Let $V = H^1(\Omega)$ and $a(v, w) = \int_\Omega \nabla v \cdot \nabla w \,\mathrm{d}x + \beta_3 h^{-1} \int_{\partial\Omega} vw \,\mathrm{d}s$ (in which case $\|\cdot\|_a^2 = |\cdot|_1^2 + h^{-1}\|\cdot\|_{\partial\Omega}^2$ where $|\cdot|_1$ is the H^1 seminorm). In this case, $\mathcal{N}_h$ is the (discrete) Ritz projection $\mathcal{N}_h : H^{-1}(\Omega) \to V_h$ defined by

$$\int_\Omega \nabla \mathcal{N}_h w \nabla \varphi_h \,\mathrm{d}x + \frac{\beta_3}{h} \int_{\partial\Omega} \mathcal{N}_h w \varphi_h \,\mathrm{d}s = \int_\Omega w \varphi_h \,\mathrm{d}x, \quad \forall \varphi_h \in V_h. \tag{3.22}$$

This gives us the following approximation.

$$\begin{aligned}
&\int_\Omega \nabla \mathcal{N}_h (A : D_h^2 u_h) \cdot \nabla \mathcal{N}_h (A : D_h^2 \varphi_h) \,\mathrm{d}x \\
&+ \frac{\beta_3}{h} \int_{\partial\Omega} \mathcal{N}_h (A : D_h^2 u_h) \mathcal{N}_h (A : D_h^2 \varphi_h) \,\mathrm{d}s + s(u_h, \varphi_h) = l_h(\varphi_h), \quad \forall \varphi_h \in V_h,
\end{aligned} \tag{3.23}$$

where we choose $p = 1, q = 2, r = -1$ in $s(u_h, \varphi_h)$ using the same logic as in example 3.3.1, remark 2.

Remark. In this case the original problem is equivalent to the minimization of $A : D_h^2 u_h - f$ in the H^{-1} norm.

Remark 2. This form for $a(\cdot, \cdot)$ comes from Nitsche's method (see Freund and Stenberg [1995]) for solving Poisson's equation. The second term is added to weakly impose boundary conditions so that $a(\cdot, \cdot)$ is invertible (the alternative would be working in $V = H_0^1$ and not using the term). We note that there exist additional terms $\int_{\partial\Omega} \nabla v \cdot \mathbf{n} w \,\mathrm{d}s - \int_{\partial\Omega} \nabla w \cdot \mathbf{n} v \,\mathrm{d}s$ in the full method that can be added for consistency, however as they do not appear to affect our numerical results we do not use them to simplify the presentation.

3.3.1 Saddle Point Formulation

One potential weakness to the forms (3.21) and (3.23) is that they can be tricky to implement numerically. For one, P_h and N_h require extra effort to implement. Another problem is the $D_h^2\varphi$ term present in these equations, since in later sections (specifically we refer to example 3.5.1) we plan to replace D_h^2 with $H[\cdot]$, and $H[\varphi]$ lacks an implementation in Dune-Fempy.

Thus we look here to rewrite the approximation into the form of a saddle point problem. This is the form we will use later in computational results, and we can also show directly the appeal of example 3.3.2 in terms of the complexity of the problem. To obtain this form, we introduce an additional variable.

$$\sigma = -\mathcal{N}_h(A : D_h^2 u_h + f). \tag{3.24}$$

Taking $a(\cdot, \varphi_h)$ of both sides of (3.24), and substituting σ into (3.17), we get two equations,

$$\begin{aligned} a(\sigma, \varphi_h) &= -a(\mathcal{N}_h(A : D_h^2 u_h + f), \varphi_h), \\ a(\sigma, \mathcal{N}_h(A : D_h^2 \varphi_h)) - s(u_h, \varphi_h) &= -\beta_2 h^q (f, A : D_h^2 \varphi_h). \end{aligned}$$

Recalling property (3.14), i.e. $a(\mathcal{N}_h w, v) = (w, v)_{L^2}$, and rearranging the first equation, this can be rewritten as

$$\begin{aligned} a(\sigma, \varphi_h) + (A : D_h^2 u_h, \varphi_h) &= -(f, \varphi_h), \\ (\sigma, A : D_h^2 \varphi_h) - s(u_h, \varphi_h) &= -\beta_2 h^q (f, A : D_h^2 \varphi_h). \end{aligned}$$

Letting $b(v, w) := (A : D_h^2 v, w)$, we can think of the above in terms of bilinear forms instead.

$$\begin{aligned} a(\sigma, \varphi_h) + b(u_h, \varphi_h) &= -(f, \varphi_h), \\ b(\varphi_h, \sigma) - s(u_h, \varphi_h) &= -\beta_2 h^q b(\varphi_h, f). \end{aligned}$$

We can then rewrite this system in matrix-vector form as

$$\begin{pmatrix} M & B \\ B^T & -S \end{pmatrix} \begin{pmatrix} \boldsymbol{\sigma} \\ \mathbf{u} \end{pmatrix} = - \begin{pmatrix} \mathbf{f} \\ \mathbf{g} \end{pmatrix} \tag{3.25}$$

where here we can think of B as representing $b(\cdot, \varphi_h)$, S as representing $s(\cdot, \varphi_h)$ and M as $a(\cdot, \varphi_h)$. The Schur complement of this is then the following.

$$\big(B^T M^{-1} B + S\big)\mathbf{u} = -B^T M^{-1}\mathbf{f} - \mathbf{g}. \tag{3.26}$$

Thus we can see the differences between the two examples in terms of the order of the complexity of the problem. In the case $a(\cdot, \cdot)$ is the L^2 inner product, M is approximately the identity, i.e. of order 0. On the other hand if $a(v, w) = \int_\Omega \nabla v \cdot \nabla w \, \mathrm{d}x + \beta_3 h^{-1} \int_{\partial\Omega} vw \, \mathrm{d}s$, then M becomes the discrete Laplace operator, so M^{-1} is of order -2.

From this we can see that the primary advantage of the H^{-1} approach in comparison to the L^2 version is that the order of the method is $\mathcal{O}(h^2 h^{-2} h^2) = \mathcal{O}(h^2)$, in comparison to $\mathcal{O}(h^4)$.

3.4 Error Analysis

3.4.1 Error Bound for H^{-1} Method

As stated previously, analysis of a method similar to example 3.3.1 has already been carried out in Mu and Ye [2017]. Thus for the rest of this chapter, we will focus on the discrete problem for the $V = H^1$ case. Let us state this formulation again.

Example 3.4.1 (H^{-1} Minimization)**.** Since we are just dealing with a single example now, let us take $p = 1, q = 2, r = -1$ in $s(u, v)$. This results in the discrete

problem of finding $u_h \in V_h$ such that

$$\begin{aligned}&\int_\Omega \nabla \mathcal{N}_h(A : D_h^2 u_h) \cdot \nabla \mathcal{N}_h(A : D_h^2 \varphi_h) \,\mathrm{d}x \\ &+ \frac{\beta_3}{h} \int_{\partial\Omega} \mathcal{N}_h(A : D_h^2 u_h) \mathcal{N}_h(A : D_h^2 \varphi_h) \,\mathrm{d}s + s(u_h, \varphi_h) = l_h(\varphi_h), \quad \forall \varphi_h \in V_h,\end{aligned} \tag{3.23}$$

where

$$s(v, w) = \int_{\mathcal{E}} \beta_1 h [\![\nabla v]\!] \cdot [\![\nabla w]\!] \,\mathrm{d}s + \beta_2 h^2 \int_\Omega A : D_h^2 v A : D_h^2 w \,\mathrm{d}x + \frac{\beta_3}{h} \int_{\partial\Omega} vw \,\mathrm{d}s,$$

and

$$l_h(v) = -a(\mathcal{N}_h f, \mathcal{N}_h(A : D_h^2 v)) - \beta_2 h^2 \int_\Omega f A : D_h^2 v \,\mathrm{d}x.$$

We also note that in this example $\mathcal{N}$ acts as the inverse Laplace operator, and we make the assumption that it has elliptic regularity, i.e. for any $v \in V_h$, we have

$$|\mathcal{N} v|_{H^2} \leq \|v\|_{L^2}, \tag{3.27}$$

where $|\cdot|_{H^2}$ denotes the H^2 seminorm. Now for the following error analysis it will be convenient to introduce a bilinear form using $\mathcal{N}$ instead of $\mathcal{N}_h$ as follows.

$$b(v, w) = a(\mathcal{N}(A : D_h^2 v), \mathcal{N}(A : D_h^2 w)) + s(v, w).$$

Note that this is equivalent to the LHS of the Euler-Lagrange formulation (3.17), save for the $\mathcal{N}$ replacing $\mathcal{N}_h$. For the choice of $a(\cdot, \cdot)$ given in the H^1 case, this becomes

$$\begin{aligned}b(v, w) = &\int_\Omega \nabla \mathcal{N}(A : D_h^2 v) \cdot \nabla \mathcal{N}(A : D_h^2 w) \,\mathrm{d}x + \frac{\beta_3}{h} \int_{\partial\Omega} \mathcal{N}(A : D_h^2 v) \mathcal{N}(A : D_h^2 w) \,\mathrm{d}s \\ &+ \int_{\mathcal{E}} \beta_1 h [\![\nabla v]\!] \cdot [\![\nabla w]\!] \,\mathrm{d}s + \beta_2 h^2 \int_\Omega A : D_h^2 v A : D_h^2 w \,\mathrm{d}x + \frac{\beta_3}{h} \int_{\partial\Omega} vw \,\mathrm{d}s.\end{aligned}$$

From this we define the norm $\|v\|_b^2 = b(v, v)$, $\forall v \in V_h$. Explicitly,

$$\|v\|_b^2 = \|A : D_h^2 v\|_{\mathcal{N}}^2 + \beta_1 h \|[\![\nabla v]\!]\|_{\mathcal{E}}^2 + \beta_2 h^2 \|A : D_h^2 v\|_0^2 + \beta_3 h^{-1} \|v\|_{\partial\Omega}^2. \tag{3.28}$$

Recall $\|\cdot\|_{\mathcal{E}}$ denotes the L^2 norm over the skeleton of the grid and $\|\cdot\|_{\partial\Omega}$ denotes the L^2 norm over the boundary.

The primary reason for defining this norm is that we can use it to show convergence results by proving that the LHS of (3.17) is coercive and bounded with respect to it. Let us show this now.

Lemma 3.4.1 (Coercivity of $b_h(v,w)$)**.** *For β_2 large enough, we have that for all $v \in V_h$,*

$$b_h(v,v) \geq C\|v\|_b^2.$$

Proof. By definition from (3.18),

$$b_h(v,v) := a(\mathcal{N}_h(A : D_h^2 v), \mathcal{N}_h(A : D_h^2 v)) + s(v,v).$$

Let us consider these terms separately. First we start with the $a(\cdot,\cdot)$ component.

$$\begin{aligned}
& a(\mathcal{N}_h(A : D_h^2 v), \mathcal{N}_h(A : D_h^2 v)), \\
=& a((\mathcal{N}_h - \mathcal{N})(A : D_h^2 v), \mathcal{N}_h(A : D_h^2 v)) \\
& + a(\mathcal{N}(A : D_h^2 v), \mathcal{N}_h(A : D_h^2 v)), \\
=& ((\mathcal{N}_h - \mathcal{N})(A : D_h^2 v), A : D_h^2 v)_{L^2} && \text{(using (3.14))} \\
& + a(\mathcal{N}(A : D_h^2 v), \mathcal{N}(A : D_h^2 v)), && \text{(using G.O. of } \mathcal{N}_h) \\
\geq& - \|(\mathcal{N}_h - \mathcal{N})(A : D_h^2 v)\|_0 \|A : D_h^2 v\|_0 && \text{(using Cauchy-Schwarz)} \\
& + \|A : D_h^2 v\|_{\mathcal{N}}^2, \\
\geq& - Ch^2 \|\mathcal{N}(A : D_h^2 v)\|_2 \|A : D_h^2 v\|_0 && \text{(using assumption 3.3.1, i.e.} \\
& + \|A : D_h^2 v\|_{\mathcal{N}}^2, && \|(\mathcal{N}_h - \mathcal{N})g\|_0 \leq Ch^2\|\mathcal{N}g\|_2.) \\
\geq& - Ch^2 \|A : D_h^2 v\|_0^2 + \|A : D_h^2 v\|_N^2. && \text{(using (3.27))}
\end{aligned}$$

We now add in the penalty term (which helps account for the negative term). We

get

$$\begin{aligned} b_h(v,v) \geq & \|A : D_h^2 v\|_N^2 - Ch^2 \|A : D_h^2 v\|_0^2 \\ & + \beta_1 h \|\nabla v\|_{\mathcal{E}}^2 + \beta_2 h^2 \|A : D_h^2 v\|_0^2 + \beta_3 h^{-1} \|v\|_{\partial\Omega}^2 \\ = & \|A : D_h^2 v\|_N^2 + (\beta_2 - C) h^2 \|A : D_h^2 v\|_0^2 + \beta_1 h \|[\![\nabla v]\!]\|_{\mathcal{E}}^2 + \beta_3 h^{-1} \|v\|_{\partial\Omega}^2. \end{aligned}$$

From here we can see that by taking $\beta_2 > C$, the above expression can be bounded from below by (3.28) multiplied by a constant. □

Lemma 3.4.2 (Boundedness of $b_h(v,w)$)**.** *For all $v, w \in V$,*

$$b_h(v,w) \leq C \|v\|_b \|w\|_b.$$

Proof.

$$\begin{aligned} & b_h(v,w) \\ = & a(\mathcal{N}_h(A : D_h^2 v), \mathcal{N}_h(A : D_h^2 w)) + \int_{\mathcal{E}} \beta_1 h [\![\nabla v]\!] \cdot [\![\nabla w]\!] \, \mathrm{d}s \\ & + \beta_2 h^2 \int_\Omega A : D_h^2 v A : D_h^2 w \, \mathrm{d}x + \beta_3 h^{-1} \int_{\partial\Omega} vw \, \mathrm{d}s, \\ \leq & C_1 \|\mathcal{N}_h(A : D_h^2 v)\|_a \|\mathcal{N}_h(A : D_h^2 w)\|_a + \beta_1 h \|[\![\nabla v]\!]\|_{\mathcal{E}} \|[\![\nabla w]\!]\|_{\mathcal{E}} \qquad (*) \\ & + \beta_2 h^2 \|A : D_h^2 v\|_0 \|A : D_h^2 w\|_0 + \beta_3 h^{-1} \|v\|_{\partial\Omega} \|w\|_{\partial\Omega}, \\ \leq & C_2 \|\mathcal{N}(A : D_h^2 v)\|_a \|\mathcal{N}(A : D_h^2 w)\|_a + \beta_1 h \|[\![\nabla v]\!]\|_{\mathcal{E}} \|[\![\nabla w]\!]\|_{\mathcal{E}} \qquad (**) \\ & + \beta_2 h^2 \|A : D_h^2 v\|_0 \|A : D_h^2 w\|_0 + \beta_3 h^{-1} \|v\|_{\partial\Omega} \|w\|_{\partial\Omega}, \\ \leq & C_2 \|v\|_b \|w\|_b + \|v\|_b \|w\|_b + \|v\|_b \|w\|_b + \|v\|_b \|w\|_b, \\ \leq & C_3 \|v\|_b \|w\|_b. \end{aligned}$$

□

(In step $(*)$ we have used the boundedness of $a(\cdot,\cdot)$ and of the Cauchy-Schwarz inequality, and in step $(**)$ we have used lemma 3.3.1.)

Now we will look to create a bound for the difference between the original solution u and discrete solution u_h for this method.

For the upcoming lemma we will make use of the standard result with regards

to the Lagrange interpolation operator I_h that is similar to assumption 3.3.1.

Lemma 3.4.3 (Lagrange Interpolation Estimate)**.** *Suppose $v \in H^r(\Omega)$ and let $I_h : H^r(\Omega) \to V_h$ where $V_h = C^0(\Omega) \cap P^k(\mathcal{T})$. Then for $0 \leq m \leq p$ and $p = \min\{k+1, r\}$,*

$$\|v - I_h v\|_m \leq C h^{p-m} \|v\|_p.$$

Proof. See e.g. [Ciarlet and Raviart, 1972, Thm 5].

Remark. Naturally in the case where v is arbitrarily smooth, this becomes

$$\|v - I_h v\|_m \leq C h^{k+1-m} \|v\|_{k+1}.$$

Then we have the following bound on the difference between the solution and its interpolation in the $\|\cdot\|_b$ norm.

Lemma 3.4.4 ($\|\cdot\|_b$ Interpolation Estimate)**.** *Let I_h be the Lagrange interpolation operator defined in lemma 3.4.3. Then for $V_h = C^0(\Omega) \cap P^k(\mathcal{T})$, where $k \in \mathbb{N}$, $k \geq 2$ and $v \in H^{k+1}(\Omega)$ we have*

$$\|v - I_h v\|_b \leq C h^{k-1} \|v\|_{k+1}. \tag{3.29}$$

Proof. Recall that the $\|\cdot\|_b$ is defined by

$$\|v\|_b^2 = \|A : D_h^2 v\|_{\mathcal{N}}^2 + \beta_1 h \|[\![\nabla v]\!]\|_{\mathcal{E}}^2 + \beta_2 h^2 \|A : D_h^2 v\|_0^2 + \beta_3 h^{-1} \|v\|_{\partial\Omega}^2. \tag{3.28}$$

For the first term, we have

$$\begin{aligned}
&\|A : D_h^2 v\|_{\mathcal{N}}^2 \\
=&a(\mathcal{N}(A : D_h^2 v), \mathcal{N}(A : D_h^2 v)) \\
=&(A : D_h^2 v, \mathcal{N}(A : D_h^2 v))_{L^2} && \text{(using (3.10))} \\
\leq&\|A : D_h^2 v\|_0 \cdot \|\mathcal{N}(A : D_h^2 v)\|_0 && \text{(using Cauchy-Schwarz inequality)} \\
\leq&C\|A : D_h^2 v\|_0 \cdot |\mathcal{N}(A : D_h^2 v)|_1 && \text{(using Poincaré inequality)} \\
\leq&C\|A : D_h^2 v\|_0 \cdot \|\mathcal{N}(A : D_h^2 v)\|_a \\
=&C\|A : D_h^2 v\|_0 \cdot \|A : D_h^2 v\|_{\mathcal{N}}
\end{aligned}$$

Thus dividing through by $\|A : D_h^2 v\|_{\mathcal{N}}$ we get

$$\|A : D_h^2 v\|_{\mathcal{N}} \leq C\|A : D_h^2 v\|_0.$$

We also note that for the last term, after substituting $v - I_h v$, we can simply use the trace theorem, i.e.

$$\begin{aligned}
\frac{\beta_3}{h}\|v - I_h v\|_{\partial\Omega} &\leq \frac{C}{h}\|v - I_h v\|_1 \\
&\leq Ch^{k-1}\|v - I_h v\|_{k+1} && \text{(using (3.4.3))}
\end{aligned}$$

Then the result follows by using [Mu and Ye, 2017, p308, Lemma 3], i.e.

$$\|A : D_h^2(v - I_h v)\|_0 + h^{-1}\|[\![v - I_h v]\!]\|_{\mathcal{E}_0} + h^{-1}\|[\![\nabla(v - I_h v)]\!]\|_{\mathcal{E}} \leq Ch^{k-1}\|v\|_{k+1},$$

where we recall $\mathcal{E}_0 = \mathcal{E}\backslash\partial\Omega$. Putting $v - I_h v$ into $\|v\|_b$, and noting that h is small, and we can see that it is bounded by the above expression times a constant. □

With these results, we can now prove the following error estimate.

Theorem 3.4.1. *Let u be the solution to (3.1) and let $u_h \in V_h$ be the solution to*

the approximation (3.23). Then we have

$$\|u - u_h\|_b \leq Ch^{k-1}\|u\|_{k+1}.$$

Proof. Via the triangle inequality, we have

$$\|u - u_h\|_b \leq \|u - I_h u\|_b + \|I_h u - u_h\|_b.$$

For the first term we can apply lemma 3.4.4, i.e.

$$\|u - I_h u\|_b \leq h^{k-1}\|u\|_{k+1}.$$

For the second, we have

$$\begin{aligned}
&\|I_h u - u_h\|_b^2 \\
\leq& Cb_h(I_h u - u_h, I_h u - u_h) && \text{(coercivity of } b_h(\cdot,\cdot)) \\
\leq& C(b_h(u - u_h, I_h u - u_h) - b_h(u - I_h u, I_h u - u_h)) && (\pm b_h(u, I_h u - u_h)) \\
\leq& C(b_h(u, I_h u - u_h) - l_h(I_h u - u_h) - b_h(u - I_h u, I_h u - u_h)) && \text{(since } b_h(u_h, v) = l_h(v)) \\
\leq& Cb_h(u - I_h u, I_h u - u_h) && \text{(lemma 3.3.2)} \\
\leq& C\|u - I_h u\|_b \|I_h u - u_h\|_b && \text{(boundedness of } b(\cdot,\cdot)) \\
\leq& Ch^{k-1}\|u\|_{k+1}\|I_h u - u_h\|_b && \text{(lemma 3.4.4)}
\end{aligned}$$

Dividing through by $\|I_h u - u_h\|_b$, we get

$$\|I_h u - u_h\|_b \leq Ch^{k-1}\|u\|_{k+1}.$$

Adding the two together gives us

$$\|u - u_h\|_b \leq Ch^{k-1}\|u\|_{k+1}.$$

This concludes the proof. □

Remark. Although this result is consistent with other results in the literature (e.g. [Mu and Ye, 2017, Thm 1]), we remark that it in practice the convergence rate is greater than indicated, which we demonstrate in section 3.4.2.

3.4.2 Numerical Demonstration of H^{-1} Interpolation Error

Recall the bound for the interpolation error given in lemma 3.4.4

$$\|v - I_h v\|_b \leq Ch^{k-1}\|v\|_{k+1},$$

which ultimately leads to the error estimate in theorem 3.4.1. In particular for the case of $k = 1$, this leads to linear basis functions and no scaling with the grid size h. This is clearly accurate if one considers that for linear basis functions of the form $I_h v = ax$, $D^2(I_h v) = 0$, thus

$$\begin{aligned}\|v - I_h v\|_b :=& \|A : D_h^2(v - I_h v)\|_{\mathcal{N}}^2 + \beta_1 h\|[\![\nabla(v - I_h v)]\!]\|_{\mathcal{E}}^2 \\ &+ \beta_2 h^2\|A : D_h^2(v - I_h v)\|_0^2 + \beta_3 h^{-1}\|v - I_h v\|_{\partial\Omega} \\ =& \|v\|_b + \beta_1 h\|[\nabla I_h v]\|_{\mathcal{E}} + \beta_3 h^{-1}\|I_h v\|_{\partial\Omega},\end{aligned} \tag{3.30}$$

which does not converge as h decreases.

On the other hand for $k = 2$ we have quadratic functions and a factor of h. Now whilst the estimate may be accurate for the linear case, numerical experiments we have done would indicate that this result might be suboptimal for the H^{-1} minimization method, even if it is still accurate for the L^2 minimization method. We demonstrate the actual computational difference between the two methods here.

To start off with, we examine the simple case where $A = I$ in (3.1), which results in $-\Delta u = f$, giving us Poisson's equation. For our experiments we suppose we have a smooth exact solution $u = \sin(2\pi x)\sin(2\pi y)$, and that we use a second order interpolation $I_h u$.

In that case the error for the L^2 method we want to examine is $\|\Delta(u - I_h u)\|_0$. For the H^{-1} method, we want to compute $\|\nabla\mathcal{N}\Delta(u - I_h u)\|_0$, which we can approximate via $\|\nabla\mathcal{N}_h\Delta(u - I_h u)\|_0$. We can then calculate $\mathcal{N}_h\Delta v$ numerically by

using (3.14) and substituting in Δv. That is to say we solve for ξ (in a P_3 space),

$$(\nabla\xi, \nabla w) = (\Delta(u - I_h u), w).$$

Additionally we can in this simple case note that since $\mathcal{N}_h$ approximates the inverse Laplace operator, $\|\nabla\mathcal{N}_h\Delta(u - I_h u)\| \approx \|\nabla(u - I_h u)\|$, so we consider this too for comparison.

To compare the convergence of the error we will compute the estimated order of convergence (EOC) using the formula.

$$EOC = \frac{\log(\text{error}_{new}/\text{error}_{old})}{\log(h_{new}/h_{old})}.$$

Calculating the above in DUNE-FEMPY and varying the grid size, we get the results in table 3.1 (letting $e_h = u - I_h u$). From this we are able to show that the kind

Table 3.1: Interpolation error in the Laplace case for different norms

Elements	$\|\Delta e_h\|$	EOC	$\|\nabla\mathcal{N}_h(\Delta e_h)\|$	EOC	$\|\nabla e_h\|$	EOC
64	20.88	-	1.483	-	0.984	-
128	10.82	0.942	0.435	1.768	0.264	1.899
512	5.462	0.985	0.113	1.940	0.0672	1.975
2048	2.738	0.997	0.0287	1.985	0.0169	1.994

of optimal interpolation estimate we would expect from the H^{-1} case would have $\mathcal{O}(h^2)$ for 2nd order interpolation, in comparison to the $\mathcal{O}(h)$ for L^2. Furthermore, the similar convergence rate when compared to the $\|\nabla e_h\|$ case shows that it retains the same convergence as a typical Laplace scheme.

A comparison of the plots for the L^2 and H^{-1} interpolation errors for 2048 elements is given in figures 3.1 and 3.2. To confirm that this still holds for non constant $A(x)$, we perform the same experiment for

$$A = \frac{16}{9}\begin{pmatrix} x^{2/3} & -x^{1/3}y^{1/3} \\ -x^{1/3}y^{1/3} & y^{2/3} \end{pmatrix}.$$

This gives us the following results in table 3.2. So once again we recover the same

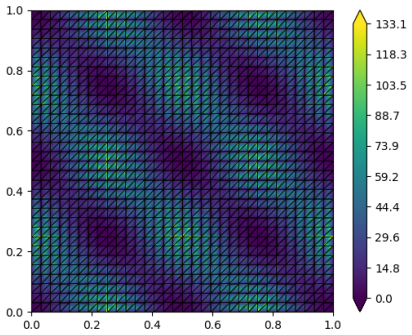

Figure 3.1: Plot of $\|\Delta(u - I_h u)\|$

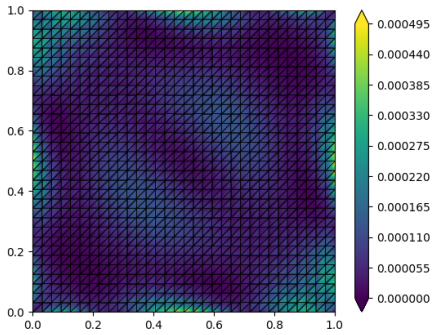

Figure 3.2: Plot of $\|\nabla \mathcal{N}_h \Delta(u - I_h u)\|$

Table 3.2: Interpolation error with non-constant A for different norms

Elements	$\|A : D^2 e_h\|$	EOC	$\|\nabla \mathcal{N}_h A : D^2 e_h\|$	EOC	$\|\nabla e_h\|^4$	EOC
32	28.44	-	1.463	-	0.984	-
128	14.15	1.005	0.404	1.855	0.264	1.899
512	7.058	1.003	0.104	1.959	0.0672	1.975
2048	3.527	1.000	0.026	1.989	0.0169	1.994

convergence rate.

We note that these are the optimal results given a smooth enough solution. In particular the theory specifies that for $k + 1 = 3$, that H^3 functions or above are necessary for convergence.

Suppose we instead use the exact solution $u = x^{4/3} y^{4/3}$, (used in [Feng et al., 2015, Test 3]) for which $u \in W^{2,p}(\Omega) \cap W^{1,\infty}(\Omega)$, where $p < 3/2$. Then we get the results in table 3.3. We note that we do not obtain optimal convergence in such a case, which is consistent with the results from said paper (i.e. $|u - u_h|_1 = \mathcal{O}(h^{5/6})$).

Table 3.3: Interpolation error for a non-smooth solution with different norms

Elements	$\|A : D^2 e_h\|$	EOC	$\|\nabla \mathcal{N}_h A : D^2 e_h\|$	EOC	$\|\nabla e_h\|$	EOC
32	0.290	-	0.0135	-	0.0249	-
128	0.207	0.483	6.509e-3	1.048	0.0140	0.833
512	0.147	0.492	2.820e-3	1.207	7.860e-3	0.833
2048	0.104	0.496	1.136e-3	1.312	4.411e-3	0.833

3.5 Finite Element Hessian

3.5.1 Derivation of FEH

In the previous section in (3.30) we demonstrated that our method may not show convergence for linear basis functions, since it uses a piecewise approximation to the Hessian. Additionally there remains the problem of there being no clear way to make use of the piecewise Hessian in the nonlinear case, since it lacks a nonlinear form.

One way to avoid these problems is to make use of the *finite element Hessian* (FEH), first derived in (3.2). For instance due to the fact that this formulation only uses first derivatives, it means linear basis functions can be used. Thus in this section we will properly introduce this concept, which we will later use in application to methods 3.3.1 and 3.3.2.

The FEH was first considered in Aguilera and Morin [2008], and was later used in a nonvariational context in Lakkis and Pryer [2010]. The principal idea is to rewrite the Hessian using a variational approach, allowing us to express it using lower derivatives. Additionally we follow the derivation used in Dedner and Pryer [2013] that considers it in a discontinuous Galerkin setting. This allows for a more efficient computation of the Hessian from a numerical point of view compared to a continuous formulation[5].

Let $v \in H^2(\Omega)$, and let $\mathbf{n} : \partial\Omega \to \mathbb{R}^d$ be the outward pointing normal of Ω. Then the Hessian $D^2 v$, satisfies the following identity.

$$\int_\Omega D^2 v\, \varphi \,\mathrm{d}x = -\int_\Omega \nabla v \otimes \nabla \varphi \,\mathrm{d}x + \int_{\partial\Omega} \nabla v \otimes \mathbf{n}\, \varphi \,\mathrm{d}s, \quad \forall \varphi \in H^1(\Omega). \tag{3.31}$$

If $v \in H^1(\Omega)$, the left hand side of (3.31) can still be expressed as a dual pair. In this case we have

$$\langle D^2 v, \varphi \rangle = -\int_\Omega \nabla v \otimes \nabla \varphi \,\mathrm{d}x + \int_{\partial\Omega} \nabla v \otimes \mathbf{n}\, \varphi \,\mathrm{d}s, \quad \forall \varphi \in H^1(\Omega).$$

[5] One reason for this is that the mass matrix can be locally constructed in a DG setting, meaning that it can be inverted much more easily.

We note that we will define $H[v]$ in such a way that it is defined elementwise. With that in mind we consider the following results for elementwise integration that can be obtained via the identities in definition 3.1.3.

Proposition 3.5.1. *For a vector valued function $\boldsymbol{p} \in H^1(\Omega)$ and scalar valued function $\varphi \in H^1(\Omega)$ we have*

$$\sum_{K\in\mathcal{T}} \int_K \nabla \cdot \boldsymbol{p}\, \varphi \,\mathrm{d}x = \sum_{K\in\mathcal{T}} \left(-\int_K \boldsymbol{p} \cdot \nabla_h \varphi \,\mathrm{d}x + \int_{\partial K} \boldsymbol{p} \cdot \boldsymbol{n}_K \varphi \,\mathrm{d}s \right), \tag{3.32}$$

where $\nabla_h = (D_h)^T$ is the elementwise gradient. Furthermore if $\boldsymbol{p} \in L^2(\mathcal{E})^d$ and $\varphi \in L^2(\mathcal{E})$, the following identity holds

$$\sum_{K\in\mathcal{T}} \int_{\partial K} \boldsymbol{p} \cdot \boldsymbol{n}_K \varphi \,\mathrm{d}s = \int_{\mathcal{E}_0} [\![\boldsymbol{p}]\!]\{\varphi\} \,\mathrm{d}s + \int_{\mathcal{E}} [\![\varphi]\!] \cdot \{\boldsymbol{p}\} \,\mathrm{d}s = \int_{\mathcal{E}} [\![\boldsymbol{p}\varphi]\!] \varphi \,\mathrm{d}s, \tag{3.33}$$

An equivalent tensor formulation of (3.32)–(3.33) is

$$\sum_{K\in\mathcal{T}} \int_K D_h \boldsymbol{p}\, \varphi \,\mathrm{d}x = \sum_{K\in\mathcal{T}} \left(-\int_K \boldsymbol{p} \otimes \nabla_h \varphi \,\mathrm{d}x + \int_{\partial K} \boldsymbol{p} \otimes \boldsymbol{n}_K \varphi \,\mathrm{d}s \right), \tag{3.34}$$

where the last term is given by

$$\sum_{K\in\mathcal{T}} \int_{\partial K} \boldsymbol{p} \otimes \boldsymbol{n}_K \varphi \,\mathrm{d}s = \int_{\mathcal{E}_0} [\![\boldsymbol{p}]\!]_\otimes \{\varphi\} \,\mathrm{d}s + \int_{\mathcal{E}} [\![\varphi]\!] \otimes \{\boldsymbol{p}\} \,\mathrm{d}s = \int_{\mathcal{E}} [\![\boldsymbol{p}\varphi]\!]_\otimes \,\mathrm{d}s.$$

By using equations (3.31) and (3.34), we formulate the following definition for the finite element Hessian in its most general form.

Definition 3.5.1 (Generalized Finite Element Hessian)**.** Let $u \in H^2(\mathcal{T})$, let $\hat{U} : H^1(\mathcal{T}) \to L^2(\mathcal{E})$ be a linear form and $\hat{\mathbf{p}} : H^2(\mathcal{T}) \times H^1(\mathcal{T})^d \to L^2(\mathcal{E})^d$ a bilinear form representing approximations to u and ∇u respectively over the skeleton of the triangulation. Then we define the **generalised finite element Hessian** $H[u]$ as

the solution of

$$\int_K H[u]\,\varphi\,\mathrm{d}x = -\int_K \hat{\mathbf{p}} \otimes \nabla_h\varphi\,\mathrm{d}x + \int_{\partial K} \hat{\mathbf{p}} \otimes \mathbf{n}\,\varphi\,\mathrm{d}s, \quad \forall\varphi \in H^1(\mathcal{T}) \cap V_h, \tag{3.35}$$

$$\int_K \hat{\mathbf{p}} \otimes \boldsymbol{\psi}\,\mathrm{d}x = -\int_K u\,D_h\boldsymbol{\psi}\,\mathrm{d}x + \int_{\partial K} \boldsymbol{\psi} \otimes \mathbf{n}\,\hat{U}_K\,\mathrm{d}s, \quad \forall\boldsymbol{\psi} \in \left(H^1(\mathcal{T})\right)^d. \tag{3.36}$$

Theorem 3.5.1. *Let $u \in H^2(\mathcal{T})$ and let $\hat{U}$ and $\hat{\boldsymbol{p}}$ be defined as in Definition 3.5.1. Then the generalised finite element Hessian $H[u]$ is given for each $\varphi \in V_h$ as*

$$\begin{aligned}\int_\Omega H[u]\,\varphi\,\mathrm{d}x = &-\int_\Omega \nabla_h u \otimes \nabla_h\varphi\,\mathrm{d}x + \int_{\mathcal{E}} [\![\varphi]\!] \otimes \{\hat{\boldsymbol{p}}\}\,\mathrm{d}s + \int_{\mathcal{E}_0} \{\varphi\}[\![\hat{\boldsymbol{p}}]\!]_\otimes\,\mathrm{d}s \\ &- \int_{\mathcal{E}_0} \{\hat{U}-u\}[\![\nabla_h\varphi]\!]_\otimes\,\mathrm{d}s - \int_{\mathcal{E}} [\![\hat{U}-u]\!] \otimes \{\nabla_h\varphi\}\,\mathrm{d}s.\end{aligned} \tag{3.37}$$

Proof. Note that in view of definition 3.1.3, for $\boldsymbol{v} \in L^2(\mathcal{E})^d$ and $w \in L^2(\mathcal{E})$ we have the following identity

$$\sum_{K\in\mathcal{T}} \int_{\partial K} \boldsymbol{v} \otimes \boldsymbol{n} w\,\mathrm{d}s = \int_{\mathcal{E}} [\![w]\!] \otimes \{\boldsymbol{v}\}\,\mathrm{d}s + \int_{\mathcal{E}_0} \{w\}[\![\boldsymbol{v}]\!]_\otimes\,\mathrm{d}s. \tag{3.38}$$

Then summing (3.35) over $K \in \mathcal{T}$ and making use of identity (3.38) we see

$$\begin{aligned}\int_\Omega H[u]\,\varphi\,\mathrm{d}x = \sum_{K\in\mathcal{T}} \int_K H[u]\,\varphi\,\mathrm{d}x &= \sum_{K\in\mathcal{T}} \left(-\int_K \boldsymbol{p} \otimes \nabla_h\varphi\,\mathrm{d}x + \int_{\partial K} \hat{\boldsymbol{p}}_K \otimes \boldsymbol{n}\,\varphi\right)\mathrm{d}s \\ &= -\int_\Omega \boldsymbol{p} \otimes \nabla_h\varphi\,\mathrm{d}x + \int_{\mathcal{E}} [\![\varphi]\!] \otimes \{\hat{\boldsymbol{p}}_K\}\,\mathrm{d}s + \int_{\mathcal{E}_0} \{\varphi\}[\![\hat{\boldsymbol{p}}_K]\!]_\otimes\,\mathrm{d}s.\end{aligned} \tag{3.39}$$

Using the same argument for (3.36)

$$\begin{aligned}\int_\Omega \boldsymbol{p} \otimes \boldsymbol{\psi}\,\mathrm{d}x = \sum_{K\in\mathcal{T}} \int_K \boldsymbol{p} \otimes \boldsymbol{\psi}\,\mathrm{d}x &= \sum_{K\in\mathcal{T}} \left(-\int_K u\,D_h\boldsymbol{\psi}\,\mathrm{d}x + \int_{\partial K} \boldsymbol{\psi} \otimes \boldsymbol{n}\,\hat{U}_K\,\mathrm{d}s\right) \\ &= -\int_\Omega u\,D_h\boldsymbol{\psi}\,\mathrm{d}x + \int_{\mathcal{E}} [\![\hat{U}]\!] \otimes \{\boldsymbol{\psi}\}\,\mathrm{d}s + \int_{\mathcal{E}_0} \{\hat{U}\}[\![\boldsymbol{\psi}]\!]_\otimes\,\mathrm{d}s.\end{aligned} \tag{3.40}$$

Note that, again making use of (3.38) we have for each $\boldsymbol{\psi} \in H^1(\mathcal{T})^d$ and $v \in H^1(\mathcal{T})$

that

$$\int_\Omega \boldsymbol{\psi} \otimes \nabla_h v \,\mathrm{d}x = -\int_\Omega D_h \boldsymbol{\psi} v \,\mathrm{d}x + \int_{\mathcal{E}} \{\boldsymbol{\psi}\} \otimes [\![v]\!] \,\mathrm{d}s + \int_{\mathcal{E}_0} [\![\boldsymbol{\psi}]\!]_\otimes \{v\} \,\mathrm{d}s. \tag{3.41}$$

Taking $v = u$ in (3.41) and substituting into (3.40) we see

$$\int_\Omega \boldsymbol{p} \otimes \boldsymbol{\psi} \,\mathrm{d}x = \int_\Omega \boldsymbol{\psi} \otimes \nabla_h u \,\mathrm{d}x + \int_{\mathcal{E}} [\![\hat{U} - u]\!] \otimes \{\boldsymbol{\psi}\} \,\mathrm{d}s + \int_{\mathcal{E}_0} \{\hat{U} - u\} [\![\boldsymbol{\psi}]\!]_\otimes \,\mathrm{d}s. \tag{3.42}$$

Now choosing $\boldsymbol{\psi} = \nabla_h \varphi$ and substituting (3.42) into (3.39) we arrive at the finite element Hessian given by (3.37). □

We can now present the definition previously stated in (3.2).

Definition 3.5.2 (Finite Element Hessian)**.** In the case where the fluxes in Definition 3.5.1 are chosen to be

$$\hat{U} = \begin{cases} \{u\}, & \text{over } \mathcal{E}, \\ 0, & \text{on } \partial\Omega, \end{cases}$$

$$\hat{\boldsymbol{p}} = \{\nabla_h u\}, \text{ on } \mathcal{E} \cup \partial\Omega,$$

then the **finite element Hessian** $H[u]$ is a unique element of $V_h^{d\times d}$ such that for all $\varphi \in V_h$,

$$\int_\Omega H[u]\, \varphi \,\mathrm{d}x = -\int_\Omega \nabla_h u \otimes \nabla_h \varphi \,\mathrm{d}x + \int_{\mathcal{E}} [\![u]\!] \otimes \{\nabla_h \varphi\} + [\![\varphi]\!] \otimes \{\nabla_h u\} \,\mathrm{d}s \tag{3.2}$$

Remark. Whilst this discrete form of the Hessian may be more complicated than its original form, we can show that when used to write the Laplace equation, it corresponds to a second order finite difference stencil.

To demonstrate this remark, let us consider an elementary problem in 1D, with linear basis functions for u and constant basis functions for H. Since we are in 1D, let the domain be the interval $[0, 1]$, with the grid constructed via N evenly spaced vertices $0 \leq i \leq N$, with intervals of length h. We will denote our current element by $K_{i+\frac{1}{2}}$, which has vertices i and $i + 1$. This lets us rewrite the equation

elementwise as

$$\int_{K_{i+\frac{1}{2}}} H[u]\varphi \,\mathrm{d}x = \int_{K_{i+\frac{1}{2}}} u'\varphi' \,\mathrm{d}x + [\![u]\!]_{i+1}\{\varphi'\}_{i+1} + [\![u]\!]_i\{\varphi'\}_i \\ +[\![\varphi]\!]_{i+1}\{u'\}_{i+1} + [\![\varphi]\!]_i\{u'\}_i.$$

Since φ is a basis function for H and is constant, $\varphi' = 0$ and $\varphi(x) = \frac{1}{h}$. Thus $\int_{K_{i+\frac{1}{2}}} H[u]\varphi \,\mathrm{d}x = H[u]_{i+\frac{1}{2}}(xh^{-1})\Big|_i^{i+1} = H[u]_{i+\frac{1}{2}}$ This lets us simplify the above to

$$\begin{aligned} H[u]_{i+\frac{1}{2}} &= \frac{1}{h}\{u'\}_{i+1} - \frac{1}{h}\{u'\}_i \\ &= \frac{1}{2h}\left(\frac{u_{i+2}-u_{i+1}}{h} + \frac{u_{i+1}-u_i}{h}\right) - \frac{1}{2h}\left(\frac{u_{i+1}-u_i}{h} + \frac{u_i - u_{i-1}}{h}\right) \\ &= \frac{1}{2h^2}(u_{i+2} - u_{i+1} - u_i + u_{i-1}) \end{aligned}$$

Finally we consider this applied to the Laplace equation for u, by testing $H[u]$ with v_i (a basis function for u). Since v_i has support only on $K_{i-\frac{1}{2}}$ and $K_{i+\frac{1}{2}}$, this gives us the following.

$$\begin{aligned} \int_\Omega H[u]v_i \,\mathrm{d}x &= H[u]_{i-\frac{1}{2}} \int_{K_{i-\frac{1}{2}}} v_i \,\mathrm{d}x + H[u]_{i+\frac{1}{2}} \int_{K_i+\frac{1}{2}} v_i \,\mathrm{d}x \\ &= \frac{1}{2}H[u]_{i-\frac{1}{2}} + \frac{1}{2}H[u]_{i+\frac{1}{2}} \\ &= \frac{1}{4h^2}(u_{i+2} - 2u_i + u_{i-2}) \end{aligned}$$

As claimed, this indeed corresponds to a second order FD stencil. It should be noted however that due to the ± 2 spaced grid points, such a stencil would rarely be used.

3.5.2 Numerical Implementation of FEH

Now that we have derived the finite element Hessian in 3.2, let us consider the implementation of this in a finite element scheme. In terms of incorporating it into our existing methods, for the L^2 and H^1 minimization methods, we simply replace the piecewise Hessian with the finite element Hessian and omit all penalty terms except the boundary term from $s(u, v)$. For instance for the H^{-1} example (originally

formulated in example 3.3.2), we use the following method.

Example 3.5.1 (H^{-1} minimization with FEH)**.** Find $u_h \in V_h$ such that

$$\begin{aligned}&\int_\Omega \nabla\mathcal{N}_h(A : H[u_h]) \cdot \nabla\mathcal{N}_h(A : H[u_h]\varphi_h)\,\mathrm{d}x \\ &+ \frac{\beta}{h}\int_{\partial\Omega} \mathcal{N}_h(A : H[u_h])\mathcal{N}_h(A : H[\varphi_h])\,\mathrm{d}s + s(u_h, \varphi_h) = l_h(\varphi_h), \quad \forall\varphi_h \in V_h,\end{aligned} \tag{3.43}$$

where

$$s(v, w) = \frac{\beta}{h}\int_{\partial\Omega} vw\,\mathrm{d}s,$$

and

$$l_h(v) = -a(\mathcal{N}_h f, \mathcal{N}_h(A : H[v])).$$

For the L^2 version we use exactly the same procedure, so we will skip it for brevity.

Now to present an idea of the numerical implementation that is used to compute the FEH, let us consider the formulation in terms of finite element basis functions. Let $u \in V_h$ be a function on a fixed element $K \in \mathcal{T}$. It will be advantageous for us to assume that $H[u] \in W_h$ which is potentially different to V_h. Thus we express V_h and W_h on each element K in terms of basis functions as

$$V_h = \operatorname{span}\{\varphi_\mu^K\}_{\mu=1,\dots,R}, \qquad W_h = \operatorname{span}\{\Psi_\nu^K\}_{\nu=1,\dots,S}.$$

We will also compute each entry of the Hessian separately as H_{ij}, since this reflects what is done numerically. With that in mind, we can express (3.2) elementwise and entrywise as follows.

$$\begin{aligned}\int_K H_{ij}^K[u]\Psi^K\,\mathrm{d}x = -\int_K \partial_i u\partial_j\Psi^K\,\mathrm{d}x + \frac{1}{2}\sum_{N\in N^K}\int_{e_N} \big((\partial_i u|_K + \partial_i u|_N)\boldsymbol{n}_j^K\Psi^K \\ + (u|_K - u|_N)\boldsymbol{n}_i^K\partial_j\Psi^K\big)\,\mathrm{d}s,\end{aligned}$$

where we denote the set of neighbours of K by N^K, and e_N as the corresponding

edge. For convenience we denote the above expression by a functional l_{ij}^K, i.e.

$$l_{ij}^K(u, \Psi^K) := \int_K H_{ij}^K[u]\Psi^K \, \mathrm{d}x. \tag{3.44}$$

From this we can define the vector $\boldsymbol{l}_{ij}^K(u)$, which contains the degrees of freedom of l_{ij}^K, by

$$\boldsymbol{l}_{ij}^K(u) = \left(l_{ij}^K(u, \Psi_\nu^K)\right)_{\nu=1,\dots,S}.$$

We use the natural notation that entry ν of $\boldsymbol{l}_{ij}^K(u)$ is $l_{ij\nu}^K(u)$. In addition we define the mass matrix in the usual way by $M_K = \left(\int_K \Psi_\nu^K \Psi_\lambda^K\right)_{\nu\lambda=1,\dots,S}$. Thus we obtain the degrees of freedom of $H_{ij}^K[u]$ (which we denote by $\boldsymbol{H}_{ij}^K[u]$) by

$$\boldsymbol{H}_{ij}^K[u] = M_K^{-1}\boldsymbol{l}_{ij}^K(u).$$

Consequently we can recover the original $H_{ij}^K[u]$ by

$$H_{ij}^K[u] = M_K^{-1}\boldsymbol{l}_{ij}^K(u) \cdot \boldsymbol{\Psi}^K. \tag{3.45}$$

where $\boldsymbol{\Psi}^K = (\Psi_\nu^K)_{\nu=1,\dots,S}$. This motivates the following algorithm.

Algorithm 3.5.1. *To compute $H_{ij}^K[u]$, we do the following.*

3.6 Numerical Implementation in Dune-Fempy

Having considered various numerical methods for tackling nonvariational problems and looking at them analytically, let us now implement these methods and compare the results. In particular, we would like to compare the aforementioned approaches from the literature, i.e. examples 3.2.3, 3.2.4 and 3.2.5, and the new methods, examples 3.3.1 and 3.3.2. Additionally we will implement the two minimization methods with the finite element Hessian from section 3.5 in place of the piecewise Hessian, for further comparison.

The structure of this section is as follows. First we will describe the details of the implementation and the methods we are testing in section 3.6.1. Then in

for $\nu = 1$ **to** S **do**

$$l^K_{ij\nu}(u) = -\int_K \partial_i u|_K \partial_j \Psi^K_\nu$$

forall $N \in \mathcal{N}^K$ **do**

$$l^K_{ij\nu}(u) += \frac{1}{2}\sum_{N\in\mathcal{N}^K}\int_{e_N}\left((\partial_i u|_K + \partial_i u|_N)n^K_j\Psi^K_\nu + (u|_K - u|_N)n^K_i\partial_j\Psi^K_\nu\right)$$

end

end

$\boldsymbol{H}^K_{ij}[u] = M_K^{-1}\boldsymbol{l}^K_{ij}(u)$

for $\nu = 1$ **to** S **do**

$$H^K_{ij}[u] += H^K_{ij\nu}[u]\Psi^K_\nu$$

end

section 3.6.2 we will examine the effectiveness of each method in terms of errors and error convergence by applying them to three different problem cases. Lastly in section 3.6.3 we will look at efficiency in terms of iterations, condition numbers and time taken.

3.6.1 Numerical Setup

PDE and General Setup

We will conduct the tests using DUNE-FEMPY[6], by writing the methods in variational form using Unified Form Language. As previously, we will look to solve equations of the form.

$$\begin{aligned} -A : D^2 u &= f \quad \text{in } \Omega, \\ u &= 0 \quad \text{in } \partial\Omega, \end{aligned}$$

where the choice of A is the main variable. For the prescribed exact solution, we will use the smooth function $u = \sin(2\pi x)\sin(2\pi y)$ unless otherwise stated, and we calculate the RHS by substituting u into $-(A : D^2_h v, w)$, as demonstrated in the

[6]In terms of the specs, the desktop for the simulations has an Intel® Xeon® CPU E5-2650 with 10 cores and 198Gb of RAM.

following DUNE-FEMPY code.

Code Listing 3.1: The right-hand side calculation

```
def rhs(A, exact):
    b = -inner(A, grad(grad(exact[0])))*v[0]*dx
    return b
```

For all examples we will carry out all the computations on the square domain, $\Omega = [0,1]^2$, i.e.

Code Listing 3.2: The initial grid for the test examples

```
grid = create.grid('ALUSimplex', cartesianDomain([0, 0], [1, 1], [
    4, 4]))
```

The initial grid here is 4 squares in each direction, and the class `'ALUSimplex'` specifies triangular elements. This choice of domain and exact solution means the Dirichlet boundary condition is consistently $u = 0$ on $\partial\Omega$. Furthermore unless otherwise specified we will use Lagrange basis functions of order 2.

For the case of the minimization method, we use the matrix-vector form (3.25), i.e.

$$\begin{pmatrix} M & B \\ B^T & -S \end{pmatrix} \begin{pmatrix} \boldsymbol{\sigma} \\ \mathbf{u} \end{pmatrix} = - \begin{pmatrix} \mathbf{f} \\ \mathbf{g} \end{pmatrix}$$

Recall B is the system matrix for $b(v,w) = (A : D_h^2 v, w)$, M is the system matrix for either $a(v,w) = (v,w)$ in the $V = L^2$ case or $a(v,w) = (\nabla v, \nabla w) + \beta_3 h^{-1}(v,w)_\Omega$ in the $V = H^1$ case, and S is the system matrix for the stabilization term $s(v,w) = \beta_1 h^p \int_{\mathcal{E}} [\![\nabla v]\!] \cdot [\![\nabla w]\!] \,\mathrm{d}s + \beta_2 h^q (A : D_h^2 v, A : D_h^2 w) + \beta_3 h^r \int_{\partial\Omega} vw \,\mathrm{d}s$.

We note that for the numerical results we add into $b(v,w)$ the extra term, $-\int_{\mathcal{E}} [\![A\nabla v]\!]\{w\} ds$. This is a DG term used for consistency, which comes from applying the DG integration by parts formula to the variational formulation (3.4). Specifically we have the following formula from [Feng et al., 2015, 2.23].

$$\int_\Omega \boldsymbol{\tau} \cdot \nabla v \,\mathrm{d}x = -\int_\Omega (\nabla \cdot \boldsymbol{\tau}) v \,\mathrm{d}x + \int_{\mathcal{E}} ([\![\boldsymbol{\tau}]\!]\{v\} + \{\boldsymbol{\tau}\} \cdot [\![v]\!]) \,\mathrm{d}s + \int_{\partial\Omega} \boldsymbol{\tau} \cdot \mathbf{n} v \,\mathrm{d}s,$$

where v is any piecewise scalar function and $\boldsymbol{\tau}$ is a vector function. In the case where $\boldsymbol{\tau} = A\nabla u_h$ and $v = \varphi_h \in V_h$, i.e. $[\![\varphi_h]\!] = 0$, this becomes

$$\int_\Omega A\nabla u_h \cdot \nabla\varphi_h \,\mathrm{d}x = -\int_\Omega A : D_h^2 u_h \varphi_h \,\mathrm{d}x + \int_\mathcal{E} [\![A\nabla u_h]\!]\{\varphi_h\} \,\mathrm{d}s, \tag{3.46}$$

Now recall the variational form, that is

$$\begin{aligned} &\int_\Omega \left(A\nabla u_h \cdot \nabla\varphi_h + (\nabla \cdot A)\cdot\nabla u_h\varphi_h\right)\mathrm{d}x \\ &+ \int_{\partial\Omega} \left(\beta h^{-1} u_h\varphi_h - A\nabla u_h \cdot \mathbf{n}\varphi_h\right)\mathrm{d}s = \int_\Omega f\varphi_h \,\mathrm{d}x. \end{aligned} \tag{3.4}$$

We substitute (3.46) into the first term and remove the $\nabla \cdot A$ term that is unsuited for nonvariational problems (and the boundary terms that are already accounted for in the minimization formulation's penalty term) and we get

$$-\int_\Omega A : D_h^2 u_h\varphi_h \,\mathrm{d}x + \sum_{e\in\mathcal{E}} \int_e [\![A\nabla u_h]\!]\{\varphi_h\} \,\mathrm{d}s = \int_\Omega f\varphi_h \,\mathrm{d}x.$$

Thus we use the LHS of this equation for $b(v, w)$.[7]

Now let us consider the implementation of this in Dune-Fempy. We can treat the above as one system of equations and use a standard linear solver (e.g. the conjugate gradient method) to calculate the solution. We assemble each component as a different scheme, e.g. to assemble B for the minimization method we have

Code Listing 3.3: Assembling B

```
a = inner(A, grad(grad(u[0])))*v[0]*dx \
    - jump(A*grad(u[0]), n)*avg(v[0])*dS
b = -rhs(A, exact)
scheme = create.scheme("galerkin", a == b, space, solver=solver)
B  = scheme.assemble(uh).as_numpy
```

We then assemble the remaining components in a similar way and construct the system matrix. As an example, for the L^2 minimization method we do the following.

[7] We note that the analysis from sections 3.3 and 3.4.1 do not account for this term, and we have added it for the numerical results simply because it appears to improve the convergence rate.

Code Listing 3.4: Assembling the system matrix for the $V = L^2$ case

```
BT = B.transpose(copy=True)
# assembling M
mass_model = inner(u, v)*dx == 0
mainScheme = create.scheme("h1", mass_model, space)
M = mainScheme.assemble(uh).as_numpy.tocsc()
# assembling S
s  = 1/he * inner( jump(grad(u[0])), jump(grad(v[0])) ) * dS \
     + inner(A, grad(grad(u[0] - exact[0]))) * inner(A, \
     grad(grad(v[0]))) * dx + beta/he0**3 * inner(u, v) * ds
penalty = create.scheme("galerkin", s == 0, space, solver='cg')
S  = -penalty.assemble(uh).as_numpy
from scipy.sparse import bmat
system = bmat([[M, B], [BT, S]])
```

The remaining methods are described below.

Methods

Here we will compare the proposed methods. First of all, we note that the weak Dirichlet boundary condition, $\beta_3 h^r \int_{\partial\Omega} vw \, \mathrm{d}s$, has been used in every method for consistency. We choose the value of $r = -3$ for the L^2 minimization methods and the method from Mu and Ye [2017], and $r = -1$ for the remaining methods. This is so the term scales correctly with the grid size h for each method.

For β_3, the value has been chosen based on the analysis from [Ainsworth and Rankin, 2008, Lemma 1]. Specifically we have the following simplified bound on the value of the parameter.

$$\beta_3 > k(k+1)\rho(A)$$

where k is the polynomial order, $\rho(A)$ is the largest eigenvalue of A from the original problem 3.1. For instance the choice of $k = 2$, and the simplest problem (where $\rho(A) = 1$), leads to $\beta_3 = 6$.

β_1 and β_2 have been chosen more empirically, by trying different values and examining convergence rates. In the following code they are taken to be the same

value, `sigma`, to avoid ambiguity with β_3 (`beta`).

Let us now list the methods, with abbreviations (**var**, **l2D2**, etc.) for labelling purposes.

- **var** - Variational approach (3.4). This is implemented in the code below.

Code Listing 3.5: The scheme for the variational method

```
a = inner(A*grad(u[0]), grad(v[0]))*dx
if div(A) != ufl.as_vector( [0, 0] ):
    print('non-constant A used')
    a += inner(div(A), grad(u[0]))*v[0]*dx
a += beta/he0*inner(u, v)*ds - dot(A*grad(u[0]), n)*v[0]*ds
b = rhs(A, exact)
scheme = create.scheme("galerkin", a==b, space, solver=solver)
```

- **l2D2** - Minimization method from 3.3.1 (refer to 3.3 and 3.4 above for details).

- **h1D2** - Minimization method from 3.3.2. This uses the same approach as the **l2D2** case, except with a different M and S as follows.

Code Listing 3.6: M and S for the **h1D2** method

```
# assembling M
laplace = inner(grad(u), grad(v))*dx + beta/he0*u[0]*v[0]*ds
laplace_model = create.model("integrands", grid, laplace == 0)
mainScheme = create.scheme("galerkin", laplace_model, space)
M = mainScheme.assemble(uh).as_numpy.tocsc()
# assembling S
sigma = 0.1
s = sigma*he*inner(jump(grad(u[0])), jump(grad(v[0])))*dS \
    + sigma*hT2*inner(A, grad(grad(u[0] - exact[0])))* \
    inner(A, grad(grad(v[0])))*dx + beta/he0*inner(u, v)*ds
penalty = create.scheme("galerkin", s == 0, space, solver='cg')
S = -penalty.assemble(uh).as_numpy
```

- **l2H** - Minimization method 3.3.1 with FE Hessian $H[u]$. To implement $H[u]$ we use an `'nv'` scheme (a new implmentation in the DUNE-FEMNV module

which was created for this thesis) which effectively maps $A : D^2u$ to $A : H[u]$. Thus our B term is almost the same, except without the added term. For S we just use the weak Dirichlet condition. The same M is used as in **l2D2** (3.4).

Code Listing 3.7: B and S for the **l2H** method

```
# assembling B
a = inner(A, grad(grad(u[0])))*v[0]*dx
b = -rhs(A, exact)
scheme = create.scheme("nv", space, a==b, penalty=0,
    solver=solver, polOrder=space.order)
B = scheme.assemble(uh).as_numpy
# assembling S
s = beta/he0**3 * inner(u, v) * ds
penalty = create.scheme("galerkin", s == 0, space, solver='cg')
S  = -penalty.assemble(uh).as_numpy
```

- **h1H** - Minimization method 3.3.2 with FE Hessian $H[u]$. Here we use the B from **l2H** (3.7) and the M from **h1D2** (3.6). The only change is the h-scaling on the penalty.

Code Listing 3.8: S for the **h1H** method

```
s = beta/he0 * inner(u, v) * ds
penalty = create.scheme("galerkin", s == 0, space, solver='cg')
S = -penalty.assemble(uh).as_numpy
```

- **nvdg** - Example 3.2.3 from Dedner and Pryer [2013]. This is simply the B from the **l2H** and **h1H** minimization methods, with the penalty terms added from within the C++ class via a penalty parameter.

- **feng** - Example 3.2.4 from Feng et al. [2015].

Code Listing 3.9: The **feng** method

```
a = -inner(A, grad(grad(u[0])))*v[0]*dx
b = rhs(A, exact)
s = jump(A*grad(u[0]), n)*avg(v[0])*dS \
```

```
    + beta/hF*inner(u, v)*ds
scheme = create.scheme("galerkin", a + s == 0, space, \
                        solver=solver)
B = scheme.assemble(uh).as_numpy
```

- **mu** - Example 3.2.5 from Mu and Ye [2017]. We use $\beta = 1$ here as it reflects the choice given in the paper. We also implement the RHS by subtracting it directly from the bilinear form, since a is slightly different here.

Code Listing 3.10: The **mu** method

```
a = inner(A, grad(grad(u[0] - exact[0])))*inner(A, \
          grad(grad(v[0])))*dx
s = 1/he * inner( jump(grad(u[0])), jump(grad(v[0])) ) * dS \
    + 1/hF**3 * inner(u, v) * ds
scheme = create.scheme("galerkin", a + s == 0, space, \
                        solver=solver)
B = scheme.assemble(uh).as_numpy
```

Symmetry

One important consideration between methods is whether they are symmetric or not. Symmetric methods allow for the use of a more efficient conjugate gradient (CG) solver over a non-symmetric solver (such as a bi-conjugate gradient (BiCGSTAB) or generalized minimal residual (GMRES) solver). In particular we note that the

Table 3.4: Table indicating which methods are symmetric

Method	**feng**	**h1D2**	**h1H**	**l2D2**	**l2H**	**mu**	**nvdg**	**var**
Symmetric	no	yes	yes	yes	yes	yes	no	no

minimization methods, and the **mu** method have the quality of being symmetric.

Remark. In the case of problems with a constant A such as the Laplace problem, **var** and **nvdg** can be made symmetric with the addition of the symmetrizing term $-\int_{\partial\Omega} A\nabla[\![\varphi_h]\!]_0 \cdot \mathbf{n} u_h \, ds$. However in general these methods will not be symmetric.

We note that in terms of linear solvers, a conjugate gradient solver is used if the system matrix is found to be symmetric (according to table 3.4), otherwise a

biconjugate gradient stabilized method is used. In both cases a tolerance of 10^{-9} is used and a max iteration cap of 10^6.

Preconditioners

For the minimization methods in particular, preconditioners are very important for efficiency. We calculate the approximation to the inverse of the system using an incomplete LU decomposition (ILU) from the SciPy package.

We note that some methods appear to require different levels of drop tolerance in order to converge, which we detail in table 3.5. These are based on whether the methods converge for the most refined grid used. Additionally we use a fill ratio

Table 3.5: Levels of drop tolerance necessary for ILU

Method	**l2D2**	**l2H**	**h1D2**	**h1H**	**mu**	**feng**	**nvdg**	**var**
Tolerance	10^{-12}	10^{-7}	10^{-7}	10^{-7}	10^{-7}	10^{-5}	10^{-5}	10^{-5}

upper bound of 30. This is not optimal for all methods but does not appear to affect efficiency.

3.6.2 Effectiveness and Convergence Rates

Let us now look at the results and discuss the effectiveness of the methods. For testing purposes we shall consider 3 examples, beginning with the following.

Example 3.6.1 (Poisson's Equation)**.** First let us look at the simplest case, Poisson's equation.

$$A = \begin{pmatrix} 1 & 0 \\ 0 & 1 \end{pmatrix}, \qquad \text{i.e.} - \Delta u = f.$$

This choice of A inserted into (3.1) leads to Poisson's equation, which can be easily compared to the variational version.

We choose this as our first example as a simple benchmark to make sure all methods including the variational approach are working. Additionally we want the nonvariational methods to behave as similarly as possible to the variational method

in the case where both are applicable. The bilinear form we use for the variational method is as follows.

$$\int_\Omega \nabla u \cdot \nabla v \, \mathrm{d}x + \int_{\partial\Omega} \beta h^{-1} uv - \nabla u \cdot \mathbf{n} v \, \mathrm{d}s = \int_\Omega f v \, \mathrm{d}x$$

We compute the solution for increasing levels of grid refinement, and consider the error e_h between the exact and computed solution in different norms. In particular we consider the norm

$$\|e_h\|_{D1} := \|A : D_h^2 e_h\|_{H^{-1}} \equiv \|\nabla \mathcal{N}(A : D_h^2 e_h))\|$$

where we approximate $\mathcal{N}$ by $\mathcal{N}_h$ in the same way as in section 3.4.2. We will also use the norm

$$\|e_h\|_{D2} := \|A : D_h^2 e_H\|_{L^2}$$

For the variational case we display in table 3.6 the errors and estimated orders of convergence (EOCs). Let us first comment on the observed orders of convergence.

Table 3.6: Variational method applied to Poisson's equation

Grid	$\|\|e_h\|\|$	EOC	$\|\|\nabla e_h\|\|$	EOC	$\|\|e_h\|\|_{D1}$	EOC	$\|\|e_h\|\|_{D2}$	EOC
32	0.02858	-	0.8902	-	1.913	-	21.66	-
128	0.003732	2.94	0.252	1.82	0.6626	1.53	11.18	0.954
512	0.0004776	2.97	0.06585	1.94	0.1842	1.85	5.518	1.02
2048	6.024e-05	2.99	0.01672	1.98	0.04759	1.95	2.743	1.01
8192	7.552e-06	3.0	0.004204	1.99	0.01203	1.98	1.37	1.0

For the L^2 norm we have roughly third order convergence, and for the H^1 seminorm and $\|A : D_h^2 e_h\|_{-1}$ (which should be approximately the same), we have second order. Lastly $\|A : D_h^2 e_h\|$ gives us first order convergence, which is expected as it is roughly the H^2 norm. These results are as expected for polynomial degree of 2. Thus we consider them to be the target for other methods to attain.

Since the **nvdg** method is identical to the **var** method in this case, we obtain the same EOCs and errors as shown in table 3.7. Now let us look at the other methods. We shall first start with the minimization methods 3.3.1 and 3.3.2.

Table 3.7: Nonvariational (DG) method applied to Poisson's equation

Grid	$\|\|e_h\|\|$	EOC	$\|\|\nabla e_h\|\|$	EOC	$\|\|e_h\|\|_{D1}$	EOC	$\|\|e_h\|\|_{D2}$	EOC
32	0.02858	-	0.8902	-	1.913	-	21.66	-
128	0.003732	2.94	0.252	1.82	0.6626	1.53	11.18	0.954
512	0.0004776	2.97	0.06585	1.94	0.1842	1.85	5.518	1.02
2048	6.024e-05	2.99	0.01672	1.98	0.04759	1.95	2.743	1.01
8192	7.552e-06	3.0	0.004204	1.99	0.01203	1.98	1.37	1.0

For the L^2 version we show the results in table 3.8. The main difference we

Table 3.8: L^2 minimization method applied to Poisson's equation

Grid	$\|\|e_h\|\|$	EOC	$\|\|\nabla e_h\|\|$	EOC	$\|\|e_h\|\|_{D1}$	EOC	$\|\|e_h\|\|_{D2}$	EOC
32	0.1085	-	1.178	-	1.753	-	21.03	-
128	0.02736	1.99	0.3396	1.79	0.5842	1.59	10.89	0.95
512	0.005443	2.33	0.08213	2.05	0.1552	1.91	5.44	1.0
2048	0.001163	2.23	0.01986	2.05	0.03951	1.97	2.726	0.996
8192	0.0002702	2.11	0.004862	2.03	0.009947	1.99	1.366	0.997

note to the variational version is that the L^2 error only attains second order instead of third. However the result is different for the H^{-1} case (table 3.9). Here we recover

Table 3.9: H^{-1} minimization method applied to Poisson's equation

Grid	$\|\|e_h\|\|$	EOC	$\|\|\nabla e_h\|\|$	EOC	$\|\|e_h\|\|_{D1}$	EOC	$\|\|e_h\|\|_{D2}$	EOC
32	0.04075	-	0.8951	-	1.49	-	20.12	-
128	0.00487	3.06	0.2558	1.81	0.4208	1.82	10.6	0.924
512	0.0005604	3.12	0.06621	1.95	0.1066	1.98	5.408	0.971
2048	6.687e-05	3.07	0.01674	1.98	0.02676	1.99	2.725	0.989
8192	8.17e-06	3.03	0.004205	1.99	0.006703	2.0	1.367	0.995

the same L^2 EOC of 3 as we saw for the **nvdg** and **var** methods, and the other EOCs remain the same. As was demonstrated previously in section 3.4.2, this would indicate the H^{-1} version of the method to be superior in terms of convergence.

Next we observe in tables 3.10 and 3.11, the results of the same method but using the finite element Hessian in place of the piecewise Hessian. Here we note in particular that in the L^2 case, the addition of the finite element Hessian improves the L^2 error's EOC from 2 to 3. Otherwise we observe the same results as before.

We now collect the EOCs for all methods including the remaining ones into table 3.12, which averages the final 3 EOCs. We plot some of these results in figures

Table 3.10: L^2 minimization method with $H[u]$

Grid	$\|\|e_h\|\|$	EOC	$\|\|\nabla e_h\|\|$	EOC	$\|\|e_h\|\|_{D1}$	EOC	$\|\|e_h\|\|_{D2}$	EOC
32	0.06574	-	0.9629	-	1.923	-	21.76	-
128	0.01092	2.59	0.2683	1.84	0.656	1.55	11.15	0.965
512	0.001549	2.82	0.06867	1.97	0.1825	1.85	5.501	1.02
2048	0.0002084	2.89	0.01715	2.0	0.04732	1.95	2.738	1.01
8192	2.711e-05	2.94	0.004265	2.01	0.01199	1.98	1.368	1.0

Table 3.11: H^{-1} minimization method with $H[u]$

Grid	$\|\|e_h\|\|$	EOC	$\|\|\nabla e_h\|\|$	EOC	$\|\|e_h\|\|_{D1}$	EOC	$\|\|e_h\|\|_{D2}$	EOC
32	0.03113	-	0.8814	-	1.932	-	21.5	-
128	0.00414	2.91	0.2505	1.81	0.6731	1.52	11.13	0.949
512	0.0005269	2.97	0.06567	1.93	0.1859	1.86	5.501	1.02
2048	6.571e-05	3.0	0.0167	1.98	0.04782	1.96	2.739	1.01
8192	8.169e-06	3.01	0.004201	1.99	0.01206	1.99	1.369	1.0

Table 3.12: Table of EOCs for the Laplace example

Method	$\|\|e_h\|\|$ EOC	$\|\|\nabla e_h\|\|$ EOC	$\|\|e_h\|\|_{D1}$ EOC	$\|\|e_h\|\|_{D2}$ EOC
feng	2.963	1.963	1.91	1.01
h1D2	3.073	1.973	1.99	0.985
h1H	2.993	1.967	1.937	1.01
l2D2	2.223	2.043	1.957	0.9977
l2H	2.883	1.993	1.927	1.01
mu	1.83	1.88	1.88	0.9937
nvdg	2.987	1.97	1.927	1.01
var	2.987	1.97	1.927	1.01

3.3 and 3.4, which show that for the L^2 error the methods are for the most part the same, with the **mu** and **l2D2** examples performing slightly worse than the others. We also compare the errors for the H^1 norm in figures 3.5 and 3.6, which demonstrate that all methods obtain a second order convergence rate, with the **mu** method being a slight underperformer.

Example 3.6.2 (Advection dominated (AD) problem)**.** For our second example we introduce an "advection dominated" problem (adapted from [Lakkis and Pryer,

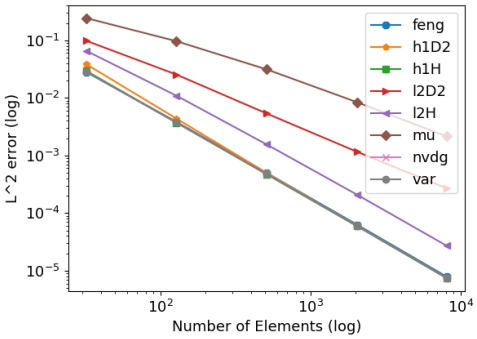

Figure 3.3: Plots of L^2 errors for Poisson's equation

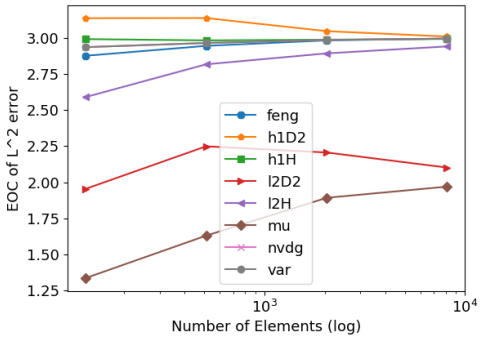

Figure 3.4: Plots of L^2 EOCs for Poisson's equation

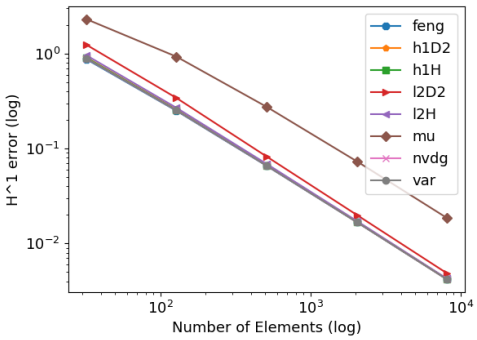

Figure 3.5: Plots of H^1 errors for Poisson's equation

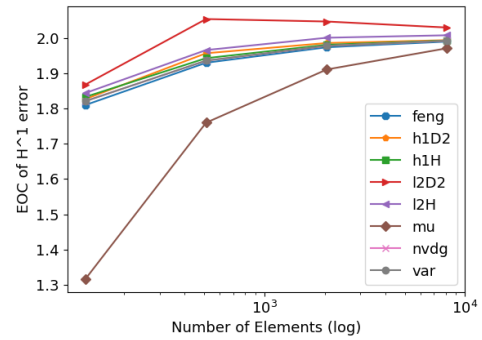

Figure 3.6: Plots of H^1 EOCs for Poisson's equation

2010, Test 4.2]).

$$A = \begin{pmatrix} 1 & 0 \\ 0 & \tan^{-1}(5000(x^2+y^2-1))+2 \end{pmatrix}$$

This equation has derivatives of the following form.

$$\frac{\partial}{\partial x_i}(\tan^{-1}(5000(x^2+y^2-1)+2) = \frac{10000x_i}{(5000(x^2+y^2-1)+2)^2+1}$$

These derivatives become particularly large on the unit circle. Recall that the variational method (3.4) includes the derivatives of A. Thus whilst this problem can still be written in such a form, and will converge for a high enough grid resolution,

the variational method is ill suited.

Let us first demonstrate this fact by presenting the results for the **var** method in table 3.13. As stated, the method does appear to converge on the final step.

Table 3.13: Variational method applied to the AD equation

Grid	$\|\|e_h\|\|$	EOC	$\|\|\nabla e_h\|\|$	EOC	$\|\|e_h\|\|_{D1}$	EOC	$\|\|e_h\|\|_{D2}$	EOC
32	0.171	-	1.452	-	1.969	-	25.27	-
128	0.1503	0.186	1.168	0.313	1.226	0.684	27.0	-0.0957
512	1.182	-2.98	9.764	-3.06	10.97	-3.16	443.1	-4.04
2048	1.302	-0.14	15.2	-0.639	24.19	-1.14	1300.0	-1.55
8192	0.05838	4.48	4.022	1.92	4.492	2.43	617.5	1.07

However the other steps seem to face significant problems, even diverging from the solution. For this reason we do not include it in the plots.

As before we can show all the remaining methods' average EOCs in table 3.14. We will also plot the L^2 errors and EOCs for the remaining methods in figures

Table 3.14: Table of EOCs for the AD problem

Method	$\|\|e_h\|\|$ EOC	$\|\|\nabla e_h\|\|$ EOC	$\|\|e_h\|\|_{D1}$ EOC	$\|\|e_h\|\|_{D2}$ EOC
feng	2.443	1.983	1.89	0.977
h1D2	2.523	2.02	1.92	0.9433
h1H	2.603	1.987	1.917	0.9813
l2D2	2.073	2.037	1.91	0.948
l2H	2.813	2.053	1.913	0.9763
mu	1.88	1.843	1.833	0.9437
nvdg	2.587	1.983	1.903	0.98
var	0.4533	-0.593	-0.6233	-1.507

3.7 and 3.8.

We note similar results to in the Laplace case, where the **mu** and **l2D2** examples show a lower convergence rate, but all other methods are roughly equivalent. We note that the decline in EOC for most of the methods in the last step shown in figure 3.8 is most likely coincidental, since for instance an additional step for the h1D2 method leads to a higher EOC of 2.96. However on the whole we can say that outside of the **var** example, this problem is not significantly different in terms of convergence rates to the Laplace problem.

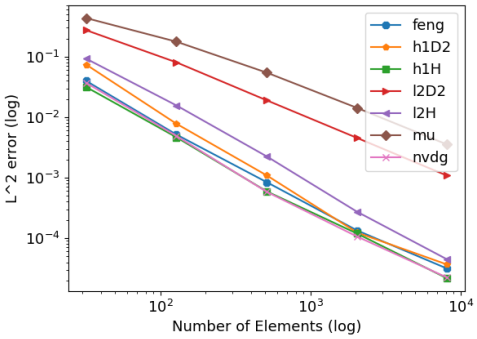

Figure 3.7: Plots of L^2 errors for the AD problem

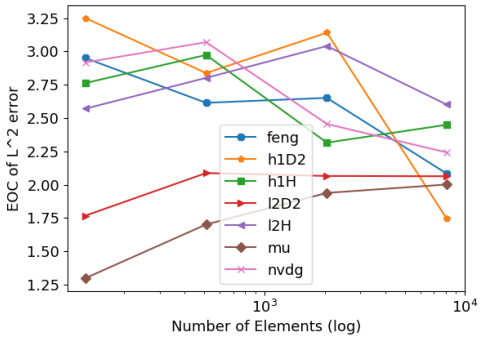

Figure 3.8: Plots of L^2 EOCs for the AD problem

For the H^1 errors and EOCs in figures 3.9 and 3.10, we obtain mostly similar results to before, in that all methods appear to converge with an order of around 2.

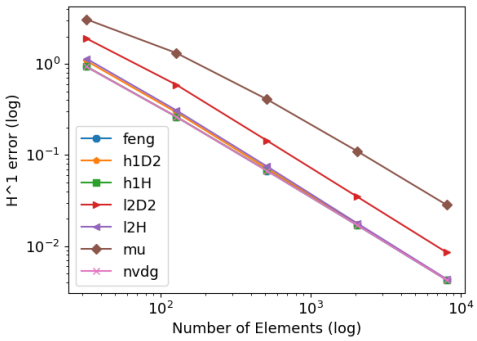

Figure 3.9: Plots of H^1 errors for the AD problem

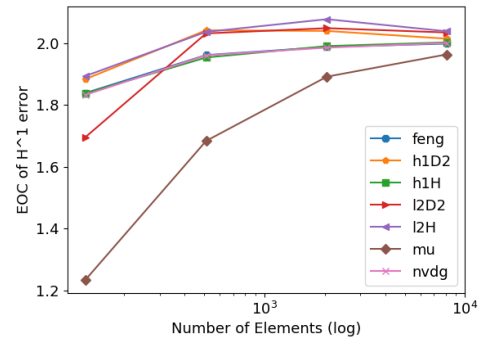

Figure 3.10: Plots of H^1 EOCs for the AD problem

Example 3.6.3 (Nondifferentiable (nonD) problem)**.** Lastly we introduce a problem where A is nondifferentiable due to a singularity at $(x, y) = (0.51, 0.61)$.

$$A = \begin{pmatrix} 1 & 0 \\ 0 & ((x-0.51)^2(y-0.61)^2)^{1/12} + 1 \end{pmatrix} \tag{3.47}$$

The singularity's location is chosen such that it does not lie directly on the mesh. This problem cannot be written in divergence form since DA does not exist. Thus

only nonvariational methods are suitable.

Let us once more present the EOCs for the nonD problem in table 3.15. In

Table 3.15: Table of EOCs for the nonD example

Method	$\|\|e_h\|\|$ EOC	$\|\|\nabla e_h\|\|$ EOC	$\|\|e_h\|\|_{D1}$ EOC	$\|\|e_h\|\|_{D2}$ EOC
feng	2.783	1.963	1.91	1.007
h1D2	2.793	1.977	1.977	0.9813
h1H	2.753	1.97	1.933	1.003
l2D2	2.453	2.033	1.957	0.9883
l2H	2.88	1.993	1.923	1.003
mu	1.847	1.913	1.91	0.9783
nvdg	2.737	1.967	1.923	1.007
var	-1.013	-0.113	0.8093	0.6153

figures 3.11 and 3.12 we plot the results for the L^2 norm. In figure 3.12 we observe a general slight decline in convergence in the final iteration, although the **l2H** and **mu** cases seems unaffected. Overall fairly similar results are obtained to the AD problem, though naturally the **var** case performs worse. For figures 3.13 and 3.14

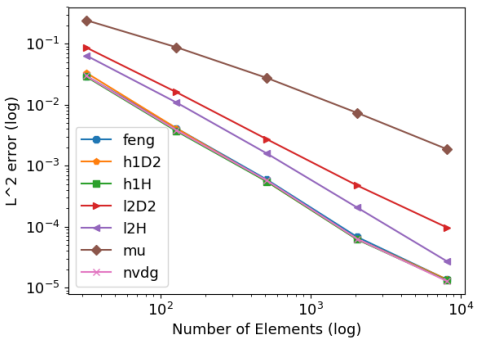

Figure 3.11: Plots of L^2 errors for the nonD problem

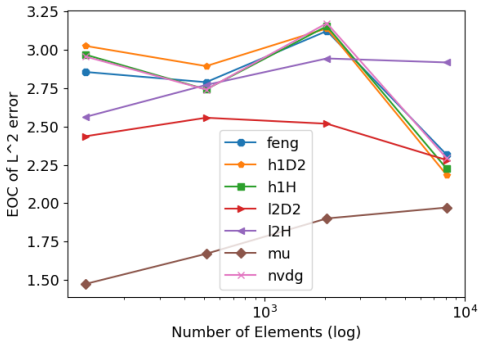

Figure 3.12: Plots of L^2 EOCs for the nonD problem

which show the H^1 errors, we once again obtain similar results.

Overall between the methods we notice the following trends with regards to convergence rates.

- The **l2D2** method appears to consistently perform better than the **mu** method despite the similarities between the two. This could possibly be the result of

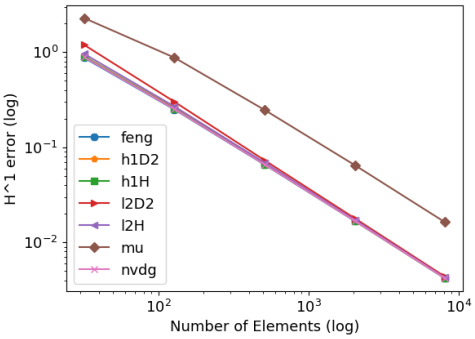

Figure 3.13: Plots of H^1 errors for the nonD problem

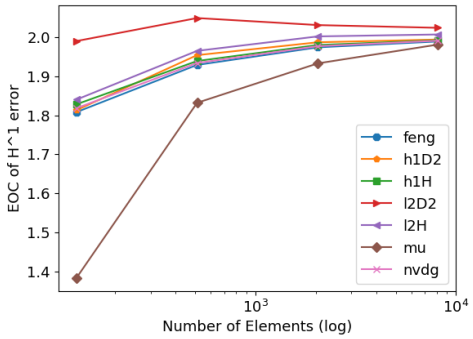

Figure 3.14: Plots of H^1 EOCs for the nonD problem

different penalty terms.

- The **h1D2** method seems to outperform the **l2D2** method on all accounts, which is consistent with prior observations.
- The **l2H** method is a clear improvement upon the **l2D2** method, however the **h1H** method is roughly equivalent to the **h1D2** method for most tests.
- Overall the **feng**, **nvdg**, **h1D2**, **h1H** and **l2H** methods all seem to consistently perform the best in terms of convergence rates.

Other Polynomial Orders

We have considered quadratic basis functions for the previous computations, but let us now examine the results for $k = 1$ and $k = 3$ polynomials. First of all let us look at first order basis functions for the nondifferentiable example in table 3.16. We note first of all that the optimal convergence decreases to approximately 2 for the L^2 EOC and 1 for the H^1 EOC. Despite our expectations, the **h1D2** method still seems to maintain optimal convergence. On the other hand the **l2D2** and **mu** methods no longer converge for first order polynomials, and despite appearing to have an average EOC close to 1, the **var** method probably does not either (the method appears to exhibit negative convergence in some steps). These results are somewhat more expected. We also note that the measures of the error which involve

Table 3.16: Table of EOCs for $k = 1$, for the nonD example

Method	$\|\|e_h\|\|$ EOC	$\|\|\nabla e_h\|\|$ EOC	$\|\|e_h\|\|_{D1}$ EOC	$\|\|e_h\|\|_{D2}$ EOC
feng	1.992	0.9747	5.881e-05	-6.13e-05
h1D2	1.959	0.9758	5.881e-05	-6.13e-05
h1H	1.991	0.9763	5.881e-05	-6.13e-05
l2D2	-0.05036	-0.01919	5.881e-05	-6.13e-05
l2H	1.17	0.9728	5.881e-05	-6.13e-05
mu	4.483e-15	-7.795e-15	5.881e-05	-6.13e-05
nvdg	1.987	0.9769	5.881e-05	-6.13e-05
var	0.843	0.9034	5.881e-05	-6.13e-05

$A : D^2$ no longer converge in this case (since the second derivative of a first order basis function is zero).

Now let us examine the results for $k = 3$ in table 3.17.

Table 3.17: Table of EOCs for $k = 3$, for the nonD example

Method	$\|\|e_h\|\|$ EOC	$\|\|\nabla e_h\|\|$ EOC	$\|\|e_h\|\|_{D1}$ EOC	$\|\|e_h\|\|_{D2}$ EOC
feng	3.846	2.998	1.908	1.985
h1D2	3.724	2.963	2.055	1.987
h1H	3.948	3.008	1.914	1.984
l2D2	2.012	2.111	1.977	1.988
l2H	4.014	3.043	1.895	1.983
mu	3.953	3.014	2.964	1.988
nvdg	3.948	3.0	1.91	1.984
var	0.0612	0.07163	0.4753	-0.2388

Here we see as expected the EOCs mostly move up by 1 compared to the $k = 2$ case, and the results are fairly uniform in this regard. One exception to this is the **l2D2** case which does not improve, though we do not have an analytical explanation as to why. Another observation is that the $\|e_h\|_{D1}$ EOC does not improve overall, which may simply be due to the fact the polynomial order used to approximate the H^{-1} norm has not changed.

3.6.3 Efficiency

Following the previous section which shows that many of the methods are roughly equivalent in terms of absolute errors and convergence rates, we now look towards other aspects with which to compare the methods.

Condition Numbers

One way of evaluating the efficiency of the schemes is to calculate the condition number of the system matrix and its growth after grid refinements. The condition number C is defined by

$$C = \frac{\max \lambda_i}{\min \lambda_i},$$

where λ_i are the eigenvalues of the system matrix. We compare the condition numbers of the L^2 and H^{-1} minimization methods below. For these tests we will use Poisson's equation (example 3.6.1) with polynomial order 2.

Table 3.18: Condition numbers for the L^2 minimization method

l2D2	Ele.	$\max \lambda_i$	$\min \lambda_i$	C	l2H	$\max \lambda_i$	$\min \lambda_i$	C
	32	11,788	0.001012	1.164e7		445.5	0.001037	429,493
	128	51,072	2.530e-4	2.016e8		1782	2.593e-4	6.871e6
	512	209,387	6.326e-5	3.310e9		7128	6.483e-5	1.099e8
	2048	843,302	1.582e-5	5.332e10		25,513	1.621e-5	1.759e9

In table 3.18, we note that for the L^2 minimization method for both the piecewise and finite element Hessian versions, the condition number C grows by roughly 16 each refinement, which is proportionate to h^{-4}.

Table 3.19: Condition numbers for the H^{-1} minimization method

h1D2	Elements	$\max \lambda_i$	$\min \lambda_i$	C	h1H	$\max \lambda_i$	$\min \lambda_i$	C
	32	24.26	0.1891	128.3		16.61	0.1860	89.31
	128	26.24	0.0475	552.8		17.07	0.04725	361.4
	512	26.88	0.01189	2261		17.21	0.01188	1449
	2048	27.06	0.002975	9096		17.25	0.002974	5798

In table 3.19, in contrast to the L^2 case, the H^{-1} version has a condition number growth rate of approximately 4 or h^{-2}. This corresponds with the observations we made in section 3.4.2.

Now, let us compare the condition numbers of all the methods in figure 3.15. For clarity we also include lines which demonstrate how the condition number grows when proportionate to h^{-2} and h^{-4}.

There are some notable observations to make. Firstly, we see that the **feng**

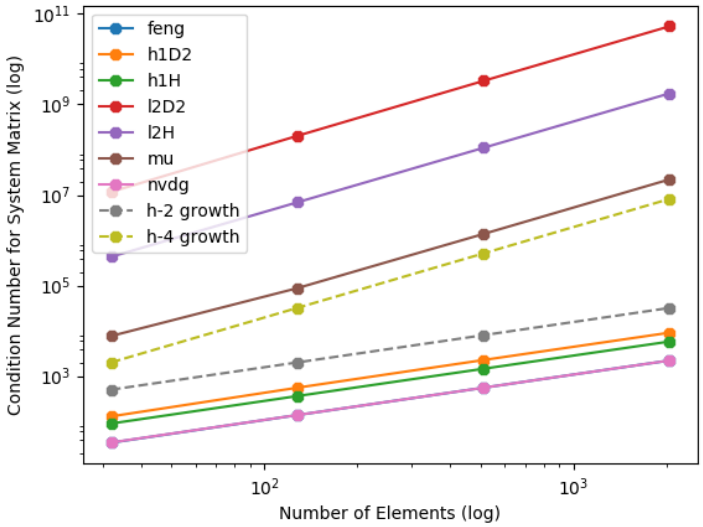

Figure 3.15: Comparison of the condition numbers for different methods

and **nvdg** appear to perform the best (obtaining almost identical condition numbers). Shortly behind this, the **h1H** method can be found, followed by the **h1D2** method, and then the remaining methods.

The second observation is regarding the slope of the lines, which can be most easily observed via comparison to the additional dotted lines. Here we see that the methods form into two categories, with the **nvdg**, **feng**, **h1H** and **h1D2** methods (showing growth numbers of about h^{-2}) comprising one, and the **mu**, **l2H** and **l2D2** (with a growth of about h^{-4}) comprising the other.

From these results we can say that the **nvdg** and **feng** methods are ideal due to their low initial condition numbers. However we do note that they seem to scale the same way as the H^{-1} method, meaning that for larger scale simulations there may not be a significant difference. These results also further show that the L^2 method is probably suboptimal.

Iteration Count

Generally speaking observing the growth in iterations made by the linear solver in solving the PDE is indicative of the efficiency of the method. In this case however

the use of preconditioning in our methods reduces this effect substantially. This can be seen in figure 3.16, where it can be seen the iterations rarely rise above 10.

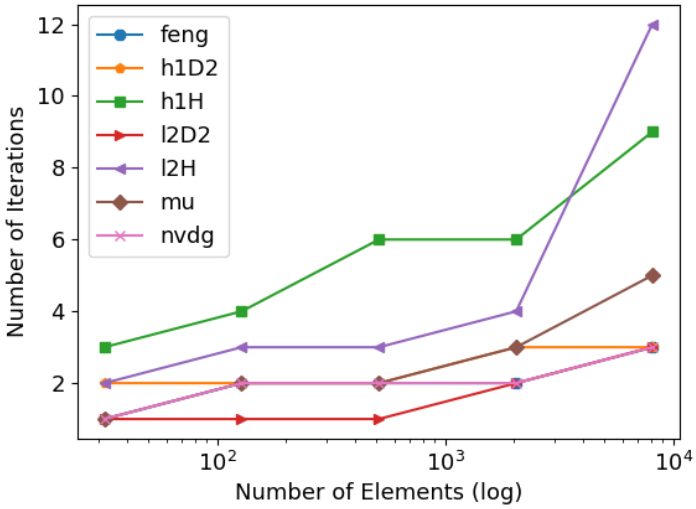

Figure 3.16: Plot of the iteration count for the nonD problem

We also note that the choice of tolerance given in 3.5 directly affects the iteration count. Thus the use of different tolerances makes the above information unreliable.

Whilst this preconditioning can be turned off for comparison purposes, the minimization methods rely heavily on preconditioning and are significantly less efficient without it. Thus we defer instead to the analysis of the condition numbers from 3.6.3.

Time Taken

One other tool we can use to compare the different methods efficiency is the time taken to run the entire solving process. In some ways this is the most direct method for analysing the efficiency, however there is no guarantee the results will remain constant when factors such as parallel processing and different hardware are taken into account. The runtimes of the simulations used are also relatively small (not exceeding half a minute after pre-processing). We also note that a method could

take less time yet have a larger error, although our tests show that the H^1 error typically does not deviate by more than 5% between methods[8].

Nonetheless we compare the methods in figure 3.17 for a relative idea of the scales involved.

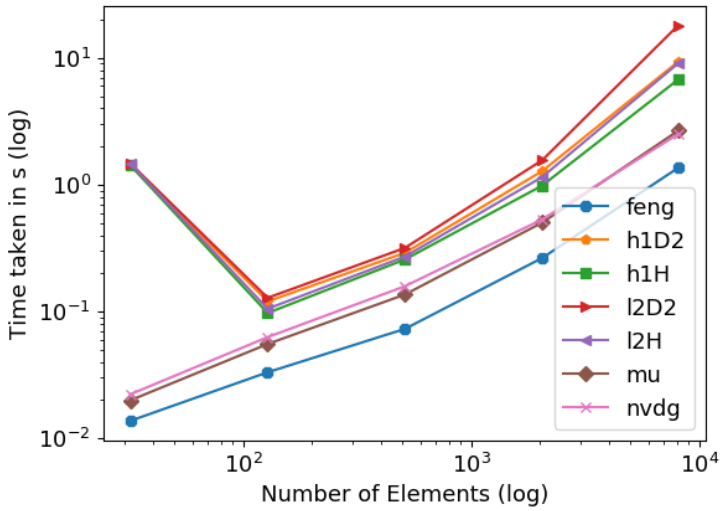

Figure 3.17: Plot of the total time taken for the nonD problem

We first note that the minimization methods all exhibit a longer initial step, most likely due to having to assemble additional schemes. Past this point they are more comparable, although the fastest methods are still the non-minimization methods, i.e. **nvdg**, **mu** and **feng**.

3.7 Nonlinear Problems

Until this point, we have looked purely at linear nonvariational PDEs taking the form $A : D^2u = f$, as that has allowed us to most easily numerically compare and analyse different methods. Now we want to take a look at the more general case,

$$F(D^2u) = f(x, u, Du),$$

[8]Although we do note the L^2 error seems to differ by a more substantial amount, the scales are still comparable enough for efficiency comparisons to be valid.

where $F : \mathrm{Sym}(\mathbb{R}^{d\times d}) \to \mathbb{R}$, and $f \in L^2(\Omega)$. This form is no longer restricted to linearly acting on each component of the Hessian, and allows for more complicated functions such as the Monge-Ampère equation and the Hamilton-Jacobi-Bellman equations.

In this section we will provide a primarily numerical-based look at a first step towards solving NV problems in a nonlinear setting in Dune-Fempy. As such we do not guarantee analytical convergence but instead focus on a practical look at whether we can solve nonlinear equations effectively. We leave the comparison of different methods for nonlinear problems as future work.

We will consider this section in two parts. First we will look at the details of the implementation, then we shall look at the implementation of the problems and their convergence rates.

3.7.1 Numerical Setup

Let us first of all describe the method we want to use to solve nonlinear nonvariational problems of the form $F(D^2u) = f$. To obtain the weak form of the PDE for the method, we will use a simple direct substitution of the Hessian for the finite element Hessian from section 3.5, equation (3.2). Thus we instead solve $F(H[u]) = f$. Next we will then use Newton's method to iteratively find the solution, i.e. we start from the well-known iterative formula,

$$0 = DF(H[u^n])(u^{n+1} - u^n) + F(H[u^n]),$$

(where DF is the derivative of F). We then rearrange and invert DF to obtain,

$$u^{n+1} = u^n - DF^{-1}(H[u^n])F(H[u^n]).$$

It then remains to choose a suitable u^0 (in this case we will just choose $u^0 = 0$ for the first two examples), and iterate until the residual error is sufficiently small.

We note that this method is applied automatically within the Dune software framework, the derivative being calculated automatically from the bilinear form via

UFL differentiation. However in the case of the finite element Hessian, we must implement this manually, which we describe below.

We reuse the notation from the original numerical implementation of the FEH in section 3.5.2 by considering the FEH elementwise for $K \in \mathcal{T}$ and entrywise for $1 \leq i, j \leq d$.

To use Newton's method with finite elements, it is necessary to compute the components $H_{ij}^K[\bar{u}]$, $H_{ij}^K[\varphi_\mu^K]$ and $H_{ij}^K[\varphi_\mu^N]$ for all $\mu \in \{1, ..., R\}$ (recall φ_μ are the basis functions for u). It will be convenient to define matrices derived from l_{ij}^K (defined in (3.44)) which contain all the basis functions as follows.

$$L_{ij}^{KK} := \left(l_{ij}^K(\varphi_\mu^K, \Psi_\nu^K)\right)_{\mu\nu}, \quad L_{ij}^{KN} := \left(l_{ij}^K(\varphi_\mu^K, \Psi_\nu^N)\right)_{\mu\nu}.$$

Note that if we let $\{\boldsymbol{e}_\mu\}_{\mu=1,...,R}$ be the standard basis for V_h, we have $L_{ij}^{KK}\boldsymbol{e}_\mu = \boldsymbol{l}_{ij}^K(\varphi_\mu)$. We also use the notation $\bar{u} = \sum_\mu \bar{u}_\mu \varphi_\mu^K = \bar{\boldsymbol{u}} \cdot \boldsymbol{\varphi}^K$, where $\boldsymbol{\varphi}^K = (\varphi_\mu^K)_{\mu=1,...,R}$. Then we can rewrite (3.45) using the above forms, giving us equations for $H_{ij}^K[\varphi_\mu^K]$, $H_{ij}^K[\varphi_\mu^N]$ and $H_{ij}^K[\bar{u}]$ as follows.

$$\begin{aligned}
H_{ij}^K[\psi_\mu^K] &= M_K^{-1} L_{ij}^{KK} \boldsymbol{e}_\mu \cdot \boldsymbol{\Psi}^K, \\
H_{ij}^K[\psi_\mu^N] &= M_K^{-1} L_{ij}^{KN} \boldsymbol{e}_\mu \cdot \boldsymbol{\Psi}^K, \\
H_{ij}^K[\bar{u}] &= M_K^{-1} L_{ij}^{KK} \bar{\boldsymbol{u}}^K \cdot \boldsymbol{\Psi}^K + \sum_{N \in \mathcal{N}^K} M_K^{-1} L_{ij}^{KN} \bar{\boldsymbol{u}}^N \cdot \boldsymbol{\Psi}^K.
\end{aligned}$$

In algorithmic form we have the following.

Algorithm 3.7.1. *To compute $H_{ij}^K[\bar{u}], H_{ij}^K[\varphi_\mu^K]$ and $H_{ij}^K[\varphi_\mu^N]$ we do the following.*

3.7.2 Effectiveness and Convergence Rates

We start off by looking at an example of a nonlinear problem that can be written in variational form.

// Part 1 - L^{KK} and L^{KN} construction
for $\mu = 1$ **to** R **do**
  for $\nu = 1$ **to** S **do**

$$(L_{ij}^{K,K})_{\mu\nu} = -\int_K \partial_i \varphi_\mu^K \partial_j \Psi_\nu^K$$

    forall $N \in \mathcal{N}^K$ **do**

$$(L_{ij}^{K,K})_{\mu\nu} += \int_{e_N} \left(\partial_i \varphi_\mu^K n_j^K \Psi_\nu^K + \varphi_\mu^K n_i^K \partial_j \Psi_\nu^K\right)$$

$$(L_{ij}^{K,N})_{\mu\nu} = \int_{e_N} \left(\partial_i \varphi_\mu^N n_j^K \Psi_\nu^K - \varphi_\mu^N n_i^K \partial_j \Psi_\nu^K\right)$$

    end
  end
end

Example 3.7.1 (p-Laplace Equation)**.** We consider the p-Laplace equation, i.e.

$$\begin{aligned} -\nabla \cdot \left(|\nabla u|^{p-2} \nabla u\right) &= f, \quad \text{in } \Omega, \\ u &= 0, \quad \text{on } \partial\Omega, \end{aligned}$$

where $|\nabla u|^{p-2}$ is defined as

$$|\nabla u|^{p-2} = (d + \nabla u \cdot \nabla u)^{\frac{p-2}{2}},$$

and $d = 0.001$ and $1 < p < \infty$. The nonvariational bilinear form is simply

$$\int_\Omega -\nabla \cdot \left(|\nabla u|^{p-2} \nabla u\right) \varphi \, \mathrm{d}x = \int_\Omega f \varphi \, \mathrm{d}x.$$

This is implemented as a scheme in Dune-Fempy as follows, for a chosen value of $p = 1.7$, and exact solution $u = \sin(2\pi x)\sin(2\pi y)$.

Code Listing 3.11: The p-Laplace problem

```
1 d = 0.001
2 p = 1.7
3 norm_gradu = pow(d + inner(grad(u), grad(u)), (p-2)/2)
```

```
// Part 2 - Obtain degrees of freedom
```

$$\boldsymbol{H}_{ij}^{K}[\bar{u}] = M_{K}^{-1} L_{ij}^{KK} \bar{\boldsymbol{u}}^{K}$$

for $\mu = 1$ **to** R **do**

$$\boldsymbol{H}_{ij}^{K}[\varphi_{\mu}^{K}] = M_{K}^{-1} L_{ij}^{KK} \boldsymbol{e}_{\mu}$$

end

forall $N \in \mathcal{N}^{K}$ **do**

$$\boldsymbol{H}_{ij}^{K}[\bar{u}] += M_{K}^{-1} L_{ij}^{KN} \bar{\boldsymbol{u}}^{N}$$

for $\mu = 1$ **to** R **do**

$$\boldsymbol{H}_{ij}^{K}[\varphi_{\mu}^{N}] = M_{K}^{-1} L_{ij}^{KN} \boldsymbol{e}_{\mu}$$

end

end

```
// Part 3 - Calculate result
```

for $\nu = 1$ **to** S **do**

$$H_{ij}^{K}[\bar{u}] += H_{ij\nu}^{K}[\bar{u}] \Psi_{\nu}^{K}$$

for $\mu = 1$ **to** R **do**

$$H_{ij}^{K}[\varphi_{\mu}^{K}] += H_{ij\nu}^{K}[\varphi_{\mu}^{K}] \Psi_{\nu}^{K}$$

forall $N \in \mathcal{N}^{K}$ **do**

$$H_{ij}^{K}[\varphi_{\mu}^{N}] += H_{ij\nu}^{K}[\varphi_{\mu}^{N}] \Psi_{\nu}^{K}$$

end

end

end

```
4 pLaplace_u = grad(norm_gradu*grad(u))[0, 0, 0] \
5              + grad(norm_gradu*grad(u))[0, 1, 1]
6 a = (-inner(pLaplace_u, v[0])) * dx
7 b = ufl.replace(a, {u: exact} )
8 scheme = create.scheme("nv", space, [a==b, dirichletBC], \
```

```
9                                    constraints='dirichlet')
```

Note that we have obtained the RHS by substituting the exact solution for u. We run our method with this form and the same numerical setup as before ($[0,1]^2$ domain, 2nd order basis functions), and this results in the table of EOCs 3.20.

Table 3.20: Table of EOCs for the nonvariational p-Laplace

Elements	$\|\|e_h\|\|$	EOC	$\|\|\nabla e_h\|\|$	EOC
32	0.04266	-	0.9627	-
128	0.004414	3.273	0.2594	1.892
512	0.0005047	3.129	0.0668	1.957
2048	6.059e-05	3.058	0.01684	1.988
8192	8.107e-06	2.902	0.004219	1.997

Here we note that we obtain the expected convergence rates of 3 for the L^2 norm and 2 for the H^1 norm[9]. We can also confirm the correctness of this result by comparing it to the variational form of this method, i.e.

$$\int_\Omega |\nabla u|^{p-2}\nabla u \cdot \nabla \varphi \,\mathrm{d}x = \int_\Omega f\varphi \,\mathrm{d}x.$$

This gives us the following errors in table 3.21.

Table 3.21: Table of EOCs for the variational p-Laplace

Elements	$\|\|e_h\|\|$	EOC	$\|\|\nabla e_h\|\|$	EOC
32	0.03386	-	0.9275	-
128	0.003885	3.123	0.2591	1.84
512	0.0004783	3.022	0.06681	1.956
2048	5.999e-05	2.995	0.01684	1.988
8192	8.061e-06	2.896	0.004219	1.997

As expected we obtain almost the same error results for the variational version compared to the nonvariational version.

Example 3.7.2 (Nonlinear NV Equation)**.** As a second example we implement a

[9]We note that quasinorms (see e.g. Barrett and Liu [1994]) could potentially be more suitable for nonlinear problems, yet we will follow the procedure of Lakkis and Pryer [2012].

simple nonlinear problem that can only be written in nonvariational form.

$$\begin{aligned} \sin(\Delta u) + 2\Delta u &= f, \quad \text{in } \Omega, \\ u &= 0, \quad \text{on } \partial\Omega. \end{aligned}$$

In DUNE-FEMPY this corresponds to the following scheme.

Code Listing 3.12: The simple nonvariational nonlinear problem

```
laplace = grad(grad(u))[0, 0, 0] + grad(grad(u))[0, 1, 1]
a = inner(sin(laplace) + 2*laplace, v[0])*dx
b = ufl.replace(a, {u: ufl.as_vector(exact)} )
scheme = create.scheme("nv", space, [a==b, dirichletBC],
    constraints='dirichlet')
```

We once again solve the code and compute the errors in 3.22.

Table 3.22: Table of EOCs for the simple nonlinear problem

Elements	$\|\|e_h\|\|$	EOC	$\|\|\nabla e_h\|\|$	EOC
32	0.0314	-	0.9254	-
128	0.003706	3.083	0.2588	1.838
512	0.000779	2.25	0.06711	1.947
2048	0.0002034	1.938	0.01705	1.977
8192	1.62e-05	3.65	0.004278	1.995

In this situation the convergence rate appears to be unstable but nonetheless converges with roughly the same results as before.

Example 3.7.3 (Monge-Ampère equation)**.** Finally we move onto the Monge-Ampère equation.

$$\begin{aligned} det(D^2 u) &= f, \quad \text{in } \Omega, \\ u &= 0, \quad \text{on } \partial\Omega. \end{aligned}$$

Here we will use the exact solution

$$u = e^{2((x-0.5)^2+(y-0.5)^2)}.$$

We note that for the solving of this equation, instead of Newton's method we instead use a specific iterative method from [Benamou et al., 2010, Def. 2.1.], i.e.

$$u^{n+1} = \Delta^{-1}\left(\sqrt{(\Delta u^n)^2 + 2(f - \det(H[u^n])}\right) \tag{3.48}$$

We are able to implement (3.48) by taking the Laplacian to the LHS and solving weakly, as shown below.

Code Listing 3.13: Monge-Ampère iterative method

```
a = laplace(u)*v[0]*dx
b = sqrt(laplace(uOld)**2 + 2*(f - detH(uOld)))*v[0]*dx
scheme0 = create.scheme("nv", space, [a==b, dirichletBC],
    solver=solver, polOrder=space.order)
```

After applying this method and solving it, this results in the EOC table 3.23. We see an EOC of approximately 2 for the L^2 error, which we note is consistent

Table 3.23: Table of EOCs for the Monge-Ampère equation

Elements	$\|\|e_h\|\|$	EOC	$\|\|\nabla e_h\|\|$	EOC
32	0.0003722	-	0.01135	-
128	8.454e-05	2.139	0.003261	1.799
512	1.980e-05	2.094	0.0006888	2.243
2048	4.822e-06	2.038	0.0001897	1.860
8192	1.167e-06	2.047	4.220e-05	2.1685

with the results from the paper the method comes from (Benamou et al. [2010]), where they observe $\mathcal{O}(h^2)$ convergence for a smooth solution.

Chapter 4

Conclusion

4.1 Achieved Goals

The first goal we have achieved in this work is the design and creation of Dune-Fempy. Primarily we sought to design a Python interface for finite element methods (via the Dune-Fem module) which facilitates simpler code design and rapid prototyping. However to justify the existence of the package beyond the confines of Dune development and to show its merit in comparison to other similar Python front-end packages we have endeavored to add additional functionality and do things in a unique way. For instance we have made efforts to maintain the similarity between the Python and C++ code structure so that translation between the two for efficiency reasons is easier. We have also facilitated the writing of additional modules in C++ that do things not currently available in Dune-Fempy, such as the Dune-Femnv module for nonvariational problems. The fact that such modules can be written independently and added to the interface easily means external development is encouraged and not limited by what is merely available to the user. Finally we have added many of the features common to finite element packages such as grid adaptivity and the integration of external solvers, which we have demonstrated throughout section 2.

With regards to nonvariational PDEs, our primary goal was to implement a new method for solving this class of problems based on minimization, that attempts

to improve upon existing methods in terms of analytical results and performance. We have shown a full mathematical derivation for the method and derived results for the existence and uniqueness and the error convergence. We then showed a derivation for an improvement to the method in terms of the DG finite element Hessian. In the numerical results we were able to implement all the methods in the same setting and compare them directly. We were able to demonstrate there was in fact an improvement when considering the H^{-1} version of the method compared to the L^2 case, although some other existing methods displayed similar results. In a preliminary look at the nonlinear case, we showed that using the finite element Hessian and Newton's method that we can also successfully solve such equations, and that an extension to the analysis would be feasible.

4.2 Future Work

Principally with regards to future work, we would like to continue the nonlinear analysis of nonvariational problems. Of particular note is that the minimization method could be brought to the nonlinear case by instead considering instead,

$$\frac{1}{2}\|F(H[u]) + f\|^2_{\mathcal{N}} \quad \rightarrow \quad \min.$$

However we do note that this would be a nontrivial extension considering F is nonlinear, so the Euler-Lagrange equation would be different. Nonetheless this would be a necessary extension to make in order to fully apply the method to interesting NV problems.

In addition to this, it would also be desirable to consider direct applications of the Monge-Ampère equation having constructed a working example, e.g. r-adaptivity on the sphere (see McRae et al. [2016]). In general the consideration of other applicable nonlinear NV problems would be an ideal extension as well.

In terms of the program itself, one useful feature for simplicity and transparency reasons would be the ability to write the finite element Hessian operator directly into the Python interface. Currently the operator is created externally

through DUNE code that is not visible to the user unless they look inside the corresponding operator file, and even then it is difficult to casually read through and modify. If this operator could be written on the Python side it would be much more transparent and easy to work with. Furthermore this functionality could also be used for other DG methods, as other lifting operators are as of yet unavailable.

Regarding Dune-Fempy, there naturally remain many different directions the project could be taken. In particular integration with other Dune modules would be a high priority in order to add new features to the code and encourage continued development. In particular the Dune-fem-dg module (see Dedner et al. [2017]) could be added to increase the complexity of DG schemes available, whilst compatibility with Dune-pdelab would be desirable since it accomplishes a similar thing of offering high-level abstraction for Dune code.

Chapter 5

Bibliography

TIOBE index. https://www.tiobe.com/tiobe-index/, 2019. Accessed: 2019-01-09.

N. E. Aguilera and P. Morin. On convex functions and the finite element method. https://arxiv.org/pdf/0804.1780.pdf, 2008.

J. Ahrens, B. Geveci, and C. Law. Paraview: An end-user tool for large data visualization. *The visualization handbook*, 717, 2005.

M. Ainsworth and R. Rankin. Constant free error bounds for non-uniform order discontinuous finite element approximation on locally refined meshes with hanging nodes. https://core.ac.uk/download/pdf/110659248.pdf, 2008.

M. Alnäes, A. Logg, K. Ölgaard, M. Rognes, and G. Wells. A Unified Form Language: A domain-specific language for weak formulations of partial differential equations. http://arxiv.org/pdf/1211.4047v2.pdf, 2013.

M. Alnæs, J. Blechta, J. Hake, A. Johansson, B. Kehlet, A. Logg, C. Richardson, J. Ring, M. E. Rognes, and G. N. Wells. The FEniCS project version 1.5. *Archive of Numerical Software*, 3(100):9–23, 2015.

G. Alzetta, D. Arndt, W. Bangerth, V. Boddu, B. Brands, D. Davydov, R. Gassmoeller, T. Heister, L. Heltai, K. Kormann, M. Kronbichler, M. Maier, J-

P. Pelteret, B. Turcksin, and D. Wells. The `deal.II` Library, Version 9.0. *Journal of Numerical Mathematics*, 2018, accepted.

I. Babuška and T. Strouboulis. *The finite element method and its reliability*. Oxford, Great Clarendon Street, Oxford, 2001.

S. Balay, S. Abhyankar, M. F. Adams, J. Brown, P. Brune, K. Buschelman, L. Dalcin, A. Dener, V. Eijkhout, W. D. Gropp, D. Kaushik, M. G. Knepley, D. A. May, L. C. McInnes, R. T. Mills, T. Munson, K. Rupp, P. Sanan, B. F. Smith, S. Zampini, and H. Zhang. PETSc Web page. http://www.mcs.anl.gov/petsc, 2018.

J. W Barrett and W. B. Liu. Quasi-norm error bounds for the finite element approximation of a non-Newtonian flow. *Numerische Mathematik*, 68(4):437–456, 1994.

P. Bastian, M. Blatt, A. Dedner, C. Engwer, R. Klöfkorn, R. Kornhuber, M. Ohlberger, and O. Sander. A generic grid interface for parallel and adaptive scientific computing. Part II: Implementation and tests in DUNE. *Computing*, (82(2–3)):121–138, 2008.

J-D. Benamou and Y. Brenier. A computational fluid mechanics solution to the Monge-Kantorovich mass transfer problem. *Numerische Mathematik*, 84(3):375–393, 2000.

J-D. Benamou, B. D. Froese, and A. M. Oberman. Two numerical methods for the elliptic Monge-Ampère equation. *ESAIM: Mathematical Modelling and Numerical Analysis*, 44(4):737–758, 2010.

J. Bezanson, A. Edelman, S. Karpinski, and V. B. Shah. Julia: A fresh approach to numerical computing. *CoRR*, 2014. URL http://arxiv.org/abs/1411.1607.

M. Blatt and P. Bastian. The iterative solver template library. In *International Workshop on Applied Parallel Computing*, pages 666–675. Springer, 2006.

Y. Cao and N. Wan. Optimal proportional reinsurance and investment based on Hamilton–Jacobi–Bellman equation. *Insurance: Mathematics and Economics*, 45 (2):157–162, 2009.

P. G. Ciarlet and P. A. Raviart. General Lagrange and Hermite interpolation in $\mathbb{R}^n$ with applications to finite element methods. *Archive for Rational Mechanics and Analysis*, 46(3):177–199, 1972.

L. D. Dalcin, R. R. Paz, P. A. Kler, and A. Cosimo. Parallel distributed computing using Python. *Advances in Water Resources*, 34(9):1124–1139, 2011.

K. Deckelnick, G. Dziuk, and C. M. Elliott. Computation of geometric partial differential equations and mean curvature flow. *Acta numerica*, 14:139–232, 2005.

A. Dedner and M. Nolte. The DUNE-PYTHON Module. *Archive of Numerical Software*, 2018.

A. Dedner and T. Pryer. Discontinuous Galerkin methods for nonvariational problems. https://arxiv.org/pdf/1304.2265.pdf, 2013.

A. Dedner, R. Klöfkorn, M. Nolte, and M. Ohlberger. A generic interface for parallel and adaptive discretization schemes: abstraction principles and the DUNE-FEM module. *Computing*, (90):165–196, 2010.

A. Dedner, S. Girke, R. Klöfkorn, and T. Malkmus. The DUNE-FEM-DG module. *Archive of Numerical Software*, 5(1):21–61, 2017.

Y. Efendiev, O. Ilieva, and V. Taralova. Upscaling of an isothermal li-ion battery model via the homogenization theory. *Berichte des Fraunhofer ITWM*, (230), 2013.

L. C. Evans. Partial differential equations and Monge-Kantorovich mass transfer. *Current developments in mathematics*, 1997(1):65–126, 1997.

X. Feng, L. Hennings, and M. Neilan. C^0 discontinuous Galerkin finite element methods for second order linear elliptic partial differential equations in non-divergence form. https://arxiv.org/pdf/1505.02842.pdf, 2015.

J. Freund and R. Stenberg. On weakly imposed boundary conditions for second order problems. In *Proceedings of the Ninth Int. Conf. Finite Elements in Fluids*, pages 327–336. Venice, 1995.

T-P. Fries. A corrected XFEM approximation without problems in blending elements. *International Journal for Numerical Methods in Engineering*, 75(5):503–532, 2008.

D. Gilbarg and N. S. Trudinger. *Elliptic partial differential equations of second order*. springer, 2015.

C. E. Gutiérrez. *The Monge-Ampère equation*, volume 44. Birkhuser, Boston, MA, 2001.

J. E. Guyer, D. Wheeler, and J. A. Warren. FiPy: Partial differential equations with Python. *Computing in Science & Engineering*, 11(3):6–15, 2009. doi: 10.1109/MCSE.2009.52. URL https://www.ctcms.nist.gov/fipy/examples/phase/generated/examples.phase.anisotropy.html.

F. Hecht. New development in FreeFem++. *Journal of numerical mathematics*, 20 (3-4):251–266, 2012.

J. D. Hunter. Matplotlib: A 2D graphics environment. *Computing in science & engineering*, 9(3):90–95, 2007.

E. Süli I. Smears. Discontinuous Galerkin finite element approximation of non-divergence form elliptic equations with Cordès coefficients. *SIAM J. Numer. Anal., 51(4):20882106*, 2013.

I. Ioslovich, P-O. Gutman, and R. Linker. Hamilton–Jacobi–Bellman formalism for optimal climate control of greenhouse crop. *Automatica*, 45(5):1227–1231, 2009.

W. Jakob, J. Rhinelander, and D. Moldovan. pybind11 – seamless operability between C++11 and Python, 2017. https://github.com/pybind/pybind11.

E. Jones, T. Oliphant, P. Peterson, et al. SciPy: Open source scientific tools for Python, 2001–. URL http://www.scipy.org/.

G. Karniadakis and S. Sherwin. *Spectral/hp element methods for computational fluid dynamics*. Oxford University Press, 2013.

Nikos Katzourakis and Tristan Pryer. A review from the PDE viewpoint of Hamilton-Jacobi-Bellman equations arising in optimal control with vectorial cost. *Journal of Nonlinear Functional Analysis*, 2018, 01 2018. doi: 10.23952/jnfa.2018.6.

A. Khoei. *Extended finite element method: theory and applications*. Wiley, Chichester, England, 2015.

T. Kieu. Galerkin finite element method for generalized Forchheimer equation of slightly compressible fluids in porous media. https://arxiv.org/pdf/1508.00294.pdf, 2015.

R. C. Kirby, A. Logg, M. E. Rognes, and A. R. Terrel. Common and unusual finite elements. In *Automated Solution of Differential Equations by the Finite Element Method*, pages 95–119. Springer, 2012.

O. Lakkis and T. Pryer. A finite element method for second order nonvariational elliptic problems. https://arxiv.org/pdf/1003.0292.pdf, 2010.

O. Lakkis and T. Pryer. A finite element method for nonlinear elliptic problems. https://arxiv.org/pdf/1103.2970.pdf, 2012.

A. Latz, J. Zausch, and O. Iliev. *Modeling of species and charge transport in li–ion batteries based on non-equilibrium thermodynamics*, volume 6046. Springer, Berlin, Heidelberg, 2011.

G. Loeper and F. Rapetti. Numerical solution of the Monge–Ampère equation by a Newton's algorithm. *C. R. Acad. Sci. Paris, Ser. I 340 (2005) 319324*, 2005.

M. Lyly, J. Ruokolainen, and E. Järvinen. ELMER–a finite element solver for multiphysics. *CSC–report on scientific computing*, 2000:156–159, 1999.

R. Malladi and J. A. Sethian. Image processing: Flows under min/max curvature and mean curvature. *Graphical models and image processing*, 58(2):127–141, 1996.

A. McRae, C. Cotter, and C. Budd. Optimal–transport–based mesh adaptivity on the plane and sphere using finite elements. https://arxiv.org/pdf/1612.08077.pdf, 2016.

J. M. Melenk. *hp-Finite Element Methods for Singular Perturbations.* Springer, 2002.

L. Mu and X. Ye. A simple finite element method for non-divergence form elliptic equations. *International Journal of Numerical Analysis and Modeling, Vol 14, Number 2, 306-311*, 2017.

S. Müthing and P. Bastian. *DUNE-Multidomaingrid: a metagrid approach to subdomain modeling.* Springer, Berlin, Heidelberg, 2012.

A. Oberman. Wide stencil finite difference schemes for the elliptic Monge-Ampère equation and functions of the eigenvalues of the Hessian. *Discrete Contin. Dyn. Syst. Ser. B, 10(1):221238*, 2008.

T. Oliphant. *A guide to NumPy*, volume 1. Trelgol Publishing USA, 2006.

W. Ożański. The Monge-Ampère equation and the two-dimensional Navier-Stokes equations. Master's thesis, University of Warwick, 2015. URL https://warwick.ac.uk/fac/sci/maths/people/staff/ozanski/ozanski_srp_dissertation.pdf.

P. Popov, Y. Vutov, S. Margenov, and O. Iliev. Finite volume discretization of equations describing nonlinear diffusion in li-ion batteries. *Dimov I., Dimova S., Kolkovska N. (eds) Numerical Methods and Applications. NMA 2010. Lecture Notes in Computer Science, vol 6046. Springer, Berlin, Heidelberg*, 2011.

F. Rathgeber, D. A. Ham, L. Mitchell, M. Lange, F. Luporini, A. T. T. McRae, G-T. Bercea, G. R. Markall, and P. H. J. Kelly. Firedrake: automating the finite element method by composing abstractions. *ACM Transactions on Mathematical Software (TOMS)*, 43(3):24, 2017.

M. Taralov. *Simulation of Degradation Processes in Lithium–Ion Batteries*. PhD thesis, University of Kaiserslautern, 2015.

M. Taralov, V. Taralova, P. Popov, and O. Iliev. Report on finite element simulations of electrochemical processes in li–ion batteries with thermic effects. *Berichte des Fraunhofer ITWM*, (221), 2012.

N. S. Trudinger and J. I. E. Urbas. The Dirichlet problem for the equation of prescribed Gauss curvature. *Bull. Austral. Math. Soc.*, 28:217–231, 1983.

M. Turner, R. W. Clough, H. C. Martin, and L. J. Topp. Stiffness and deflection analysis of complex structures. *Journal of the Aeronautical Sciences*, 23(9), 1956.

J. Urbas. Global continuity estimates for two dimensional graphs of prescribed Gauss curvature. *manuscripta mathematica*, (115.2):179–193, 2004.

R. Verfürth. A posteriori error estimation and adaptive mesh-refinement techniques. *Journal of Computational and Applied Mathematics*, 50(1-3):67–83, 1994.

C. Wang and J. Wang. A primal-dual weak Galerkin finite element method for second order elliptic equations in non-divergence form.

Appendix A

Running this code

The code in this thesis can be run by using the accompanying docker repository. Docker is a software package that allows one to run programs from within a self-contained container without having to download extra software. Provided that docker has been installed (using `sudo apt install docker.io` or some equivalent), the container can be accessed on the command line in linux via

```
$ docker run --rm -v dune:/dune -p 127.0.0.1:8888:8888
    lloydconnellan/thesis
```

The examples can then be run by opening a web browser and typing the address `http://127.0.0.1:8888`, which opens up a Jupyter notebook. The password for the login is `dune` .

Appendix B

Derivation of Forchheimer Model

The origin of this equation stems from Darcy's law, an equation that describes flow through porous media, and is applied regularly to groundwater flow models.

$$-\nabla p = \frac{\mu}{\kappa} v,$$

where p, v, μ and κ are the pressure, velocity, absolute viscosity and permeability. For situations where the Reynolds number is greater than $\sim$ 10, inertia begins to have an effect on the system, which is accounted for in the Darcy-Forchheimer equation. In its most general form we have the following.

$$-\nabla p = \sum_{i=0}^{N} a_i |v|^{\alpha_i} v,$$

where a_i and α_i are obtained empirically. Through some manipulations, we can simplify this to an equation for just the pressure ρ.

$$\rho_t - \nabla \cdot (K(|\nabla \rho|)\nabla \rho) = f,$$

where the function $K : \mathbb{R}^+ \to \mathbb{R}^+$ is dependent on the a_i and α_i above. Adding in boundary data and initial values gives us the **boundary value problem**.

$$\begin{aligned}
&\rho_t - \nabla \cdot (K(|\nabla\rho|)\nabla\rho) = f, && \text{in } \Omega \times [0,T],\\
&\rho(x,0) = \rho^0(x), && \text{in } \Omega,\\
&K(|\nabla\rho|)\nabla\rho \cdot \mathbf{n} = g(x), && \text{on } \partial\Omega \times [0,T],
\end{aligned}$$

where ρ^0 and g are initial and boundary data given. Thus the **weak form** or variational formulation follows.

$$(\rho_t, \varphi_h) + (K(|\nabla\rho|)\nabla\rho, \nabla\varphi_h) =< g, \varphi_h > +(f, \varphi_h), \quad \varphi_h \in V_h,$$

with $\rho(x,0) = \rho^0(x)$. Finally it remains to discretize the equation in time. Let the time domain $I = [0,T]$ be divided into N intervals $t_0 = 0 < t_1 < \cdots < t_N = T$ such that $\Delta t = t_n - t_{n-1}$ and $\rho^n = \rho(x, t_n)$. Then we have the time discretized PDE.

$$\left(\frac{\rho^{n+1} - \rho^n}{\Delta t}, \varphi_h\right) + \left(\frac{1}{2}K(|\nabla\rho^{n+1}|)\nabla\rho^{n+1} + \frac{1}{2}K(|\nabla\rho^n|)\nabla\rho^n, \nabla\varphi_h\right)$$
$$=< g, \varphi_h > +(f, \varphi_h), \quad \varphi_h \in V_h,$$

where we have used Heun's method (i.e. half-implicit/half explicit) on the term with K. We can see that this is the same as equation (2.5) after replacing ρ with u.

Appendix C

C++ Version of Forchheimer Example

Here we present the C++ version of the Forchheimer example from section 2.1 using DUNE-FEM, that we compare to the Python version in section 2.3.3.

```
1  #include <config.h>
2
3  // iostream includes
4  #include <iostream>
5  #include <complex>
6  #include <ctime>
7
8  #include <dune/grid/yaspgrid.hh>
9  #include <dune/grid/io/file/dgfparser/dgfyasp.hh>
10
11 #include <dune/fempy/grid/gridpartadapter.hh>
12 #include <dune/fem/space/lagrange.hh>
13 #include <dune/fem/function/adaptivefunction.hh>
14 #include <dune/fem/function/localfunction/const.hh>
15 #include <dune/fem/function/localfunction/bindable.hh>
16 #include <dune/fem/solver/krylovinverseoperators.hh>
17 #include <dune/fem/operator/linear/spoperator.hh>
18 #include <dune/fem/io/file/dataoutput.hh>
19
```

```
20 // include header of elliptic solver
21 #include <dune/fem/schemes/elliptic.hh>
22 #include <dune/fem/schemes/femscheme.hh>
23
24 // include generated model
25 #include <forchheimer/forchheimer.hh>
26
27
28 template <class GridPart>
29 struct Initial : public Dune::Fem::BindableGridFunction< GridPart,
       Dune::Dim<1> >
30 {
31   typedef Dune::Fem::BindableGridFunction<GridPart, Dune::Dim<1> >
         Base;
32   using Base::Base;
33   template <class Point>
34   void evaluate(const Point &xhat, typename Base::RangeType &ret)
         const
35   {
36     auto x = Base::global(xhat);
37     ret[0] = 1./2.*x.two_norm2() - 1./3.*(pow(x[0],3) -
           pow(x[1],3)) + 1.;
38   }
39   unsigned int order() const { return 5; }
40   std::string name() const { return "Initial"; }
41 };
42
43 int main ( int argc, char **argv )
44 try
45 {
46   Dune::Fem::MPIManager::initialize( argc, argv );
47   Dune::Fem::Parameter::append( argc, argv );
48   for( int i = 1; i < argc; ++i )
49     Dune::Fem::Parameter::append( argv[ i ] );
50   Dune::Fem::Parameter::append( "parameter" );
51
52   typedef Dune::YaspGrid<2> HGridType ;
```

```
53  const std::string gridkey =
        Dune::Fem::IOInterface::defaultGridKey( HGridType::dimension
        );
54  const std::string gridfile = Dune::Fem::Parameter::getValue<
        std::string >( gridkey );
55  Dune::GridPtr< HGridType > gridPtr( gridfile );
56  HGridType& grid = *gridPtr ;
57
58  auto gridView = grid.leafGridView();
59  Dune::FemPy::GridPartAdapter<decltype(gridView)>
        gridPart(gridView);
60  typedef Dune::Fem::FunctionSpace< double, double,
        HGridType::dimensionworld, 1 > FunctionSpaceType;
61  Dune::Fem::LagrangeDiscreteFunctionSpace<FunctionSpaceType,decltype(gridPart),2>
        space(gridPart);
62  Dune::Fem::AdaptiveDiscreteFunction<decltype(space)>
        solution("solution",space);
63  decltype(solution) previous(solution);
64
65  Dune::Fem::interpolate(Initial<decltype(gridPart)>(gridPart),solution);
66
67  forchheimer::Model<decltype(gridPart),typename
        decltype(previous)::LocalFunctionType> model(
        previous.localFunction() );
68
69  typedef FemScheme< DifferentiableEllipticOperator<
70          Dune::Fem::SparseRowLinearOperator<decltype(solution),decltype(solution)>
71          Dune::Fem::KrylovInverseOperator<decltype(solution)> >
                SchemeType;
72  SchemeType scheme( space, model );
73
74  std::tuple< decltype(solution)* > ioTuple( &solution );
75  Dune::Fem::DataOutput<HGridType,decltype(ioTuple)> dataOutput(
        grid, ioTuple );
76  dataOutput.writeData( 0 );
77
78  Dune::Fem::GridTimeProvider< HGridType > timeProvider( grid );
```

```
79    double timeStep = 0.05;
80    model.dt() = timeStep;
81
82    auto start = std::clock();
83    for( timeProvider.init( timeStep ); timeProvider.time() < 1.0;
          timeProvider.next( timeStep ) )
84    {
85      previous.assign(solution);
86      model.t() = timeProvider.time();
87      scheme.solve( solution );
88    }
89    std::cout << double(std::clock() - start) / CLOCKS_PER_SEC <<
          std::endl;
90
91    dataOutput.writeData( 1 );
92
93    return 0;
94  }
95  catch( const Dune::Exception &exception )
96  {
97    std::cerr << "Error: " << exception << std::endl;
98    return 1;
99  }
```

Appendix D

List of Dune-Python modules

Here we list the different modules that are available to DUNE-PYTHON and DUNE-FEMPY at the time of writing. We will divide them by component into different sections that reflect the structure we have previously introduced.

D.1 Grids

Grids by default take the following form.

Code Listing D.1: The default form for grid creation

```
1 grid = create.grid('class-name', constructor, dimgrid=None,
      dimworld=None)
```

Where in particular we have the following arguments.

1. `'class-name'`: One of the strings from the table below.
2. `constructor`: Either a dgf *dune grid format* file, a gmesh file, or a preset object similar to what is demonstrated in section 2.1.1.
3. `dimgrid` (optional): The dimension of the grid.
4. `dimworld` (optional): The dimension of the space the grid is in.

The dimensions of the grid do not have to be passed to the constructor if they can be determined from the `constructor` argument.

The table below shows a list of possible grid implementations for which binding are available at the time of writing.

Table D.1: Grids

Class	Module	Description
'aluconform'	dune.alugrid	Confirming simplex grid
'alucube'	dune.alugrid	Nonconforming cube grid
'alusimplex'	dune.alugrid	Nonconforming simplex grid
'oned'	dune.grid	One-dimensional grid
'polygon'	dune.polygongrid	Polygonal grid
'ug'	dune.uggrid	Hybrid nonconforming unstructured grid
'yasp'	dune.grid	Structured grid
'spgrid'	dune.spgrid	Structured grid

Grids can also be constructed to provide a different grid view:

Code Listing D.2: Creating a custom grid view

```
1 view = create.view('class-name', grid)
```

The first argument can be any of the ones allowed for the grid construction (in which case the same `LeafGridView` is constructor as when directly constructing the grid). In addition the following views can be constructed.

Table D.2: Gridviews

Class	Module	Description
'adaptive'	dune.fem	Adaptive grid view
'filtered'	dune.fem	Filtered grid view for separated domains. Usage: subGrid = create.view("filtered", grid, filter, domainID)
'geometry'	dune.fem	Convert a coordinate function into a grid view. Usage: geometry = create.view("geometry", function)

D.2 Spaces

Now we move on to spaces. By default, they take the form

Code Listing D.3: The default form for space creation

```
space = create.space('class-name', grid, dimrange=1, order=1,
                     storage='fem', field='double')
```

where we have the following arguments.

1. `'class-name'`: A string from the table below.
2. `grid`: A grid object from above.
3. `dimrange` (optional): The range dimension of the space.
4. `order` (optional): The polynomial order of the basis functions.
5. `storage` (optional): `'fem'` by default. Specifies the storage used for discrete functions (as shown in D.3).
6. `field` (optional): The field of the range space (`'double'` or `'complex'`).

Table D.3: Discrete Functions

Class	Module	Description
'adaptive'	dune.fem	An adaptive function
'eigen'	dune.fem	Function from the eigen package
'fem'	dune.fem	The default DUNE-Fem function
'istl'	dune.fem	Function from DUNE-Istl
'petsc'	dune.fem	Function from the PETSc package
'petscadapt'	dune.fem	An adaptive function using PETSc

Available spaces are:

Table D.4: Spaces

Class	Module	Description
'bdm'	dune.fem	Space for Brezzi-Douglas Marini elements
'combined'	dune.fem	Discrete function space formed from a tuple of DF spaces
'dglagrange'	dune.fem	DG space using Lagrange basis functions
'dglegendre'	dune.fem	DG space with elementwise Legendre tensor product basis function. This space allows for an additional argument: hierarchical which defaults to True. This argument determines if the basis functions are sorted hierarchically according to their polynomial order or lexicographically.
'dglegendrehp'	dune.fem	'dglegendre' with hp-adaption
'dgonb'	dune.fem	DG space with elementwise orthonormal basis functions
'dgonbhp'	dune.fem	'dgonb' with hp-adaptation
'finitevolume'	dune.fem	Space for the finite volume method
'lagrange'	dune.fem	Space for Lagrange elements
'p1bubble'	dune.fem	P1 space with bubble elements
'product'	dune.fem	Discrete function space formed from a tuple of DF spaces
'rannacherturek'	dune.fem	Space for Rannacher-Turek elements

D.3 Grid Function

Grid functions can be constructed in a variety of ways, though the explicit way to make a grid function is

Code Listing D.4: The default form for function creation

```
1 create.function('class-name', grid, 'function-name', order,
```

```
2                    constructor)
```

with the following arguments.

1. `'class-name'`: A string from the table below.
2. `grid`: A grid object from D.1.
3. `'function-name'`: A string for the name of the created function.
4. `order`: The order of the function used for quadrature.
5. `constructor`: An object described in the table below used to construct the function.

For the below table we list the available strings for `'class-name'` together with the compatible argument for the `constructor` parameter.

Table D.5: Grid Functions

Class	Module	Constructor
'cpp'	dune.fem	A c++ string, e.g. "value[0] = 2;"
'global'	dune.fem	A Python function or lambda taking the global coordinate as a single argument
'levels'	dune.fem	This is a special piecewise constant grid function used for visualization which returns the level of each element
'local'	dune.fem	A Python function or lambda taking an entity and a local coordinate as arguments
'numpy'	dune.fem	A numpy expression
'partitions'	dune.fem	This is a special piecewise constant grid function used for visualization which returns the partition number for each element
'ufl'	dune.fem	A UFL expression

In addition `'discrete'` can be used to construct discrete functions. But typically these are made using the `space.interpolate(expression)` syntax, using the stor-

age type for the space by default. The arguments for the `interpolate` method are the same used to construct general grid functions given in the previous table.

D.4 Schemes and Operators

As discussed in section 2.1.4, schemes can be constructed directly with a UFL form and contain the method for solving the PDE. Addtionally as shown in section 2.3, it is also possible to create models and operators that store the operator separately. While schemes have to have identical domain and range spaces, operators can map between different spaces. We review this below.

Code Listing D.5: The default form for scheme creation

```
scheme = create.scheme('class-name', equation, space,
                       parameters=dict, solver='solver-name')
```

1. `'class name'`: A string from the table below.
2. `equation`: A UFL equation (`a == b`), or a model object. In addition a tuple or list can be used here where the first entry is the equation and further arguments can provide Dirichlet boundary conditions.
3. `space`: A space object from D.2. (This is optional if the trial/test UFL functions are initialized with a Dune-Fempy discrete function space, as in code listing 2.9).
4. `parameters` (optional): A dictionary of Dune parameters that can be used to specify things like the solver behaviour, e.g. `{'fem.solver.newton.tolerance':1e-3}`.
5. `solver` (optional): `'fem'` by default. Used to specify the solver used, from D.6.

The two main schemes available in Dune-Fempy are `galerkin` and `h1`. The distinction between them is described in section 2.3. In addition the Dune-nvdg module provides an `nvdg` scheme.

There are a number of parameters that can be passed to the scheme to influence the solving procedure. Most importantly tolerances for the iterative solvers can be provided and verbosity can be turned on and off. In addition preconditioners can be set via the parameters. Available options depend on the `storage` backend used to construct the space. For the `istl` backend available options include: `none`, `ssor`, `sor`, `ilu-0`, `ilu-n`, `gauss-seidel`, `jacobi` and `amg-ilu-0`. They are set using the following syntax.

Code Listing D.6: How preconditioning is set via parameters

```
from dune.fem import parameter
parameter.append({"istl.preconditioning.method": "ilu",
                  "istl.preconditioning.iterations": 1,
                  "istl.preconditioning.relaxation": 1.2})
```

For the `petsc` backend options include: `none`, `oas`, `sor`, `jacobi`, `hypre`, `ml`, `ilu`, `icc`, and `lu`. Which of these can actually be used will depend on the PETSc implementation, e.g. `hypre` requires that PETSc was build with support for the `hypre` package.

Finally we list the possible solving methods available that can be selected during scheme creation above. There is also the possibility of constructing an operator that can be applied using the `__call__` method and linearised using the `jacobian` method but does not provide a `solve` method. This is especially of interest in the case where the operator maps between different spaces. Creating an operator is similar to the scheme construction.

Table D.6: Solvers

Class	Description
'bicgstab'	Biconjugate gradient method
'cg'	Conjugate gradient method (for symmetric problems only)
'gmres'	Generalized minimal residual method
'minres'	Minimal residual method
'suitesparse'	This is a tuple where the second argument determines which suitesparse solver to used
'superlu'	Solve method from SuperLU package

Code Listing D.7: The default form for operator creation

```
scheme = create.operator('class-name', equation, domainSpace,
                         rangeSpace)
```